

---

# Characterization of nanobubbles & effectiveness in breakdown of organic micropollutants

---



Master Thesis  
Victor Lütken & Andreas Rasmus Petersen  
Aalborg University  
Chemistry



# AALBORG UNIVERSITY

## STUDENT REPORT

Final year of study at Institute For Chemistry  
and Biotechnology

Fredrik Bajersvej 7H  
9220 Aalborg Øst  
<http://www.bio.aau.dk>

**Title:**

Characterization of nanobubbles  
& effectiveness in breakdown of  
organic micropollutants

**Theme:**

Master Thesis

**Project Period:**

Fall semester 2023 and spring semester 2024

**Project Group:**

Separation group

**Participant(s):**

Victor Lütken  
Andreas Rasmus Petersen

**Supervisor(s):**

Morten Lykkegaard Christensen

**Copies:** 1**Page Numbers:** 73**Date of Completion:**

June 2024

**Abstract:**

In this project the physical properties of air, CO<sub>2</sub> and O<sub>2</sub> nanobubbles (NB) were investigated along with NB ability to break down organic micropollutants (OMP) or concentrate them with membrane technology. The size and zeta potential of the NB was measured before and after being exposed to acid, ultrasound or UV light in the presence of benzoic acid. A general increase in size for both O<sub>2</sub> and air on all methods was found, while CO<sub>2</sub> showed a decrease in ultrasound and a small increase while exposed to acid. The zeta potential analysis showed no overall trend, except for acid consistently increasing the zeta potential. The dissolved gas content was determined to see if the NB had gone into solution when exposed to acid, ultrasound or UV light as a bursting method. It was not possible to correlate dissolved gas content with the bursting of NB. The stability over time of the NB was investigated where it was found that CO<sub>2</sub> had the shortest lived NB followed by air and O<sub>2</sub> in that order. An experiment was performed in order to determine the effect of NB on the breakdown of benzoic acid when exposed to acid, ultrasound or UV light where no effect of the NB was found. The effect on membrane retention of OMP by NB was tested and it was found that the NB either had no effect on the amount of OMP that came through the membrane or allowed more OMP to come through.

*The content of this report is freely available, but publication (with reference) may only be pursued due to agreement with the author.*

# List of abbreviations

• Abbreviation	Meaning
• AOPs	Advanced oxidation processes
• BOD	Biological oxygen demand
• BPA	Bisphenol-A
• DLS	Dynamic light scattering
• DO	Dissolved oxygen
• ELS	Electrophoretic scattering
• ESR	Electron spin resonance
• HPLC	High pressure liquid chromatography
• kcps	Kilo counts per second
• MF	Microfiltration
• MS	Mass spectrometry
• NB	Nanobubble
• NF	Nanofiltration
• OMP	Organic micro pollutant
• PDI	Polydispersity index
• PFAS	Per-and polyfluoroalkyl substances
• RO	Reverse osmosis
• SDS	Sodium dodecyl sulphate
• UF	Ultrafiltration
• UV	Ultraviolet light
• UV-vis	Ultraviolet-visible light

# Contents

<b>List of abbreviations</b>	<b>ii</b>
<b>Preface</b>	<b>v</b>
<b>1 Introduction</b>	<b>1</b>
1.1 Current methods . . . . .	1
1.1.1 Sand filtration . . . . .	2
1.1.2 Membrane filtration . . . . .	2
1.1.3 Flocculation & coagulation . . . . .	3
1.1.4 Biological breakdown . . . . .	3
1.2 Advanced oxidative processes . . . . .	3
1.3 Nanobubbles . . . . .	4
<b>2 Problem statement</b>	<b>6</b>
<b>3 Theory</b>	<b>7</b>
3.1 Nanobubbles . . . . .	7
3.1.1 Surface properties of NB . . . . .	7
3.2 Radical formation & bursting methods . . . . .	10
3.2.1 Radicals . . . . .	10
3.2.2 Detection of radicals . . . . .	10
3.2.3 Bursting method . . . . .	11
3.2.4 Influence of gas on radical formation . . . . .	11
3.3 Analysis methods . . . . .	12
3.3.1 Measuring gas content . . . . .	12
3.3.2 Analysis of bubbles . . . . .	12
<b>4 Experimental considerations</b>	<b>14</b>
4.1 CO <sub>2</sub> Measurements . . . . .	14
4.1.1 CO <sub>2</sub> titration . . . . .	14
4.2 Lasertest . . . . .	15
4.2.1 UV-vis . . . . .	15
4.3 DLS and Zeta measurement . . . . .	16
4.3.1 DLS . . . . .	16
4.3.2 Zeta . . . . .	16
4.4 Radical formation & OMP breakdown . . . . .	17
4.5 Transport of OMP . . . . .	17



<b>5</b>	<b>Methods</b>	<b>18</b>
5.1	Initial generation of NBs . . . . .	18
5.2	DLS & Zeta . . . . .	18
5.2.1	DLS . . . . .	18
5.2.2	Zeta . . . . .	19
5.3	DO measurements . . . . .	19
5.3.1	Optical DO meter . . . . .	19
5.3.2	Winkler method . . . . .	19
5.4	Radical generation & breakdown of OMP . . . . .	20
5.4.1	HPLC . . . . .	20
5.5	Saturation of surface . . . . .	20
5.6	Mass transfer experiment . . . . .	20
5.6.1	pH & conductivity . . . . .	21
5.6.2	HPLC . . . . .	21
<b>6</b>	<b>Results &amp; Discussion</b>	<b>23</b>
6.1	Characterization . . . . .	23
6.1.1	Size and zeta-potential . . . . .	23
6.1.2	Dissolved gas measurements . . . . .	35
6.2	Radical formation & OMP breakdown . . . . .	39
6.2.1	HPLC . . . . .	39
6.3	Mass transfer experiment . . . . .	41
6.3.1	HPLC . . . . .	41
6.3.2	pH & conductivity . . . . .	42
<b>7</b>	<b>Conclusion</b>	<b>45</b>
<b>8</b>	<b>Further research</b>	<b>46</b>
	<b>Bibliography</b>	<b>47</b>
<b>9</b>	<b>Appendix - Winkler method</b>	<b>53</b>
<b>10</b>	<b>Appendix - HPLC for breakdown experiment</b>	<b>54</b>
<b>11</b>	<b>Appendix - Laser test</b>	<b>57</b>
11.1	Air . . . . .	57
11.2	CO <sub>2</sub> . . . . .	57
11.3	O <sub>2</sub> . . . . .	60
<b>12</b>	<b>Appendix D - Dissolved CO<sub>2</sub></b>	<b>64</b>
<b>13</b>	<b>Appendix - kcps values</b>	<b>66</b>
<b>14</b>	<b>Appendix - p and F values values</b>	<b>69</b>

# Preface

We would like to thank Morten Lykkegaard Christensen for his guidance throughout the project, Mette Helene Sahl Haferbier & Timo Kirwa for their assistance in the lab.

Aalborg Universitet, 3. June 2024

Andreas Rasmus Petersen  
arpe19@student.aau.dk  
Studynumber: 20193532

Victor Lütken  
vlatke18@student.aau.dk  
Studynumber: 20184494

# Chapter 1

## Introduction

As knowledge and understanding of the adverse effects on health and environment of organic micropollutants (OMP) has increased in recent years, a heightened interest in their removal has grown. Therefore quantifying/analyzing a method for their removal is highly favourable [1, 2].

As a group, OMP include a wide array of different anthropogenic and natural compounds in the concentration scale between ng/L to g/L. OMP include many different groups of chemicals, such as pharmaceuticals like diclofenac and ibuprofen, personal care products like triclosan and benzophenone-3, steroid hormones like estradiol and estrone, industrial chemicals like bisphenol-A (BPA), pesticides like atrazine and many others [1, 2]. As the group is diverse, the currently employed removal methods not be effective in removing some of these like diclofenac, metoprolol, TCEP and atrazine [1].

This diverse list also includes toxic, carcinogenic and endocrine-disrupting compounds that are dangerous to health and the environment [3, 4]. As the group of chemicals is wide-ranging, there is no overall characteristic to characterise OMP, other than being organic and present in small concentrations.

With the current methods of wastewater treatment, newer, more persistent OMP cannot be removed as, among other things, these methods have not been designed to remove the low concentrations of OMP from wastewater [1, 5, 6]. This leads to wastewater containing OMP being discharged into aquatic environments. The discharge of wastewater containing OMP results in several negative effects like short- and long-term toxicity, antibiotic-resistant microbes, endocrine disruption effect, and bioaccumulation of hazardous materials in various food chains. An example of this is per- and polyfluoroalkyl substances (PFAS) found in fish [7–9].

The interest in OMP, and chemicals of emerging concern, is increasing as documented by the European watch list for surface water under the Water Framework Directive [10].

Technology also follows this trend as can be seen by the use of more sensitive detection methods like MS-QTOF, which enables the detection of OMP [11, 12].

These new detection methods have led to the discovery of many chemicals of emerging concern that aren't removed from waste effluent by currently employed removal methods [11].

As some of the newer pollutants, like OMP, cannot be removed by currently employed methods, such as mechanical treatment or activated sludge, other more complex and difficult-to-implement solutions may be needed to remove these [13]. Some examples include filtration, flocculation and ozonation [14, 15].

### 1.1 Current methods

Looking at the currently implemented methods through the lens of OMP removal, two distinct paths appear for their removal; namely up-concentration and breakdown and/or conversion to

broken-down organic matter which bacteria may consume.

A tried and tested method for up concentration is filtration, where solids are removed from a fluid by passing through a porous medium, depending on the requirements, different media can be used from coarse to fine [16].

### 1.1.1 Sand filtration

An example of this is sand filtration, which uses absorption or physical encapsulation; where particles larger than the grains of sand get filtered, and smaller particles get lodged in between the grains or adsorbed to the sand through different atomic forces [16]. Sand filtration can work effectively down to suspended solid (typically 10-100  $\mu\text{m}$ ) [17, 18]. Some OMP can be removed through sand filtration. However, they may not have as high an effectiveness as is desired. Furthermore, the effectiveness can be increased through additional biological break-down within the sand column itself [17]. The method is, however, slow as the flow is limited by gravity down through the sand column, and its capacity is thus limited, as the filter cannot handle an increased flow, which may come as the flow of wastewater varies over time.

### 1.1.2 Membrane filtration

Another filtration media, which can be used to up concentrate OMP, is membranes, which can be divided into four different categories based on their pore size; microfiltration (MF), ultrafiltration (UF), nanofiltration (NF), and reverse osmosis (RO) as can be seen on **figure 1.1**. MF has a pore size of 0.1-10  $\mu\text{m}$  and removes bacteria and suspended solids whereas UF has a pore size of 10-100 nm and removes viruses. NF can remove most organic compounds and most divalent ions and have a pore size of around 1-10 nm. Lastly, RO can remove all organic compounds and nearly all ions [19, 20].

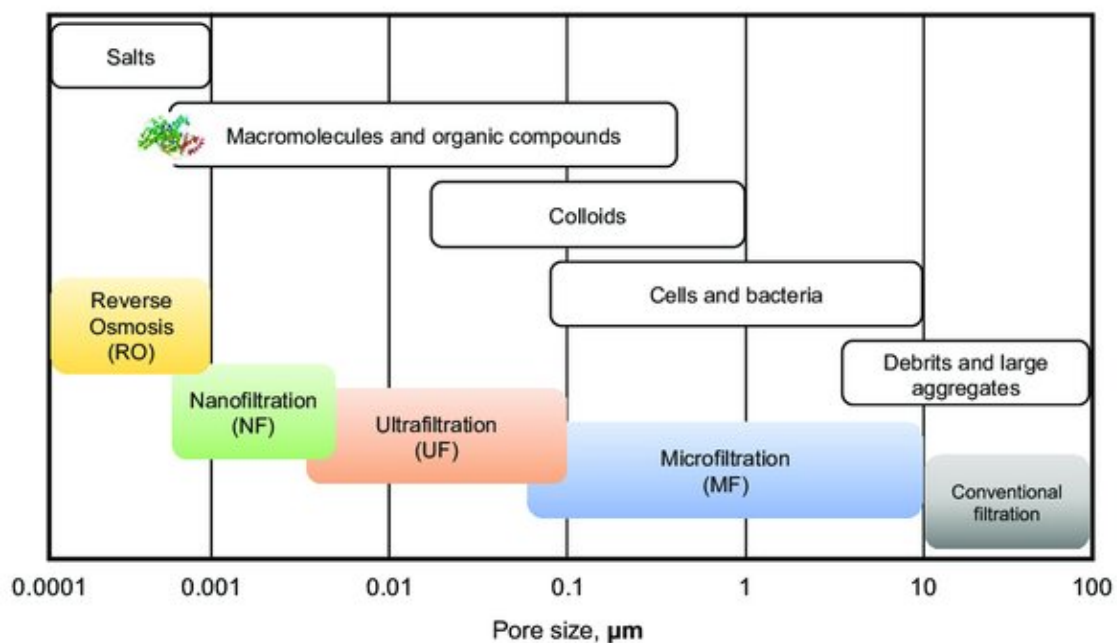


**Figure 1.1:** Figure showing the different pore sizes of membranes and what they exclude [21].

Among these, UF, NF, and RO seem to be the most promising, in regards to removing OMP [22–24].

By using membranes, OMP cannot only be removed by size exclusion but also adsorb to either the membrane surface or to bigger particles in the solution.

As OMP cover an extensive list of molecules with very different properties, it may prove difficult to remove all OMP effectively, as another key factor in membrane removal is the interaction between the OMP and membrane. Furthermore, the characteristics of the solution and the membrane itself also influence the rejection mechanism [25].

Adsorption and size exclusion can for instance be done by activated carbon, but as for all filtration systems, fouling will increase over time and the membrane will have to be cleaned or replaced. Although activated carbon can be regenerated by many different methods, it is resource intensive [26]. To exclude OMP based on size, the use of NF or RO is needed, but OMP may still penetrate the membrane and are thus not optimal as well as resource intensive [1].

### **1.1.3 Flocculation & coagulation**

Another method of removal for suspended particles is coagulation and flocculation [27, 28].

In coagulation, a coagulant is added to a suspension which neutralizes the surface charge of particles, like colloids, allowing them to stick together into floc or flake. Flocculation is the physical process of floc/flake coming out of the solution to the sediment [29].

Both, include the addition of compounds to promote the coagulation of particles together, as it is a necessary step for flocculation. Some particles may be able to sediment if the wastewater is still standing. However, as some particles have a surface charge, they repel each other and will not clump together and will need a coagulant [30].

Although the coagulation-flocculation process is versatile, it requires maintaining several different conditions for optimal efficiency. Of note is a desorption which happens during sedimentation. The desorption depended on several factors, such as pH, slow mixing time, natural organic material concentration, powdered activated carbon and  $\text{FeCl}_3$  dosage [31].

### **1.1.4 Biological breakdown**

One of the main treatment paths in biological breakdown for organic pollutants, and OMP, is aerobic biological breakdown [1]. The pollutants that are commonly broken down by the biological processes are aliphatic molecules, with short side chains, unsaturated aliphatic molecules, and molecules with electron-donating functional groups, while electron-withdrawing groups are not broken down to the same extent by the biological breakdown [1]. Furthermore, to maintain the microorganisms responsible for the breakdown of OMP, a specific environment is required like a specific oxygen content, otherwise, the microbes may not be effective [32].

As OMP have proven difficult to remove with current methods, more thorough methods must be deployed to deal with them.

## **1.2 Advanced oxidative processes**

Advanced oxidative processes (AOPs) is a broad term describing processes that are designed to break down organic compounds in water through oxidation. Ozonation is done by adding ozone ( $\text{O}_3$ ) to the effluent, which will decompose into byproducts, including radicals like  $\text{OH}^\cdot$ . The radicals can contribute to the oxidation of OMP and help oxidize them down to primarily

CO<sub>2</sub> and H<sub>2</sub>O. The effect of the hydroxyl radicals can also be achieved by using H<sub>2</sub>O<sub>2</sub> with or without exposure to UV-light [1]. Due to radicals having an unpaired electron, they are highly reactive and well-suited for breaking down pollutants in wastewater.

Ozone is effective against biological matter, viruses, bacteria, and parasites as well as having a better effect than other cleaning chemicals like chlorine [33]. It has shown an effectiveness against active pharmaceutical ingredients of >85% [34]. Furthermore, it works on a range of different pHs and does not introduce any waste products to the effluent. Unless bromide ions are present, in which case brominated byproducts will be created, therefore to avoid these byproducts careful control of the pH is necessary [33]. The actual chemical reaction in the effluent is quick, and will not provide any blockage of capacity if there is a sudden increase in the amount of effluent.

Ozonation is not as financially viable compared with other methods of cleaning effluent. Both equipment and operational costs are high and need a professional in ozone wastewater treatment. Ozone is in its nature difficult to transport, as it has a short lifetime, due to its propensity to degrade, and must be generated onsite [35].

The short lifetime of ozone also necessitates a small cross-section where the effluent is transported through to ensure equal ozonation.

Furthermore, ozone is a toxic gas as well as corrosive and will need extra measures to ensure a safe and secure working environment.

### 1.3 Nanobubbles

As the ozonation both adds complexity and increases the need for safety precautions, other AOPs may prove attractive.

One such AOP is nanobubbles (NB) from which radicals can be formed [36].

Bubbles with a diameter of below 1 µm are defined as NB and offer many of the same benefits as ozonation does, but have key differences like the ability to control when the radicals are formed, removing the requirement from ozonation for a speedy process, as well as the need for a small constricted space for the effluent. NB have many of the same properties as colloids as in they are stable, have a charge (zeta-potential), and are the same size as colloids [37].

As the low concentration of OMP often poses an additional barrier to their removal, a method of collecting them may be needed to ensure efficient removal. NB will nucleate on hydrophobic particles, which increases the likelihood of a radical interacting with the OMP. Furthermore, the NB can help agglomerate hydrophobic molecules through capillary forces [38].

Due to the size of NB, the literature suggests that the surface tension is dominating the Laplace pressure equation where [39]:

$$P_{in} = P_{out} + \frac{4 \cdot \gamma}{d} \quad (1.1)$$

Where  $P_{in}$  (Pa) is the internal pressure,  $P_{out}$  (Pa) is the external pressure,  $\gamma$  is the surface tension ( $\frac{N}{m}$ ) and  $d$  is the diameter in (m). As the size decreases, the surface tension stays the same and the pressure increases drastically within the nm scale diameter.

Another model expands upon the theory by taking the electrostatic repulsion into account. The equation goes as follows:

$$P_{in} = P_{out} + \frac{2 \cdot \gamma}{R} - \frac{\epsilon \zeta^2}{R^2} \quad (1.2)$$

$\epsilon$  is the relative permittivity of the solution,  $\zeta$ (mV) is the zeta-potential and  $R$  (m) is the radius of the bubble.

The effect of the electrostatic repulsion can be seen on **figure 1.2**.

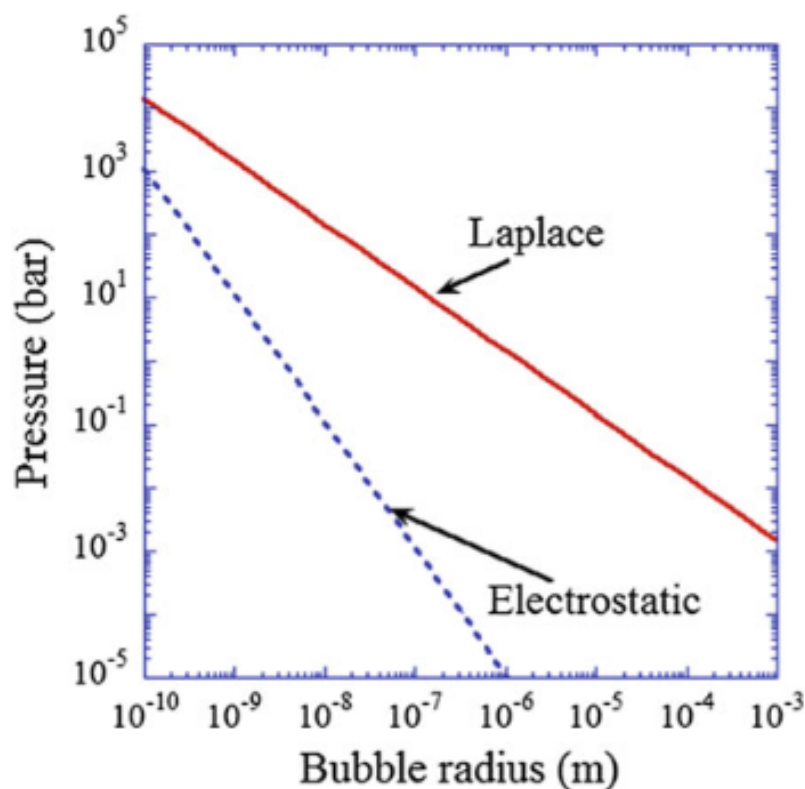


**Figure 1.2:** Figure showing the effect of electrostatic repulsion of the zeta-potential at -40 mV compared with the Laplace pressure. Figure taken from [40, 41]

The effect of the electrostatic repulsion is not enough to cover the Laplace pressure, and may thus not fully explain the stability. Another model, the Dynamic equilibrium model, postulates that the NB is partly covered with hydrophobic matter. As hydrophobic material in water repels liquid water and forms a depletion layer, the density of water drops. This depletion layer is 0.2-5 nm thick and the density of water is reduced 44-98 % [42, 43]. The concentration of gas increases in the depletion layer as the dissolved gas is trapped [44]. The gas then diffuses into the bubble alongside the contact line, while it diffuses out of the bubble on the uncovered part. The bubble is stabilised when an equilibrium influx and outflux of gas is reached [40].

The surface of NB has an increased affinity to electrons, as the bandgap between the conduction and valence band is lower on the surface than in bulk, which means less energy is required for electrons to jump up to the conduction band [45, 46]. Furthermore, the surface of droplets have been found to easily facilitate reactions with a high thermodynamic barrier, as well as helping cause spontaneous redox reduction of bio-molecules with up to 95% effectiveness, scaling with surface area [46, 47].

The inherent energy and potential of NB to facilitate reactions, along with the very favourable environment to certain reactions indicates that NB, could potentially create radicals if burst [48].

The combination of the favourable environment for reactions, the collection of hydrophobic material and the possibility of creating free radicals, indicates that NB are a promising novel way to remove OMP, in many different ways, from wastewater.

## Chapter 2

# Problem statement

How do different gasses affect the physical properties of nanobubbles and their use in the breakdown or removal of organic micropollutants?

The problem statement will be examined through the following goals:

- Characterization of nanobubbles by way of:
  - Measuring the zeta potential.
  - Measuring the size.
- Characterization of the breakdown/removal of organic micropollutants by different methods using nanobubbles:
  - Breakdown by way of bursting nanobubbles:
    - \* To produce radicals to break down organic micropollutants.
    - \* To saturate the surface with compounds causing the nanobubbles to burst.
  - Removal by way of collecting organic micropollutants on the surface of nanobubbles and removal with a membrane.



# Chapter 3

## Theory

### 3.1 Nanobubbles

To understand NB, normal bubbles must first be understood, as they differ from each other in several ways.

Bubbles are gas-filled cavities within liquids or solids. As the focus is on water treatment, only liquids will be considered here. Bubbles can act as a reserve for dissolved gas and have an internal equilibrium pressure of at least the external environment. Bubbles in water contains saturated water vapour at 100% relative humidity [39].

All bubbles have an interface surrounding the surface, which has different properties compared with the bulk liquid. Surfactants can help stabilize any size of bubble but are not necessary for the formation of bubbles [49]. The surface area of a volume of bubbles is in inverse proportion to the bubble diameter as can be seen in **equation 3.1**. On the small scale, the surface area thus plays a more significant role compared with larger sizes. For the same volume, the surface area increases proportionally to the reduction in bubble diameter:

$$\frac{\text{surface area}}{\text{volume}} = \frac{6}{\text{Diameter}} \quad (3.1)$$

Thus a total volume of 10 mL of 100 nm diameter bubbles, have a have a 1000 times more surface ( $600m^2$ ) compared with 10 mL of 100  $\mu m$  NB ( $0.6m^2$ ).

A defining feature of bubbles is their buoyancy causing them to rise up through the liquid until they reach a surface. The rising of bubbles (up to 25 $\mu m$  diameter) is governed by the Stokes equation which is valid for particles at low Reynolds numbers:

$$R = \frac{\rho \cdot g \cdot d^2}{18 \cdot \mu} \quad (3.2)$$

Where the rising rate is R (m/s),  $\rho$  is the density ( $kg/m^3$ ), g is the gravity of the earth ( $m/s^2$ ), d is the bubble diameter (m) and  $\mu$ , is the dynamic viscosity ( $Pa \cdot s$ ).

This relationship dictates that a 2.5  $\mu m$  bubble rises 100 times slower than a 25  $\mu m$  bubble [50]. Microbubbles (1 - 100 $\mu m$ ) rise slowly ( $10^{-6} - 0.01m/s$ ) and indirectly towards the surface. Smaller bubbles ( $\leq 20\mu m$ ) will shrink due to the external pressure from the bulk into smaller more stable NB ( $< 1\mu m$ ) which are stable for long periods in suspension [51].

NB rise at ( $< 1\mu m/s$ ) and are counteracted by Brownian motion of greater than ( $1\mu m/s$ ) [39] as can be seen on **figure 3.1**.

The size of NB, as well as their longevity, classify them as colloids. The requirements being the size is between 1-1000 nm and the particles being stable and dispersed in solution [37].

#### 3.1.1 Surface properties of NB

The properties of colloids, specifically NB, are strongly linked to the gas-liquid interface as ions of negative charge have been shown to gather on the surface of NB [52, 53]. The surface charge

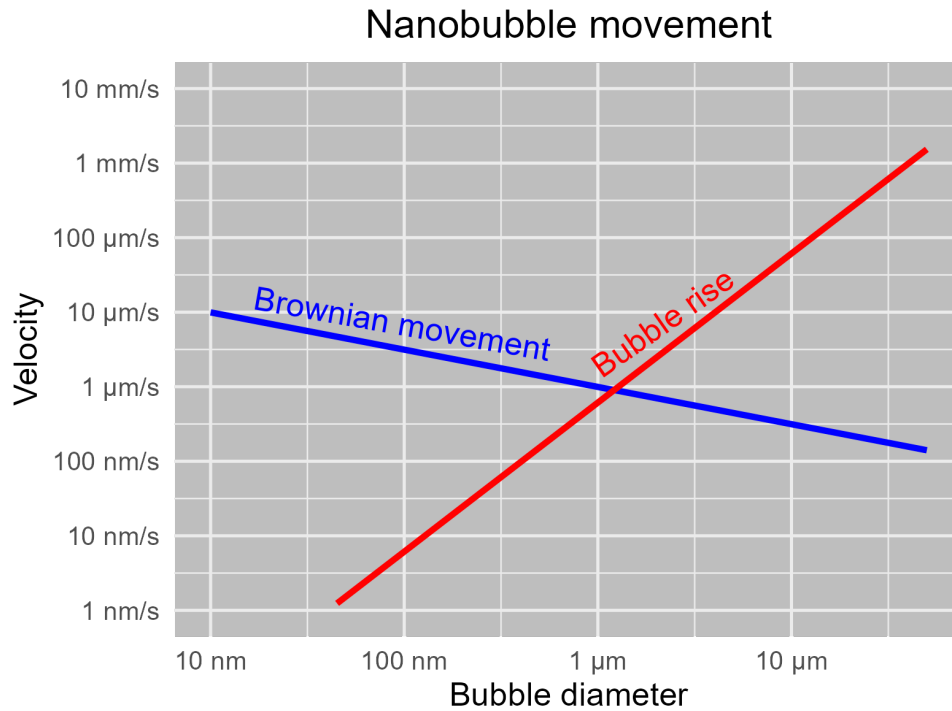


**Figure 3.1:** Velocity of the buoyancy and Brownian motion vs. bubble diameter. The bubble rise is described in equation 3.2. The equation for Brownian motion is described in [39].

is reinforced by the liquid water surface's strong affinity for electrons [46].

In the absence of counteracting forces, like charges, surface stabilizing hydrophobic material and solute interactions, the excess pressure of a spherical bulk NB at 125 nm is 2.336 MPa according to the Laplace equation 1.1, which is related to the surface tension and affected by the size.

The surface charge is theorized to partially be the reason behind the long lifetime of NB, as the negative charges repel each other on the surface and thus oppose the surface tension. It has been shown by molecular dynamics simulations that NB are charged and counteracting part of the surface tension [54].

The surface charge of the NB will attract the opposite charge, and thus an "atmosphere" of opposite charges will surround the NB called the Stern layer as seen on **figure 3.2**. The surface charge along with the stern layer and slipping plane is called the electrical double layer [56].

The charge on the double layer can be quantified by measuring the zeta potential, which is the difference between the bulk media and the slipping plane of charge in the NB.

As described previously, bubbles under 50-25 μm in diameter will shrink which is also affected by the saturation of the surrounding liquid [39, 51]. Smaller bubbles have higher internal pressure and will release gas to dissolve into the immediate surrounding under-saturated liquid, while larger bubbles have lower pressures, and grow by taking gas from supersaturated solutions. Thus large bubbles grow and small bubbles shrink (also known as Ostwald ripening) [57].

The rate at which they grow or shrink depends on many different factors. Another stabilizing factor of NB is the electrostatic interactions between them which usually prevents coalescence, and slows any rise from growing bubbles [50].

The charge on the bubbles (zeta potential) can be determined from their horizontal velocity ( $v_e$ )

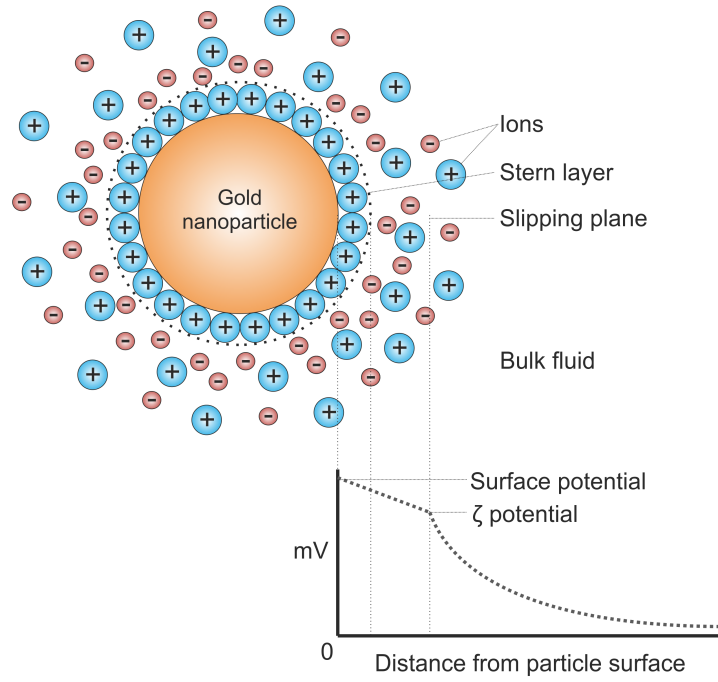


**Figure 3.2:** The different charge layers on a colloid. Taken from [55].

in a horizontal electric field:

$$v_e = \frac{\epsilon_{rs} \cdot \epsilon_0 \cdot \zeta}{\eta} \cdot E \quad (3.3)$$

Where  $v_e$  is the speed of the particle  $\frac{m}{s}$ ,  $\epsilon_{rs}$  is the relative permittivity of the solution,  $\epsilon_0$  is the electric permittivity of vacuum in  $(\frac{F}{m})$ ,  $\zeta$  is the zeta-potential (V),  $\eta$  is the viscosity  $Pa \cdot s$  and  $E$  is the electric field strength in  $\frac{V}{m}$ .

The zeta-potential is generally negative and is affected strongly by pH and the ionic strength [58, 59]. It is reported as independent of the bubble diameter, though some analyses show that a strongly negative zeta-potential is consistent with smaller NB hydrodynamic radii [60].

Due to the gas in the NB having a low electron density (gas being less dense than other states of matter), there is a lack of Van der Waals interaction between bubbles, thus preventing coalescence. Therefore the NB grow or contract but rarely coalesce or divide.

The surface may contain surface active materials, like proteins or surfactants, which stabilize the bubble by lowering the surface tension by having a smaller surface area of the bubble [61]. Growth or shrinkage in NB depends on diffusion to the surrounding solution, which in turn depends on whether the surrounding solution is over- or under-saturated. The solubility of a gas is proportional to the partial pressure of the gas [62]. This pressure is exerted by the surface tension and is inversely proportional to the diameter of the bubbles and increases significantly at small bubble diameters as can be seen in **equation 1.1**.

Due to the significant increase in pressure for smaller bubbles, the dissolution process is accelerated. The accelerated dissolution also increases the bubble's movement and contraction which helps the removal from/of the surrounding gas-saturated solution.

NB are also known to gather both hydrophobic and hydrophilic compounds in water [63]. The hydrophobic gathering is due to the hydrophobic effect, where water forms a clathrate structure around the hydrophobic surface to minimize the loss of hydrogen bonds that are broken by the

hydrophobic particle [64]. The hydrophobic effect also causes other hydrophobes to clump together onto the NB surfaces, helping them stabilize as they decrease the surface tension and the total amount of clathrated water making it more energetically favourable [65]. As described, NB are affected by many different forces and mechanisms which all affect the stability of the NB.

## 3.2 Radical formation & bursting methods

The forces at play with surface tension and pressure indicate that radicals may form in the last moments of a bursting NB. These forces have been shown to help create radicals, when a dynamic stimulus is applied, shown with both simulation and experiments [36, 66, 67]. There are disagreements on the mechanism behind the radical generation in NB, however, some things are common for all theories. Namely, the rapid increase in pressure and temperature as the bubbles collapse making the conditions ripe for radical formation [51].

### 3.2.1 Radicals

Radicals are molecules or atoms that have an unpaired valence electron. This makes the molecule highly reactive as it is not favourable for the molecule [68]. Radicals can be formed in different ways. One method is to break a covalent bond homolytically in the molecule with the help of additional energy either in the form of heat or light. The energy requirements are significant, for example, turning  $\text{Cl}_2$  into  $2\text{Cl}\cdot$  has a bond dissociation energy of +243 kJ/mol [68].

Homolytic bond cleavage often occurs between atoms of similar/same electronegativity, like O-O or O-N bonds [68].

This will create two radical species as can be seen in **reaction 3.4**. Radicals can also be formed by giving or removing an electron from the molecule.



The radicals present depend on which gas is used in making the NB. For Fenton reactions, Illés et al. has shown that if the solution contains bicarbonate at a neutral pH, the main radical is the carbonate anion radical  $\text{CO}_3^{\cdot-}$  [69]. Lan et al. also concluded that some  $\cdot\text{OH}$  related radical reaction may produce the carbonate radical.

The hydroxyl radical, ( $\cdot\text{OH}$ ), is important in water-based radical formation and is one of the main reactive species used in advanced oxidation processes (AOPs) due to its high redox potential and low selectivity with most organic pollutants [71, 72].

AOPs can produce radicals through several different methods such as Fenton oxidation, photochemical oxidation, electrochemical oxidation, ozonation and ultrasonic oxidation [73]. A common point for these AOPs is their reliance on mostly hydroxyl radicals to perform the oxidation.

### 3.2.2 Detection of radicals

As radicals are very reactive, their detection is normally done indirectly through probes. A probe will chemically change when the radical reacts with it, producing a stable product that is measurable. One such method is HPLC, where a probe such as benzoic acid reacts with  $\text{OH}\cdot$  to produce ortho, meta and para variants of hydroxybenzoic acid which may be separated and analyzed by high-pressure liquid chromatography (HPLC) and UV-vis spectroscopy [74, 75].

### 3.2.3 Bursting method

To release the energy contained in the nanobubble, a dynamic stimulus is needed [76]. Different methods have been tested in literature including ultrasonication, UV and reducing the zeta-potential.

#### Ultrasonication

Ultrasound can be used to burst NB's, as when a strong ultrasonic wave irradiates water, tiny gas bubbles will appear and collapse violently known as acoustic cavitation. The speed of the collapse is limited by the speed of sound in water. The temperature increases many fold upwards to ca. 3000-5000K where radicals are formed by decomposing water vapour and noncondensable gases inside the bubble [51, 77].

#### UV

UV has been shown to have synergistic effects when during photo-degradation which is theorized to be caused by the consumption of oxygen in solution improved the bursting/collapse of the NB's [78–80]. As UV is known to create radicals from  $H_2O$ , this can lead to consumption of  $O_2$ , for example through a reaction with a carbon-centered radical as in equation 3.5, the product of the reaction is an unstable intermediate that will react further towards mineralization of the compound [79].



#### pH

One of the stabilizers of NB is the zeta potential. As such one method of bursting the NB is by neutralizing it by changing the pH of the solution [48]. This moves the solution to the isoelectric point where the electrical double layer becomes filled with ions of opposite charge. If the primary surface ion is an acid or base, like  $OH^-$ , the opposite charged acid/base will react and therefore reduce the surface charge. This method depends on which ions are present in the solution as each ion has its separate isoelectric point.

The neutralization also leads to an increased coalescence rate and an increase in the size of NB [39]. The isoelectric point for both  $O_2$  and air NB is around pH 4 [81, 82]. Where  $CO_2$  NB has an isoelectric point around pH 6 [83].

### 3.2.4 Influence of gas on radical formation

The type of gas influences what kind of radicals can be produced, as well as other properties, like size and surface properties. The primary radicals produced from  $O_2$  include:  $O_2^{\cdot -}$ ,  $^1O_2$ ,  $\cdot OH$  and  $HO_2 \cdot$ . Collectively called reactive oxygen species (ROS) [60]. Other gasses have different radicals, for instance,  $CO_2$  has  $CO_2^{\cdot -}$  amongst other carbon-containing radicals.

The reactivity between radicals differs depending on several factors. Hydroxyl radicals are highly reactive with a redox-potential vs. normal hydrogen electrode (NHE) of 2.7V in acidic solution, and 1.8 V in neutral solution [84]. It reacts like an electrophile, extracting hydrogen atoms, adding to  $\pi$ -systems and doing electron transfer reactions [79]. The superoxide,  $O_2^{\cdot -}$ , reacts as a nucleophile, and has a redox potential of -0.33 V, with very different rate constants depending on the substrate [84–86].

Organic-based radicals, (carbon-containing), will yield peroxy radicals from reacting with  $O_2$ . These will further begin a cascade of different oxidation reactions, leading to mineralization of the compounds [87, 88].

The gas also impacts what analysis methods are available, for instance, the dissolved oxygen (DO)-meter is not capable of measuring the amount of dissolved  $CO_2$ . Methods are available for  $CO_2$ , as there is a difference between the gaseous and dissolved state in the IR-spectrum [89–91]. As  $CO_2$  forms an acid when dissolved in water, titration is possible [92].

### **3.3 Analysis methods**

#### **3.3.1 Measuring gas content**

There are different methods for measuring the gas content of a solution.

Depending on the gas, different methods are available.

For oxygen, a colourimetric method is available called the Winkler method, as well as spectroscopic methods.

##### **Winkler method**

The Winkler method measures the dissolved oxygen content in water by titration [93]. The method is described further in **appendix 9**.

##### **Dissolved oxygen meter (DO-meter)**

To measure the DO content optical DO-meters were used. Optical DO meters have a fluorescent dye that can be excited by blue light, this dye emits red light in a short period after it has been excited [94]. Instead of emitting red light, it is also possible for the dye to excite oxygen molecules and therefore when oxygen is present the lifetime of the signal will be shorter and the intensity will be lower [95].

##### **FTIR**

For  $CO_2$  there is a difference in the IR-spectra between dissolved and gaseous  $CO_2$ , making it possible to differentiate between them [90, 91].

#### **3.3.2 Analysis of bubbles**

The NB are analyzed on their defining features, namely size and charge.

##### **Dynamic light scattering**

Dynamic light scattering (DLS) is a spectroscopy method used for determining the size of particles in a suspension. The method uses the scattering of light by the particles and how it fluctuates, to determine the size of the particles by observing a change in the intensity of the scattered light over time. This change in intensity can be correlated to size by observing how fast the particle moves. As smaller particles diffuse faster, they will create a faster change in intensity than larger particles, which diffuse slower. DLS measures the hydrodynamic diameter of particles, which is the diameter of a sphere with the same diffusion coefficient as the particle, as calculated by the Stokes-Einstein equation [96, 97].

$$D = \frac{k_B T}{3\pi\eta d_H} \quad (3.6)$$

Where  $D$  is the diffusion constant,  $k_b$  is Boltzmann's constant,  $T$  is the absolute temperature in kelvin,  $\eta$  is the viscosity of the liquid and  $d_H$  is the hydrodynamic diameter. The diffusion coefficient is found from the rate at which the intensity of the scattered light changes with the help of a correlation function[96, 97].

### **Zeta-potential**

The zeta potential of a particle is typically measured with electrophoretic light scattering (ELS). ELS uses the movement of a charged colloidal particle in a liquid under an electric field to determine the zeta potential of the particle [98, 99]. The speed of the particles is determined with laser Doppler velocimetry where the laser is split into two beams [100]. One is sent through the sample where it scatters off the particles and undergoes a Doppler shift. The Doppler-shifted light is then combined with the other laser beam and is sent to a detector where a difference in intensity over time is measured. The intensity fluctuations at the detector arise from constructive and destructive interference between the Doppler shifted and the non-Doppler shifted light [98–100]. The Doppler shift is converted to a speed and the zeta potential is calculated with **equation 3.3**.

# Chapter 4

## Experimental considerations

### 4.1 CO<sub>2</sub> Measurements

#### 4.1.1 CO<sub>2</sub> titration

Two methods were tested for the determination of concentration of CO<sub>2</sub>, namely titration and FTIR. Titration works by the reaction of CO<sub>2</sub> in water, where it turns into H<sub>2</sub>CO<sub>3</sub> and lowers the pH as can be seen on **reaction mechanism 4.1**. The concentration of H<sub>2</sub>CO<sub>3</sub> could be determined by titration. The method is adapted from [92].



Titration was tested as a viable analysis method on batch 9, the results of which can be seen on **table 4.1**. A couple of drops of a phenolphthalein solution was added to the sample, hereafter titrated with a 0.02 M solution of NaOH.

Some titrated amounts seemed unstable after repeating the titration, indicating that the equilibrium reaction between H<sub>2</sub>CO<sub>3</sub> and CO<sub>2</sub> had not stabilized. If the samples were obtained after the equilibrium had stabilized, the concentration of CO<sub>2</sub> would have differed from the actual values, as the gas in solution would not be in equilibrium with the atmosphere. The solutions that had been exposed to the different degradation mechanisms contain benzoic acid, which influences the result. The concentration of the benzoic acid corresponds to a large part of the titrated amount which can be seen on **table 4.1**. Some of the blank samples (with benzoic acid but without NB) needed a larger amount of the 0.02M NaOH solution than the samples exposed to NB and a degradation method.

As a large part of the titrated solution accounts for benzoic acid, and not the CO<sub>2</sub> in solution, along with the instability of the equilibrium, it was decided that determination of CO<sub>2</sub> concentration by titration would be too unreliable.

**Table 4.1:** The titrated amount of NaOH for the first batch of CO<sub>2</sub> along with the theoretical amount needed to neutralize 25 mL 5 mM benzoic acid

	0.02M NaOH [mL]
NB	4,6520
Ultrasound	7,015
Acid	8,387
UV	6,95
Blank	7,953
5 mM benzoic acid	6,25



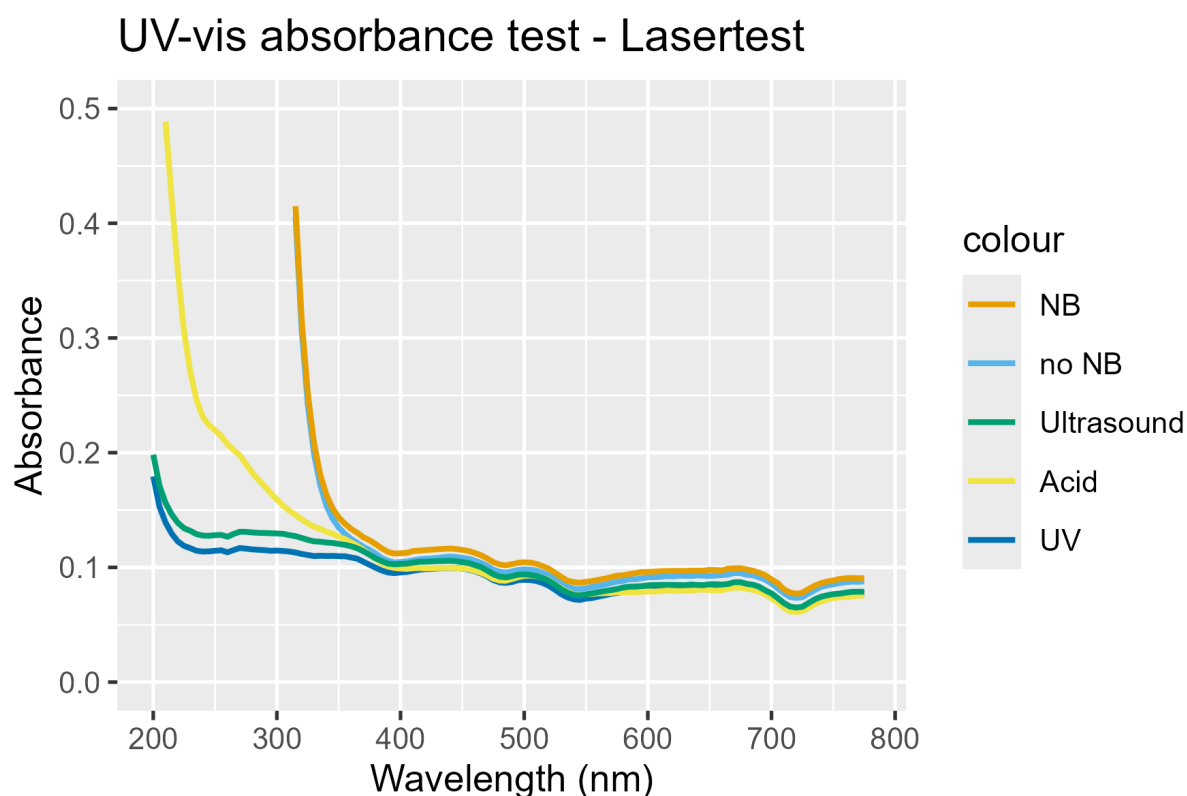


**Figure 4.1:** UV-vis test of air NB in 5 states: NB, No NB, Ultrasound, Acid and UV.

## FTIR

To supplement the determination of the concentration of  $\text{CO}_2$  in water, FTIR spectroscopy was tested [91]. The spectra were recorded by attenuated total reflectance (ATR) technique, using a Brüker Tensor II platinum ATR with a diamond as the ATR crystal. The range recorded was ( $400 - 4000\text{cm}^{-1}$ ) with a resolution of  $2\text{ cm}^{-1}$  and 64 scans.

The measurements were performed by placing a sample droplet on the ATR crystal and measuring the spectra. The ATR crystal was cleaned with ethanol between each sample.

It proved difficult to determine the concentration due to several reasons. These include water's high IR absorption and that the spectra of both dissolved and gaseous  $\text{CO}_2$  overlap, although they should be discernible due to their different shapes. Dissolved  $\text{CO}_2$  has a single band around  $2340\text{ cm}^{-1}$  and gaseous  $\text{CO}_2$  has a broad double peak from approx.  $2300$  to  $2380\text{ cm}^{-1}$  [101]. The overlap along with the low concentration of the  $\text{CO}_2$  made it difficult to determine the concentration.

## 4.2 Lasertest

### 4.2.1 UV-vis

The Tyndall effect is characteristic of colloidal suspensions and is the scattering of light by colloids. As the Tyndall effect was visible when the laser beam was pointed through the NB water it was theorized that a difference might be observed in UV-vis spectroscopy.

As can be seen on 4.1, there is no significant difference between NB and no NB. The difference between NB, no NB and the other samples is explained by the switch to a quartz cuvette instead

of a plastic. The difference between Acid and UV/Ultrasound is explained by the acid or the added dye which is present in the acid.

## **4.3 DLS and Zeta measurement**

### **4.3.1 DLS**

In this project, a Zetasizer nano ZS was used to measure the size distribution of the NB [100]. Some considerations must be taken when using the machine. In preparation for a sample, considerations must be taken regarding the concentration, with too high concentrations leading to light being scattered multiple times and too low concentrations leading to not enough light being scattered. Furthermore, high concentrations lead to particle interactions which should be avoided, as they may interfere with the scattering path.

Low concentrations may also lead to signal fluctuations that are not accounted for and should be avoided. The recommended minimum number of particles (i.e. the concentration) is 1000 [100].

Sample liquids used to dilute a sample should be filtered, to remove impurities, as they may interfere or distort the measurement leading to erratic or unreadable data.

It is recommended that samples themselves are not filtered, as filters may remove samples by absorption or size exclusion[100]. However, if larger particles are present, and a rough estimate of the sample size is known, it can be filtered to improve data quality. This isn't possible with NB as they exist in an equilibrium of multiple sizes, that may also filter out NB.

When measuring size, the zetasizer has two detectors it can use to detect the scattered light, namely front scatter and back scatter with each their advantages and disadvantages.

Backscatter was chosen as it has been used and tested against front scatter in the literature for NB [81, 102].

### **4.3.2 Zeta**

The zeta potential also uses a laser in the measurement. It is affected by some of the same factors, like the optical properties of the particles, the particle size and the polydispersity of the particle size distribution.

The minimum concentration is dependent on the relative refractive index between the medium and the particle. If the relative refractive index becomes lower, the minimum concentrations will be higher [100]. Furthermore, larger particles scatter more light and lower concentrations can be measured.

As the scattered light is detected in a forward angle with a zeta potential measurement, the concentration has a greater effect on the incident beam, as it must travel through the entire sample and is thus attenuated. To compensate, the attenuator position can be adjusted between 11 different positions from 100 % intensity to 0.0003 % [100].

As the maximum and minimum concentrations are dependent on sample-specific conditions, ultimately they must be determined experimentally.

To determine if the sample is clean of impurities, like dust or other things, the count rate can be analyzed.

If the count rate, measured in kilo counts per second (kcps), is relatively stable, it indicates no problems. Sharp peaks indicate dust in the sample, the sharp peak containing data will automatically be removed unless all measurements contain spikes. A drifting count rate indi-

cates a thermal gradient, while an increasing/decreasing count rate indicates an aggregating or sedimenting sample.

The kcps indicates the concentration of colloids but isn't directly proportional as multiple factors affect the count like size and attenuator position [100].

## 4.4 Radical formation & OMP breakdown

Benzoic acid was chosen as a radical probe because the reaction between it and the  $\text{OH}\cdot$  radical is well understood [74, 75]. Benzoic acid reacts with  $\text{OH}\cdot$  and forms ortho, meta and para hydroxybenzoic acid with a slight preference for ortho. The distribution between ortho, meta and para is 36%, 34% and 30% respectively [74]. The isomers of hydroxybenzoic acid all have a different absorption and retention time with HPLC than benzoic acid and it is therefore possible to determine the fall in concentration of the benzoic acid using HPLC. However, with  $\text{CO}_2$  as mentioned in section 4.1 benzoic acid influences the titration results for determining the gas concentration.

## 4.5 Transport of OMP

One of the problems with OMP is the low concentration in wastewater, making their removal/detection difficult. Furthermore, many OMP are hydrophobic, making them difficult to dissolve in water.

As mentioned in **chapter 3.1**, NB collects hydrophobic matter. This collection combined with the Brownian motion distributing NB in the solution could concentrate the OMP on the surface of the NB, while increasing the size.

The membrane should retain the NB, which otherwise would allow the OMP to pass through without trouble.

The low solubility in water complicates detection, as many detection methods rely on the matter being dissolved. This was also observed with two of the tested OMP, as HPLC didn't detect them in NB water.

# Chapter 5

## Methods

### 5.1 Initial generation of NBs

To ensure a uniform and sufficient ionic strength to stabilise the NBs, a standardized salt solution was added to demineralised water. BOD consists of 126 mM  $\text{CaCl}_2$ , 0.9 mM  $\text{FeCl}_3$  85 mM  $\text{MgSO}_4$  and a 0.1 M phosphate buffer solution. 1 mL of each solution was added per litre of demineralised water.

Hereafter the solution was run through NB generator setup as seen on **figure 5.1**. to ensure comparability, the following parameters were kept the same: Gas flow into setup at 5 L/min. Pressure in the generator chamber at >0.2 MPa runtime at 15 min. The flowrate was kept somewhat consistent due to its dependency of the pressure in the chamber, with the rate itself being 13-15 L/min.

The experimental setup consists of a Foras PE50F pump (1), a 30L barrel with an outlet at the bottom (2), the NB generating module (JBL10G5 from asuplus nanobubble technology) (3) with a pressure gauge (4), an SM8400 Magnetic-inductive flow meter from IFM electronic (5), a LZT-08A02M-V 1-10LPM gas flowmeter (6) and a pressure gauge on the gas outlet (7). The setup is illustrated in 5.1.

13 batches were produced in total. batches 2-11 for the OMP breakdown experiment, 12-14 for the lasertest and 15 for the mass transfer experiment.

Batch 2, 3 and 4.5 were made with  $\text{O}_2$ , batch 5, 6 and 7 with air and 9, 10 and 11 with  $\text{CO}_2$ .

Similarly batch 12 was made with air, batch 13 with  $\text{CO}_2$  and 14 with  $\text{O}_2$ .

Batch 15 was made with  $\text{O}_2$ .

### 5.2 DLS & Zeta

Both the size and the zeta potential were measured on a Zetasizer nano ZS.

The sample preparation for both is the same, with the only difference being the volume of sample.

Before the measurements, the cuvette was rinsed with milli-q water, that had been filtered through a 0.2  $\mu\text{m}$  regenerated cellulose filter, 2-3 times to remove particles from the cuvette that could interfere with the measurements.

The cuvette for size measurement was filled, while for zeta potential it was filled to 1/3 to make space for the dip cell necessary for zeta potential measurement.

#### 5.2.1 DLS

The size of the nanobubbles was measured with dynamic light scattering (DLS).

All samples were run with backscatter per the literature as discussed in 4.3. The measurement is dependent on the relative reflective index between the water and the sample itself. The  $\text{O}_2$

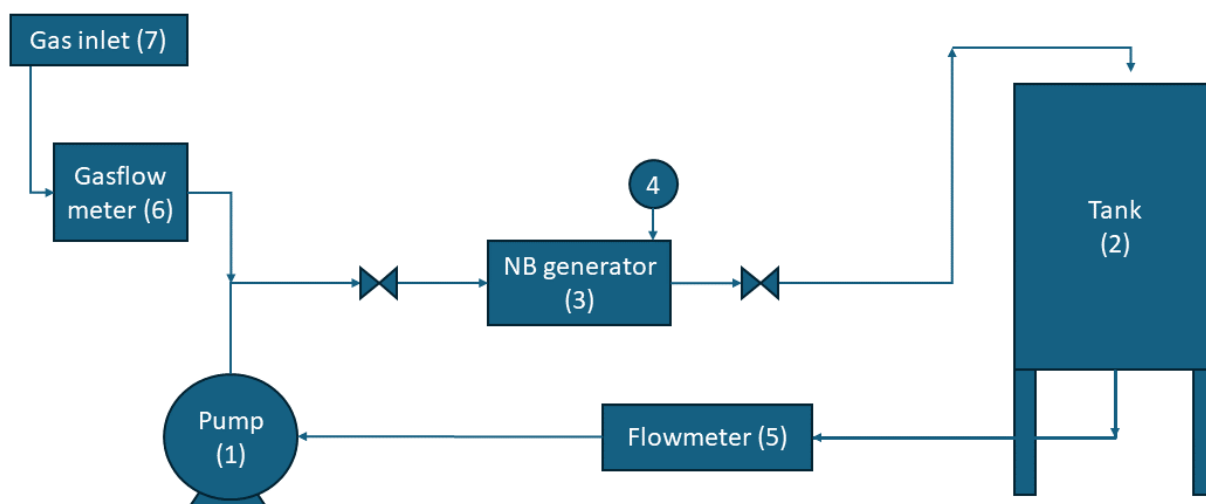


**Figure 5.1:** Illustration of the setup used to produce a NB solution. The setup is designed to run in batches. Own production.

and air batches were run with a reflective index of 1 and absorption of 0.001, while CO<sub>2</sub> had a reflective index of 1.004 and an absorption of 0.025.

### 5.2.2 Zeta

The zeta potential was measured with the standard settings. The relative refractive index and absorption were the same as for size measurement for each gas.

## 5.3 DO measurements

### 5.3.1 Optical DO meter

The dissolved oxygen meter (Loligo Systems Witrox 4) was calibrated by a two-point calibration. A solution with 100 % DO was obtained by bubbling compressed air into a beaker with demineralised water for 15 min. A 0 % solution was obtained by dissolving 10 g Na<sub>2</sub>SO<sub>3</sub> in 500 mL demineralised water. The DO meter was then calibrated with the two solutions. The measurements were performed by inserting the DO probes into the solution and waiting for the probes to reach a steady state. The DO % was then noted.

The DO measurements for batch 5 acid, ultrasound and UV along with batch 6 and 7 NB was measured with a wtw multi 3430 DO meter.

### 5.3.2 Winkler method

Other methods of determining the concentration of DO are available, such as the Winkler method [103]. Several solutions were prepared for the Winkler method as described in 9.

### Measurement of O<sub>2</sub> content

To determine the DO concentration a sample is first added carefully to a Winkler bottle to avoid the introduction of air to the sample. When the Winkler bottle is full, 250 µL MnCl<sub>3</sub> solution is added to the bottle followed by 250 µL NaI and NaOH solution. The bottle is sealed with

a stopper and mixed by carefully flipping the bottle a few times. The stopper was removed and 250  $\mu\text{L}$  concentrated sulfuric acid ( $\text{H}_2\text{SO}_4$ ) was added and the bottle was sealed again and flipped a few times. Then 50 mL of the solution was transferred to a beaker and titrated with the thiosulfate ( $\text{Na}_2\text{S}_2\text{O}_3$ ) solution from which the  $\text{O}_2$  concentration was determined.

## 5.4 Radical generation & breakdown of OMP

A standard solution of 20 mM benzoic acid was prepared which was diluted to 5 mM with either different NB solutions or demineralized water. For each batch, seven solutions were prepared. For each degradation method, two samples were prepared, one with NB and one without.

- one blank without NB which was not exposed to a degradation method.
- Exposed to ultrasound (Branson 3210) at 40 kHz for 45 min.
- Exposed to a Vilber Lourmat VL-4.LC UV lamp (254 nm) at 4W for 24 hours
- Exposed to an adjusted pH of 4 for 24 hours.

### 5.4.1 HPLC

To determine the degradation, the samples were prepared for HPLC by adding 10mM phosphoric acid  $\text{H}_3\text{PO}_4$  to ensure the benzoic acid was in its acid form [104]. Each sample was then filtered through a 0.2  $\mu\text{m}$  filter to remove impurities and any leftover NB from the sample.

The samples were tested on an HPLC with a C18 column with a mobile phase of 50% methanol and 50% water and a flowrate of 1 mL/min.

Data was collected at 227 nm [104].

Furthermore, size and zeta potential were measured afterwards.

## 5.5 Saturation of surface

A solution of Sodium dodecyl sulfate (SDS) 0.4 g/L was diluted with an NB solution to 40, 80, 120, 160 and 200  $\mu\text{g/L}$ . The solutions were left for 24 hours hereafter the size and the zeta-potential were measured.

## 5.6 Mass transfer experiment

The experiment was performed on four different compounds BPA, atrazin, diclofenac and estradiol. A standard solution was prepared for each of the four compounds by dissolving it in one litre of demineralized water the amount that was weighed can be seen in table 5.1.

Compound	Weighed [mg]
BPA	3.6
Atrazine	5.0
Diclofenac	2.0
Estradiol	3.2

**Table 5.1:** The weight of each compound dissolved in 1 L water.

The membranes (Sterlitech microdyn nadir flatsheet membrane NP010, PES, NF) were prepared by running Milli-Q water through them for half an hour.

The solutions with OMP were prepared approximately five minutes before the start of the filtration, by diluting 100 mL of the standard solution to 250 mL with either demineralised water or NB water. Thereafter the experiments were performed for each compound.

First 250 mL sample was added to the filtration cell (Sterlitech HP4750) and the cell was run with a gas pressure of 6 bar. The filtrated water was collected and weighed as it came through. The filtration was stopped when 10 g filtrate was collected corresponding to approximately 10 mL of retentate. This was repeated for each sample in the order: milliQ water, water with OMP, NB water and NB water with OMP. The membrane was changed between each OMP.

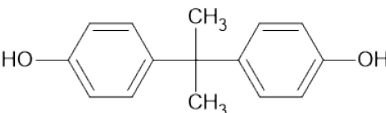
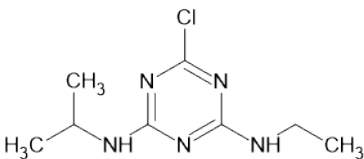
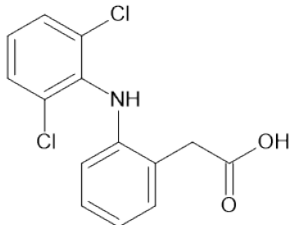
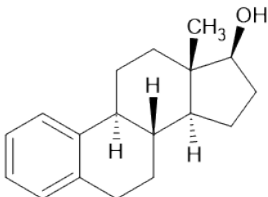
#### 5.6.1 pH & conductivity

To help determine the retention rate of the OMP, both conductivity and pH were measured. A S47 SevenMulti dual meter pH/conductivity from Mettler Toledo was used. A measurement was taken for each sample before filtration and in both the retentate and the permeate.

#### 5.6.2 HPLC

To determine the retention rate of the OMP, HPLC was performed. A standard row was prepared for each OMP, described in **table 5.2**, by diluting the standard solution by adding 5, 2.5, 1.25 and 0.625 mL respectively to a 10 mL volumetric flask and filling it to the line with demineralised water.

The samples from the membrane experiment and the standard rows were prepared by filtering them through a 0.45 µm regenerated cellulose filter into an HPLC vial. All samples were run through a C18 column. The settings used for each compound are described in **table 5.2**.

Compound	Mixture ratio	Flow rate	Wavelength	Structure
BPA	50% MeOH 50% water [105]	0.5 mL/min	224 nm	
Atrazine	60% MeOH 40% water [106]	1 mL/min	230 nm	
Diclofenac	60% MeOH 40% water [107]	1 mL/min	282 nm	
Estradiol	70% MeOH 30% water [108]	1 mL/min	280 nm	

**Table 5.2:** The settings used for HPLC and the structure of each compound.



# Chapter 6

## Results & Discussion

### 6.1 Characterization

#### 6.1.1 Size and zeta-potential

Before any attempt at making radicals or OMP breakdown, the NB solutions were analyzed by size, zeta potential and (if possible) gas content. The size of NB is affected by many different processes, and thus their size may not always be uniform. This can be seen on the polydispersity index (PDI), which goes from 0-1, where values above 0.4 are classified as polydisperse. The general tendency for all samples measured shows a PDI generally above 0.4 and often near 1 as well. Furthermore, size measurement only gives the size distribution and the % of total intensity and not the concentration of NB. Multiple peaks may arise as the NB aren't uniform, which can be seen on **figure 6.1**.

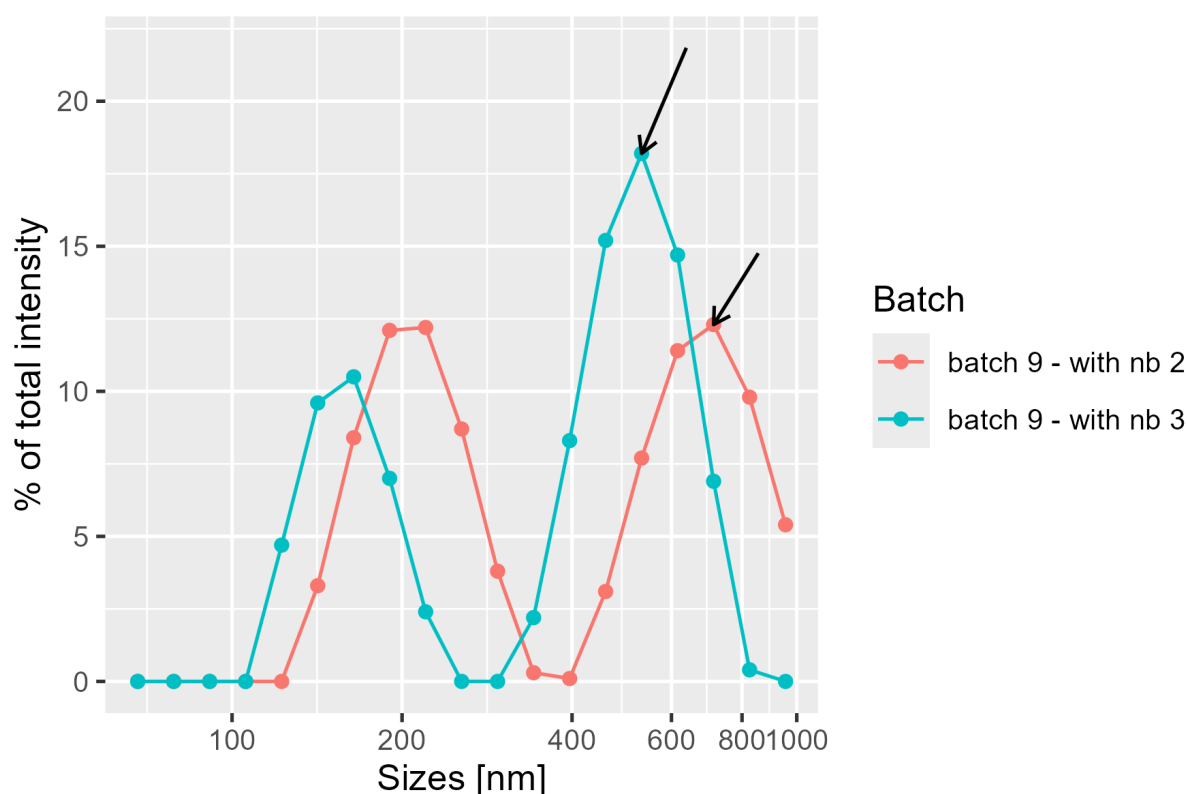


**Figure 6.1:** The selection of peaks to represent the size of 1 of 10 runs. The black arrows point to the points with the highest % of total intensity, which is chosen for each measurement. The X-axis is logarithmic and shows the data points equally spaced out.

The zetasizer outputs data for both size and zeta potential in specific steps between data points.

For size measurement, the step size increases with larger sizes.

This makes it difficult to find the area under the curve where the majority of the NB should be seen.

If the sample contains impurities or dust, it is discarded, and a new sample is taken and tested. Particles that fall in between size data points will get lumped together into the data points, skewing the data more for bigger sizes compared to smaller sizes.

Thus, to determine the size of a sample, the highest peak % of total intensity is found and the corresponding size is chosen to represent the sample as seen on **figure 6.1**.

As NBs are easily affected by many local conditions, as described in **section 3.1.1**, outliers are removed from the data, which is if they are 1.5 times above or below Q3 or Q1. The remaining values are filtered such that only sizes within the definition of NB (ie. <1000 nm) are kept. The mean and standard deviation are then found with the remaining data.

The zeta potential also has some of the same considerations as when looking at size, as the measurement also relies on the same principles. The zeta potential does not suffer the same problems regarding the multiple peaks unless the sample itself is contaminated. The stepsize for the zeta potential is around 4-5 mV. The same method is applied where the highest peak is chosen to represent the whole sample, the outliers are removed and the mean and standard deviation are found.

A further consideration for the measurement of zeta potential is when a sample is diluted. The ionic strength of a sample affects the zeta potential of a sample and should be kept constant if diluted, to not affect the double layer of the NB [109].

## Radical generation & breakdown of OMP

To characterize the NB and the effect of bursting methods, the size and zeta potential were recorded of the starting solution without NB, with NB and after each bursting method. The results in **table 6.1**, show the average of both the size and zeta potential and the standard deviation.

**Size** The no NB measurements are not expected to follow any tendency found in NB samples, as they shouldn't contain NB. This can partially be seen by the kcps values listed in **appendix 13**. Presence of colloids/NB is not determinable from the size distribution, as it doesn't show the concentration. The kcps is affected by the concentration of particles as well as other parameters like size. Thus the value gives an indication of the concentration of colloids, but not a direct comparison. In theory, if no other impurities are present, this will give an indication of the range of concentration. As many different sources of contamination are possible, this claim is not possible to make.

The results of the size measurement from the radical generation & OMP breakdown experiment can be seen on **figure 6.2 & table 6.1**.

The general expectation of all gases and bursting methods is an increase in size and a decrease in kcps, as NB lose their stabilization from zeta potential. As the stabilization is removed, the NB will coalesce together into larger NB or dissolve into the solution. Thus the size should increase and the kcps should be trending downwards. The ultrasound shouldn't show the exact same evolution but should have a bigger variance as both creation of NB of a certain size as well as coalescence of present NB into larger ones occur. A larger kcps should also be expected from the ultrasound.

**Table 6.1:** Size and zeta potential of O<sub>2</sub>, Air and CO<sub>2</sub> with standard deviation. Results are from radical generation & breakdown of OMP. Numbers have been rounded to the nearest 10 for size, and to the nearest whole number for zeta potential, and standard deviations have been rounded to the nearest 10 for size and the nearest 5 for zeta potential. Some standard deviations are written as zero due to the large step size between data points.

		Size±std	zeta±std
O <sub>2</sub>	With NB	310 ± 120	−9 ± 10
	No NB	580 ± 370	−16 ± 5
	Acid	450 ± 100	−16 ± 5
	Ultrasound	430 ± 170	−9 ± 10
	UV	430 ± 60	−12 ± 5
Air	With NB	280 ± 130	−11 ± 0
	No NB	160 ± 40	−3 ± 5
	Acid	400 ± 150	−15 ± 5
	Ultrasound	480 ± 160	−16 ± 0
	UV	630 ± 190	−9 ± 5
CO <sub>2</sub>	With NB	220 ± 140	−10 ± 10
	No NB	510 ± 120	−10 ± 5
	Acid	270 ± 130	−24 ± 5
	Ultrasound	180 ± 130	−14 ± 5
	UV	400 ± 240	−11 ± 0

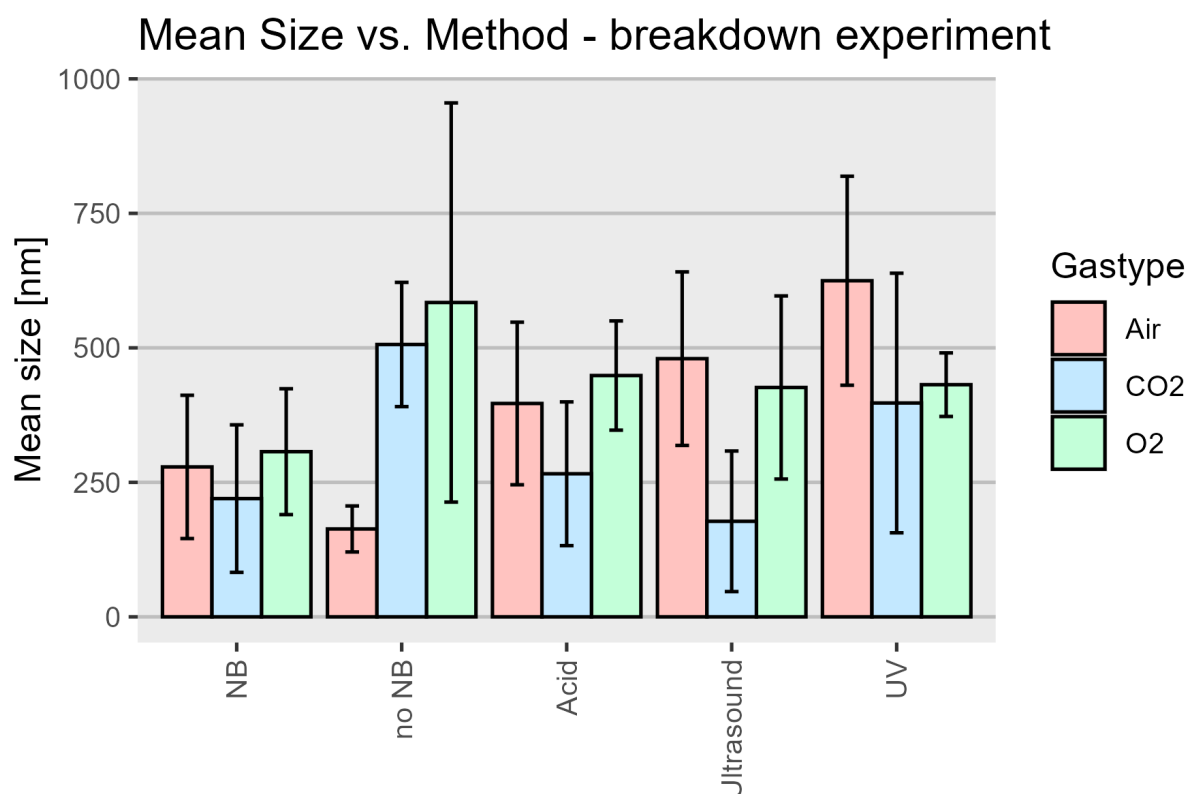


**Figure 6.2:** The mean size with standard deviation is shown per method for 3 gas types. Data from the radical generation & breakdown of OMP

All kcps values can be found in **appendix 13**.

In the **air** series, the sizes increase after each bursting method, with acid having the smallest

mean size, and UV having the largest mean size. The kcps values for the size decrease when comparing the methods to the NB sample as seen on **table 13.3**. The small size of the acid sample may be due to the increase of ions changing the ionic strength of the solution, and thus affecting the thickness of the double layer of the NB [109]. The standard deviations are stable throughout the air series except UV and no NB.

In the  $\text{CO}_2$  series, the bursting methods do not seem to have as clear an effect on the size of the NB as for air. The kcps values do show the expected tendency for all except ultrasound which shows an increase, as well as a single acid sample which also showed an increase in kcps. The ultrasound may be caused by  $\text{O}_2$  NB being more stable than  $\text{CO}_2$ .

The difference between NB and acid is only 40 nm, which may be explained by the equilibrium of  $\text{CO}_2$  in water making carbonic acid  $\text{H}_2\text{CO}_3$ , as well as the acid from the bursting method, both increase the concentration of electrolytes, thus affecting the surface even more compared to the other gas types. Ultrasound showed a decrease in size, which may be due to the equilibrium of  $\text{CO}_2(\text{aq})$  with  $\text{CO}_2(\text{atmosphere})$  and the mechanical stimulus from ultrasound. UV again showed the largest increase in the size of the methods. Furthermore, the standard deviations are quite similar for all the samples in the  $\text{CO}_2$  series except for UV. The large standard deviation along with the large size might indicate that UV have an effect on the  $\text{CO}_2$  NB.

Additionally, the  $\text{CO}_2$  showed a propensity to go out of solution and create large bubbles on the sides of the cuvettes when performing both size and zeta potential measurement, which further discredits the results for  $\text{CO}_2$ .

In the  $\text{O}_2$  series, all bursting methods showed a similar increase in size. This may indicate that the methods have no effect on the sizes for  $\text{O}_2$ . Only one batch shows the expected outcome of the kcps trending downward from the NB sample. The other batches either show an increase for all, and a decrease for ultrasound, or an increase for all. This could be due to contamination or another effect on the NB themselves.

The standard deviations remain when comparing the methods to the NB sample. Of note is the UV sample which has a lower standard deviation, which means the size is stable across batches, indicating that an effect is present from the UV.

When comparing across methods, only air and  $\text{O}_2$  show a tendency for increasing size, while  $\text{CO}_2$  doesn't show any clear tendency. Of note is ultrasound for  $\text{CO}_2$  showing a decrease in size.

The effect of pH on the size of  $\text{O}_2$  and air NB has been studied and it was found that a decrease in pH leads to an increase in size [81, 110]. That corresponds with the observations made in this study as both air and  $\text{O}_2$  show an increase in size when the pH is lowered.

**Zeta potential** The results of the zeta potential measurement from the **radical generation & OMP breakdown** experiment can be seen on **figure 6.3 & table 6.1**.

Some of the same considerations for samples without NB/colloids should be taken for zeta potential as for size measurement. The kcps gives a sort of range of concentration, but not a direct comparison nor exclusively from NB, as contaminants can easily be present and show the same zeta potential as the NB due to being exposed to the same treatments.

The general expectation of all gases and bursting methods is a decrease in zeta potential and a decrease in kcps, as NB lose their stabilization from zeta potential. As the stabilization is removed, the NB will coalesce together into larger NB or dissolve into the solution. Thus the size should increase and the kcps should be trending downwards. The ultrasound shouldn't

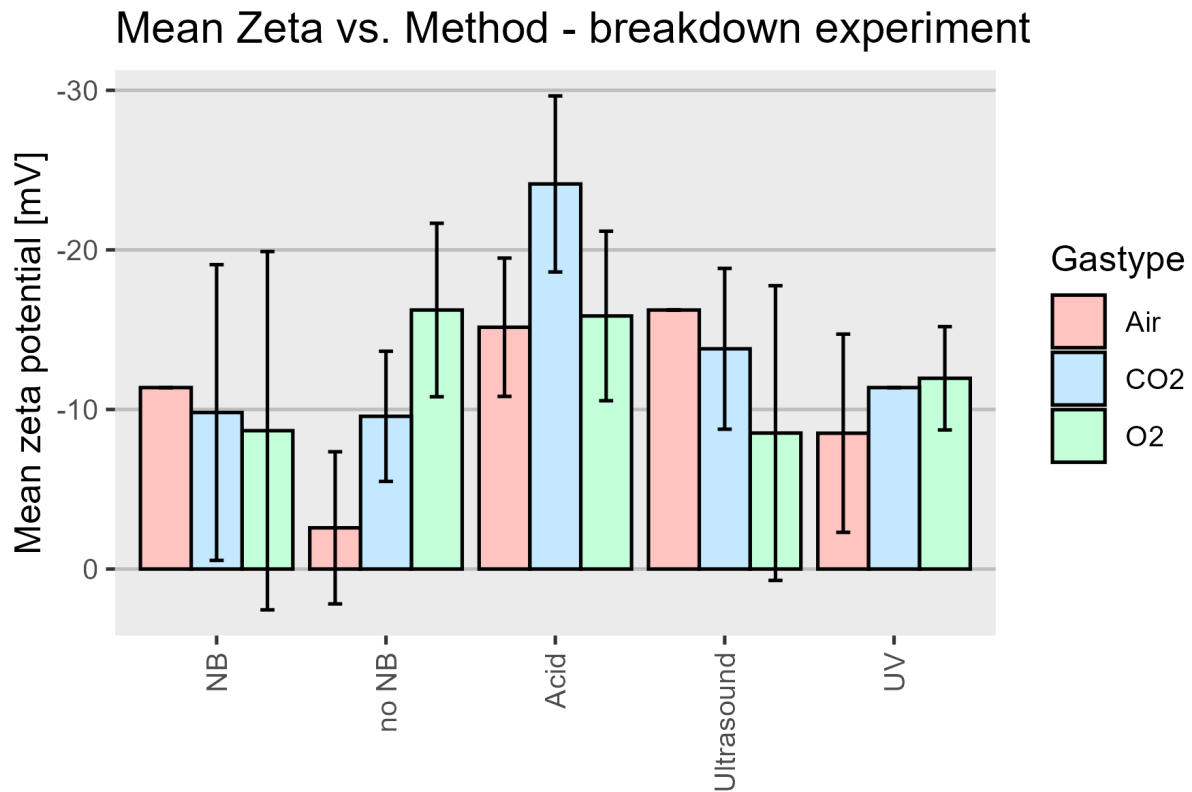


**Figure 6.3:** The mean zeta potential with standard deviation is shown per method for 3 gas types. The standard deviation for Air NB, Air Ultrasound and CO<sub>2</sub> UV is 0. This is due to the nature of the data as discussed at the beginning of the chapter.

show the exact same evolution, but should have a bigger variance as both creation of NB of a certain size as well as coalescence of present NB into larger ones occur.

In the **air** series, the zeta potential is more negative for acid and ultrasound when compared with NB. The UV sample shows a small decrease, indicating that the method may not have a significant effect. The effect from an increased electrolyte concentration may explain the larger negative zeta potential in the acid sample [109].

The NB and ultrasound samples have no standard deviation, due to the problem discussed at the beginning of the chapter.

In the **CO<sub>2</sub>** series, an increase in the value is seen for all bursting methods, with acid having the largest increase, which can be attributed to the effect of increasing the electrolyte concentration. Ultrasound and UV have similar zeta potentials, with UV being more uncertain due to the standard deviation problem discussed earlier. The samples may also have poor data quality, which is cooperated by the kcps values being above the recommended values for 1 of 3 ultrasound samples, and below the recommended threshold on 2 of 3 for UV.

In the **O<sub>2</sub>** series, acid and UV showed a more negative zeta potential than the NB sample, with ultrasound showing the same zeta potential as the NB sample. The NB sample showed a large standard deviation, indicating that the zeta potential is not stable, whereas the standard deviation for acid and UV indicates they are stabilized compared to NB. The kcps varies between 6-100, with the recommended minimum is 10 kcps. Furthermore, the no NB sample shows a similar zeta potential and standard deviation as acid. This may indicate that whatever is mea-

sured in the no NB is the same as in acid, meaning that NBs are not the dominating species, either due to removal or contamination.

The Zeta potential for the acid samples gets more negative or are around the same as other bursting methods. This is opposed to the findings in the literature where an increase in zeta potential is found when the pH is lowered [81, 83, 110, 111]. For CO<sub>2</sub> NB the isoelectric point is around pH 5.5-6 with a further decrease in pH leading to a positive zeta potential [83, 111]. For air and O<sub>2</sub> the isoelectric point is around pH 4-5 [81, 110, 111]. The measurements in the literature were performed with demineralized water and the pH was adjusted with HCl and NaOH. This means that the composition of the NB solution is different from the one used in this experiment, however, this doesn't explain the fact that the opposite effect of pH when compared to the literature.

In order to understand if there is a correlation between the size and zeta potential of the NB a comparison is made. A comparison between size and zeta potential is made on **figure 6.4, 6.5 & 6.6**.

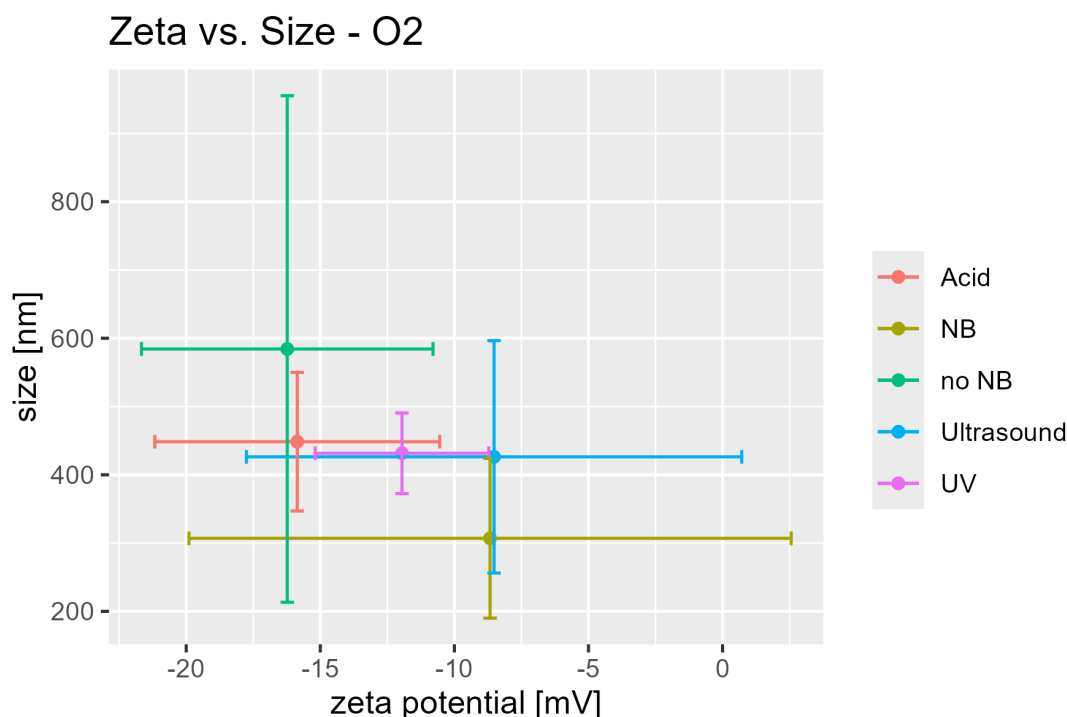


**Figure 6.4:** The mean size vs. the mean zeta potential for O<sub>2</sub> from the radical generation & OMP breakdown experiment.

No clear tendency is observed between the size and zeta potential for any of the gas types, indicating that any influence may be more of a complex character.

The only observed trend across gas types, is Acid giving a relatively stable zeta potential. This trend may indicate that the acid method affects the NB, making them more stable.

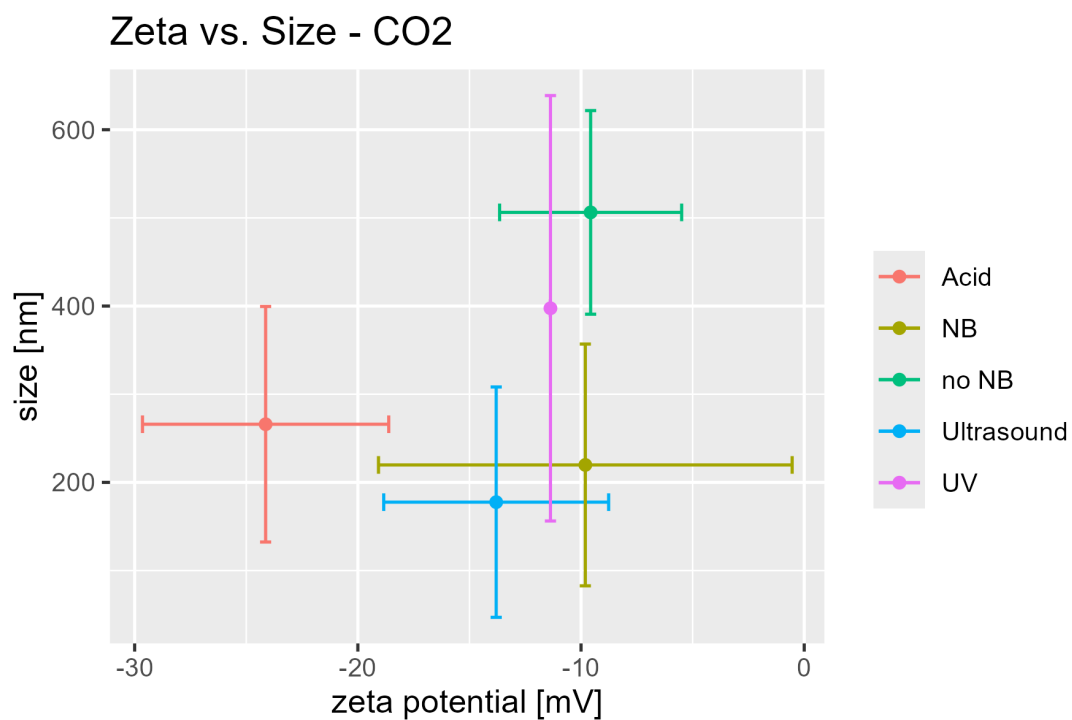


**Figure 6.5:** The mean size vs. the mean zeta potential for CO<sub>2</sub> from the radical generation & OMP breakdown experiment.

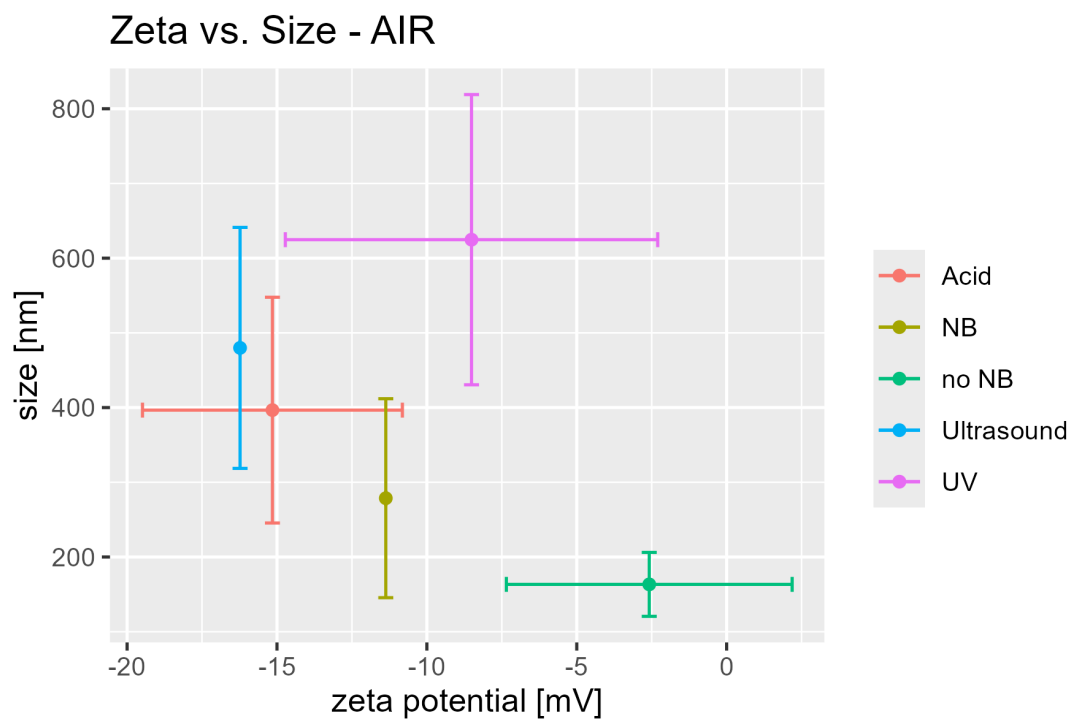


**Figure 6.6:** The mean size vs. the mean zeta potential for air from the radical generation & OMP breakdown experiment.

## Age experiment

As the NBs are affected by several different variables in equilibrium and yet are supposedly stable for long periods of time [39], the stability was tested over time by size measurement and zeta potential measurement. In the age experiment, the batch solutions of NB were analyzed by size and zeta potential over time. An overview of the age of each sample can be seen on **table 6.2**.

**Table 6.2:** The results of the age test are displayed, where the age is the number of days since the sample was produced. The size and zeta potential with standard deviation are also shown for each sample. Some standard deviations are written as zero due to the large step size between data points.

Air	Age [days]	16	23	30	58		
	Size [nm]	250 ± 60	220 ± 70	180 ± 30	390 ± 110		
	zeta potential [mV]	-15 ± 5	-15 ± 5	-15 ± 5	-15 ± 0		
CO <sub>2</sub>	Age [days]	1	5	12	19	47	
	Size [nm]	390 ± 90	460 ± 110	>1000	580 ± 200	170 ± 30	
	zeta potential [mV]	-15 ± 5	-10 ± 0	-5 ± 5	-10 ± 0	-25 ± 5	
O <sub>2</sub>	Age [days]	2	6	23	30	37	65
	Size [nm]	460 ± 140	390 ± 60	320 ± 110	350 ± 140	390 ± 30	400 ± 90
	zeta potential [mV]	-10 ± 15	-15 ± 0	-15 ± 0	-15 ± 0	-5 ± 0	-20 ± 5

The results from the size measurement of the age experiment can be seen in **figure 6.7**. The **Air**

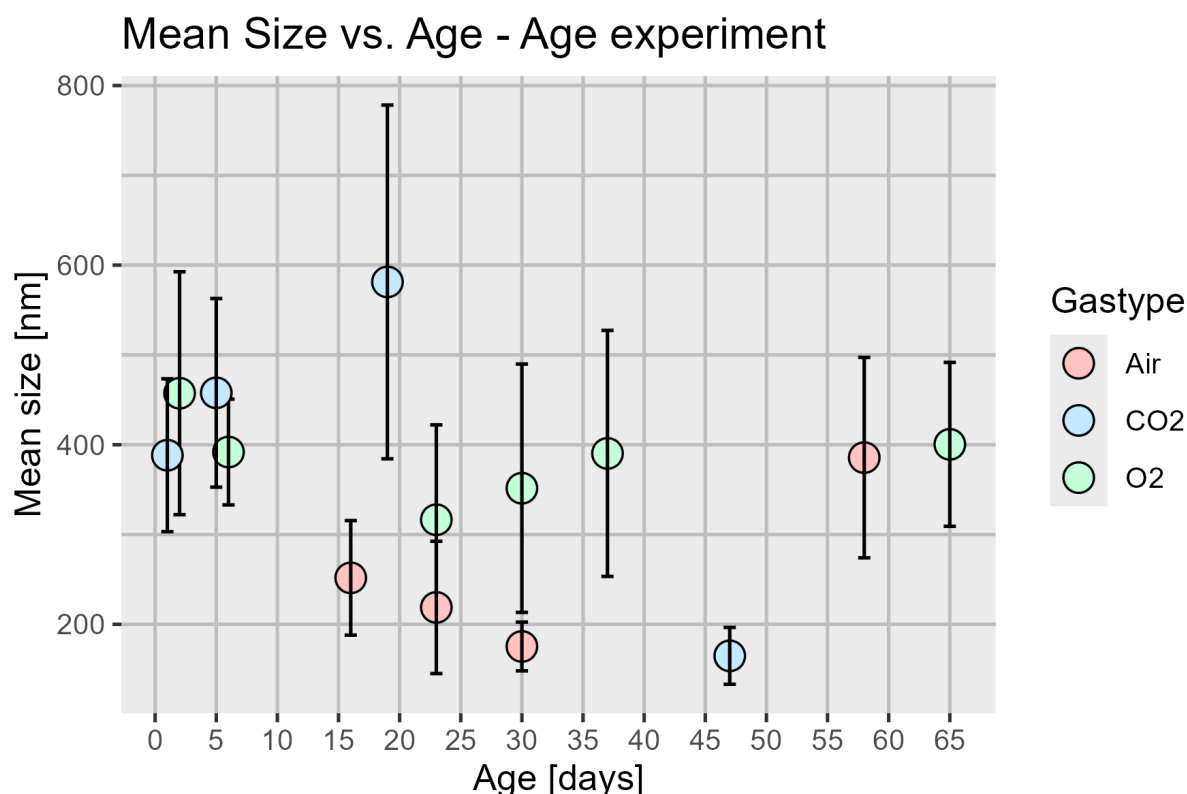


**Figure 6.7:** The mean size with standard deviation of the age experiment. The missing value for CO<sub>2</sub> at 12 days of age is due to the measurement being above 1000 nm, and is not considered as NB.

series shows a slight decrease in size to below 200 nm until day 30, and increases drastically



between day 30 and 58. The drastic change indicates either a coalescence of NBs into larger NBs, or that the sample contained dust or other impurities as suggested by the quality report which can be found in the supplementary data.

The  $\text{CO}_2$  series shows a slight upward trend between days 1 and 5 and seemingly goes out of solution between days 5 and 12, as sizes above the definition of NB are removed. This indicates that the lifetime of  $\text{CO}_2$  NB is short, compared with both  $\text{O}_2$  and air.

The  $\text{O}_2$  series shows a slight downward trend from day 2 to day 23 and stabilizes hereafter, indicating that the NB are relatively stable, compared with the other series.

The mean zeta potentials for the age experiments are shown on **figure 6.8**.

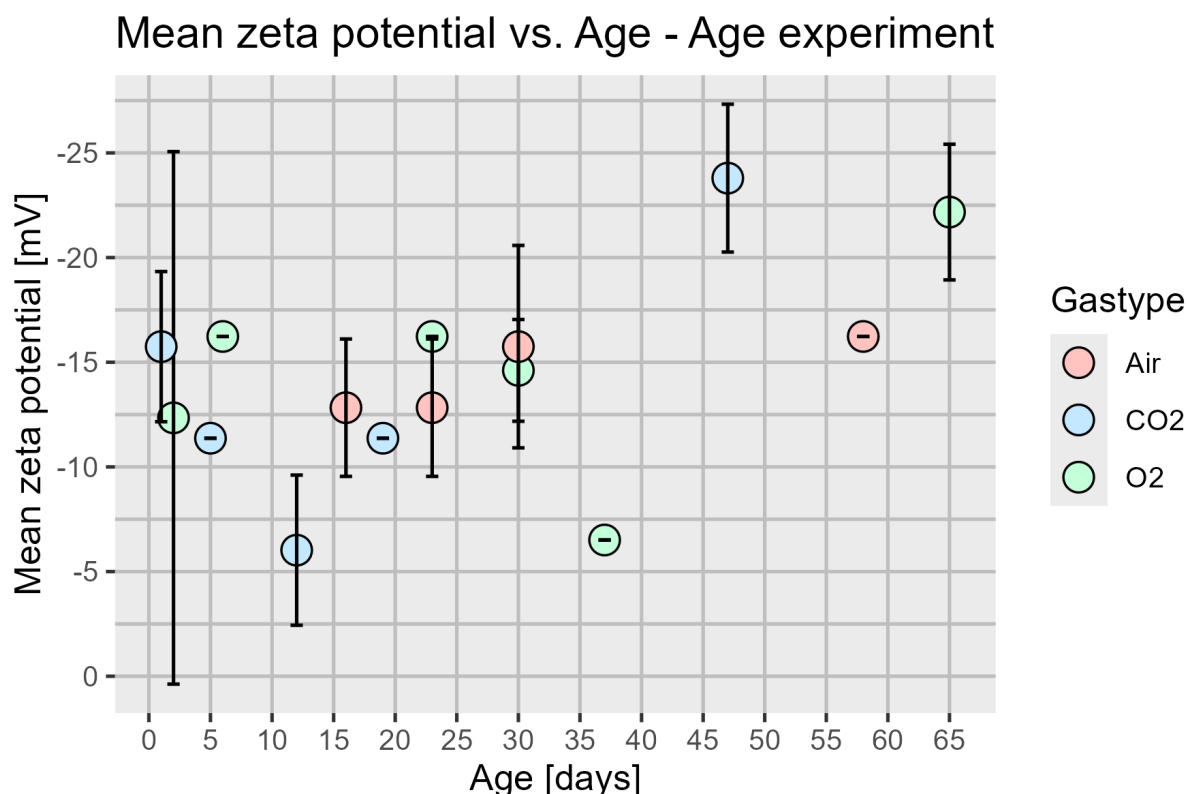


**Figure 6.8:** The mean zeta with standard deviation of the age experiment. The missing standard deviations are due to the nature of the data extracted from the Zetasizer as discussed in the beginning of this chapter.

The **Air** series is stable until between day 16 and day 23. Hereafter the zeta potential rises and remains stable between day 30 and day 58. The standard deviation for day 16 and day 23 are quit low and it increase a little to day 30 where it becomes 0 to day 58. this indicate that the zeta potential is stable for the tested period of 58 days.

The **CO<sub>2</sub>** series decreases from age 1-3. This aligns with the apparent disappearance of the NB in age 3 size. Hereafter it rises drastically through to age 5. The standard deviation is low for all days and for day 5 and 19 it is 0.

The **O<sub>2</sub>** series increases from day 1 to day 12 and stabilizes until day 30. Hereafter it varies wildly, indicating a change occurring between day 30-37 and day 37-65. Furthermore, the standard deviation here is 0, indicating a very homogeneous zeta potential.

A study on the effect of time on the stability of different gas type NB found that O<sub>2</sub> and air NB were stable for over 60 days in demineralised water and CO<sub>2</sub> NB was stable for 5 days [111]. This is in agreement with the findings from the age experiment performed in this experiment.

### Saturation of surface

A further method of bursting NBs was tested with the same experimental parameters as with the O<sub>2</sub> batches.

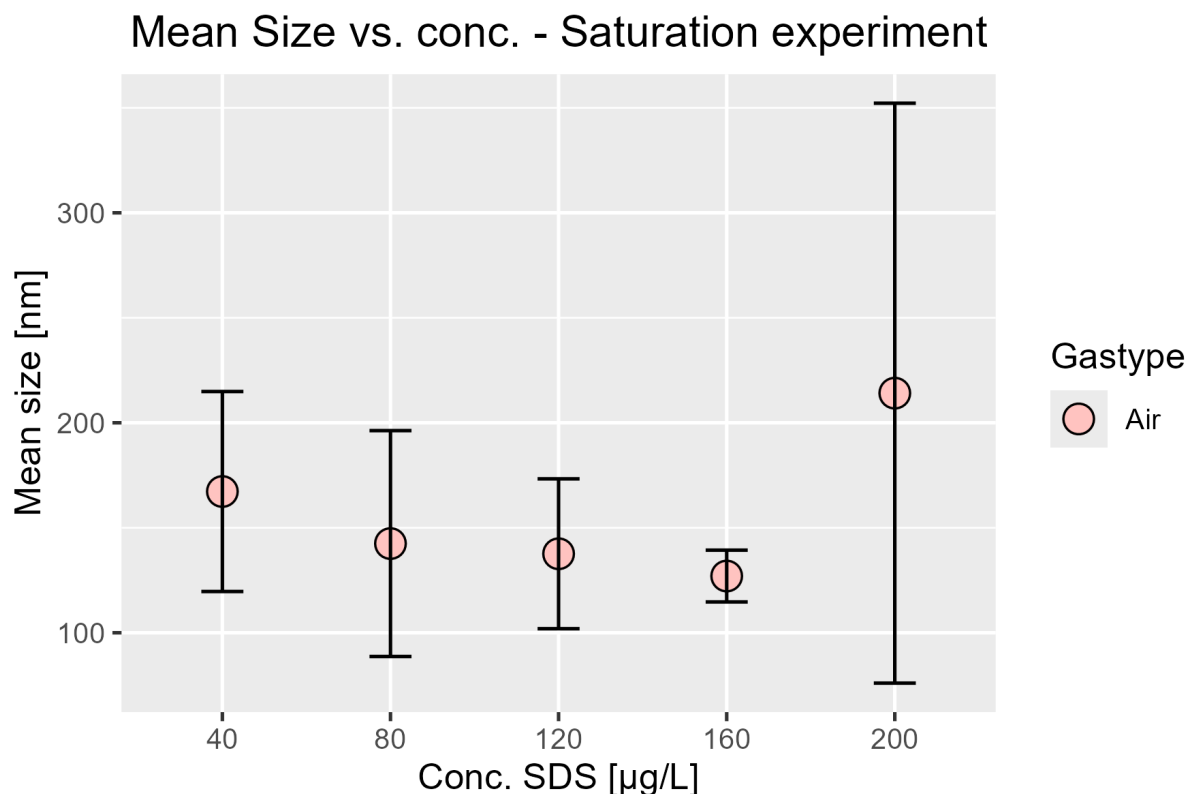


**Figure 6.9:** The mean size with standard deviation of the concentration in the saturation experiment.

The results of the saturation experiment are observed on **figure 6.9**. The addition of SDS affects the size of the NB, as a clear downward trend is visible from SDS NB 40-160 µg/L. Furthermore, the most stable sample is 160 µg/L as they have the smallest standard deviation of the samples with both NB and SDS.

160 µg/L shows a small standard deviation, indicating a homogeneous size. The kcps value of 19.5 indicates a low concentration of NB. The quality report, also showed that insufficient signal was collected to produce accurate results.

200 µg/L shows a large standard deviation and a large increase in size from 160 µg/L indicating that the stability from 160 µg/L is not present in 200 µg/L. The sizes of NB and 200 µg/L are similar, indicating that the NB are similarly polydisperse.

The mean zeta potentials for the saturation experiment is shown on **figure 6.10**.

The zeta potential of SDS NB 40-120 µg/L has a downward trend with 40 µg/L starting with a larger value compared with the NB sample. The standard deviation shows a somewhat stable zeta potential. 80 µg/L has a smaller negative zeta potential and a larger standard deviation, indicating that the NB may be more unstable due to the increasing concentration of

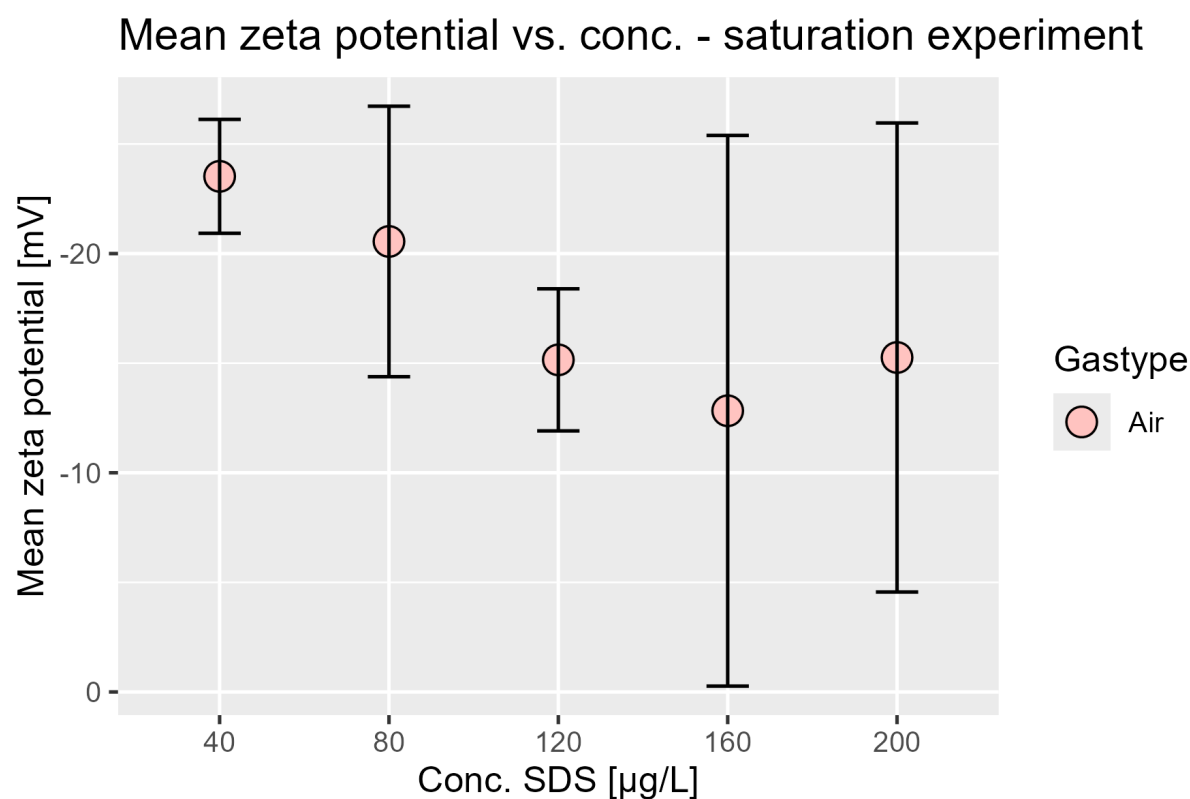


**Figure 6.10:** The mean zeta with standard deviation of the concentration in the saturation experiment.

SDS. The 120 µg/L shows a smaller still value with a smaller standard deviation, indicating the equilibrium of NB with their surroundings remains and has stabilized.

The 160 µg/L shows a smaller still value, but a large standard deviation, indicating the stability of the NB is compromised by a different zeta potential meaning that the surface may contain a significant amount of SDS. When comparing with the size, the NBs still seem to be present but are unstable.

The 200 µg/L sample shows a slight increase in the value, but still a significant standard deviation. Both the size and zeta potential of the 200 µg/L show the NBs are unstable, as the size has increased with a large standard deviation alongside the lower zeta potential when compared with the NB sample.

There is no clear tendency across all samples. However, if the samples suspected of having either burst or unstable NBs are removed (160-200 µg/L), a tendency is found that increasing concentration both decreases the zeta potential and the size. This tendency is based on 3 data points, and may not give an accurate picture. The accuracy is also lowered, as some of the standard deviations overlap.

### Statistical significance

As large standard deviations are observed in both size and zeta potential throughout the different experiments, a one-way ANOVA test was performed to examine whether any statistical difference exists in the samples. The full results can be seen in **appendix 14**. The p-values under 0.05 for both zeta potential and size are observed on **table 6.3**.

Batch 5 ultrasound zeta potential is low due to the spread of data points as described at the

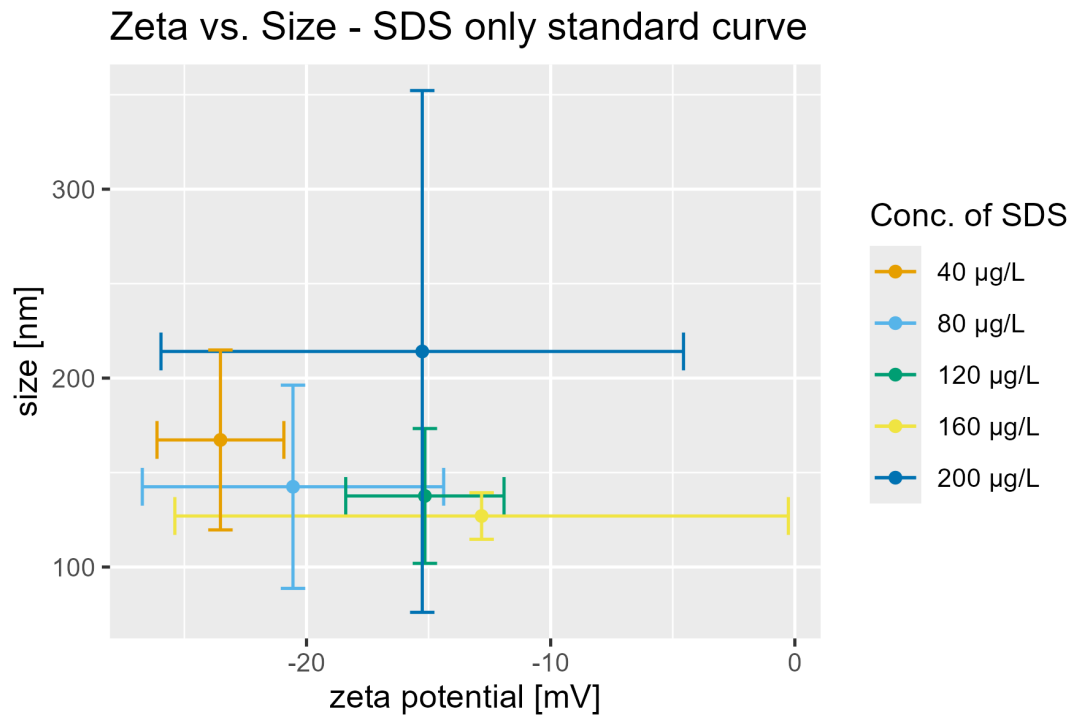


**Figure 6.11:** Mean zeta vs. mean size with standard deviation of the saturation experiment. Only the samples with NB and SDS are shown.

**Table 6.3:** Table of F- and P-values, where only samples with P-values under 0.05 are shown for all batches.

Batch	measurement type	method	F-Value	P-Value
batch 5	size	no NB	9.203553	0.02895741
batch 6	size	acid	8.13224	0.03575207
batch 11	size	acid	8.760427	0.01815171
batch 11	size	no NB	5.599912	0.04986859
batch 11	size	ultrasound	18.83602	0.002478225
batch 11	size	UV	18.59472	0.002573146
batch 12	size	acid	6.971896	0.04595213
batch 12	size	blank acid	7.723726	0.03203254
batch 13	size	blank UV	5.793063	0.04271578
batch 14	size	ultrasound	7.739497	0.02385102
batch 14	size	blank acid	15.89997	0.01045268
batch 15	size	NB SDS 2	7.163203	0.02808156
batch 2	zeta	UV	9.599206	0.03628233
batch 5	zeta	ultrasound	1.01412e+35	5.834077e-64

beginning of this chapter, as a very small variance is observed within the NB sample ( $\pm 0$ ), as well as within the ultrasound. This leads to an artificial P- and F-value. Relatively few are below the 95% confidence interval, which is partially due to the large standard deviation on some samples. The F-values show that the variance of the NB or the sample is small enough that the distance between the means of each sample creates a difference.

As relatively few samples have a small variance, and the majority of samples have a large

variance, only a few samples are statistically different. High F-values and P-values under 0.05 are primarily seen if the NB sample has a small variance, as all others are compared to it. Furthermore, the one-way ANOVA test makes the assumption that the data is normally distributed, which is not observed for a significant part of the samples. This may partially be explained by the way the mean of each run is found, the data should be normally distributed within each run if the size or zeta potential is stable.

### 6.1.2 Dissolved gas measurements

The DO content in the samples from the radical formation & OMP breakdown experiment was measured with the Winkler method and a DO meter.

The Winkler method is very precise if performed correctly but several factors can have an influence on the result during preparation of the samples. For instance, it is important to avoid air bubbles in the flask as this can increase the measured amount of DO. Furthermore, it can be difficult to determine the endpoint of the titration colour-change, as some of the colour comes from suspended particles that are slow to change colour and some comes from dissolved compounds that change colour rapidly.

Most of the DO meter values were obtained from an optical DO meter that gave the value in percent saturation. However, the acid, ultrasound and UV samples from batch 5 along with the NB samples from batches 6 and 7 were all performed with a DO meter that gave the concentration in mg/L. The Winkler method also provides the values in mg/L and thus, to produce the diagrams the values obtained in mg/L were converted to percent concentration using Henry's law[112].

#### O<sub>2</sub>

From **figure 6.12** and **table 6.4** it can be seen that the Winkler method for O<sub>2</sub> generally shows a higher concentration than the DO meter for acid and UV. For ultrasound, the average is nearly the same with a slightly smaller standard deviation for the Winkler method than for the DO meter. The concentration in the NB sample is significantly higher than the other samples for Winkler and is missing for DO meter. This is due to the limit of detection being 475 % saturation according to the data sheet which varies temperature [113]. All the samples have similar standard deviation, except UV measured with the DO meter having a very small standard deviation.

The higher concentration for the NB sample could arise from the fact that it is measured just after the NB have been produced, whereas the samples exposed to the bursting methods have stood for 24 hours in an enclosed atmosphere. The sample that had been exposed to ultrasound had a lower concentration than the others except for UV with the DO meter. This can be explained by the increased mechanical stimuli that can increase the reaction rate towards the equilibrium with the atmosphere.

#### Air

On **figure 6.13** the results from the Winkler method and the DO meter for air NB samples can be seen. The measurements from the DO meter are higher than the Winkler results and the standard deviation is small for the DO meter and large for the Winkler method. There is a small difference in gas concentration between the bursting methods as measured with the DO meter. For the Winkler measurements, there is a slight difference where UV is the highest followed by

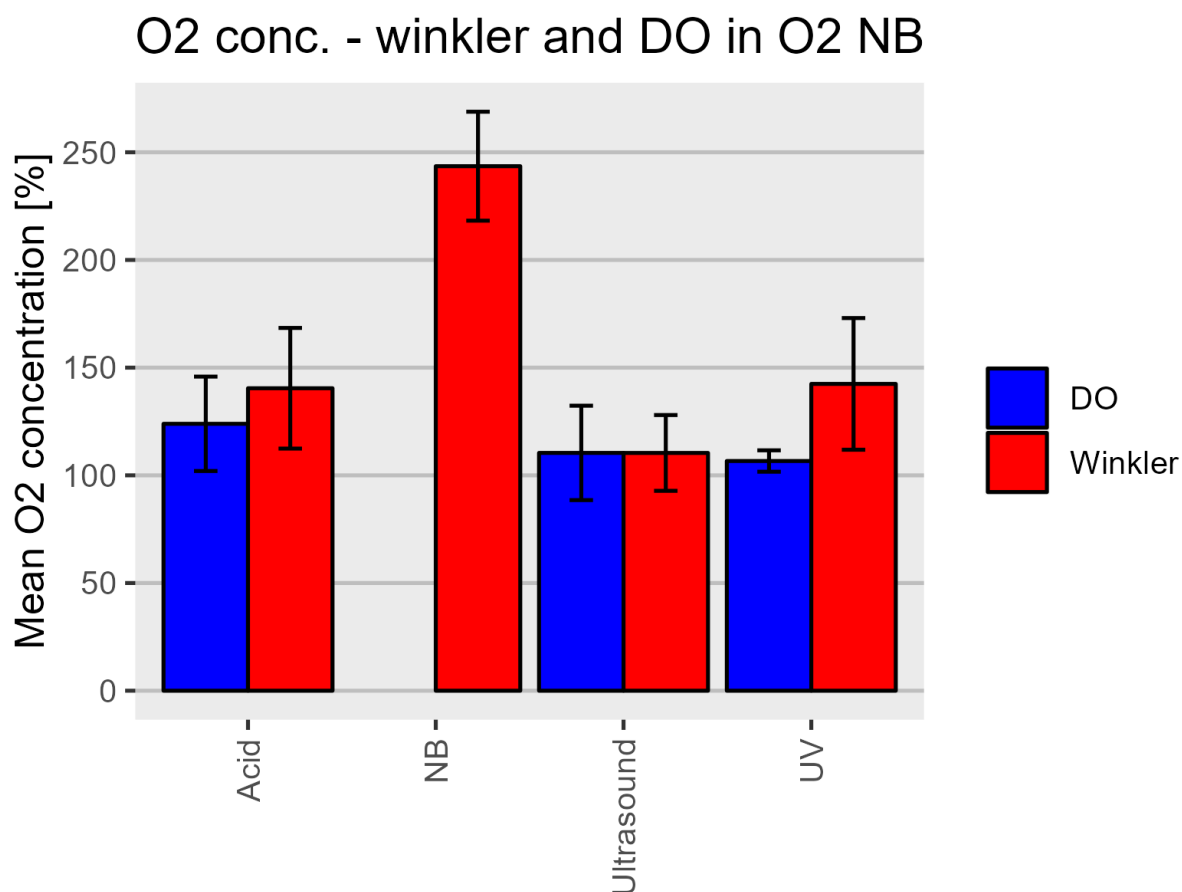


**Figure 6.12:** The mean O<sub>2</sub> concentration with standard deviation per method for O<sub>2</sub> as measured by the Winkler method and DO meter.

ultrasound and acid but the standard deviation is too large to determine a difference between the points.

The results from the DO method are expected as the gas content has stabilised around 100 % saturation of O<sub>2</sub> and there is a fall from the NB sample where the solution is over-saturated. From the Winkler method, the gas concentration starts around 100 % saturation and then falls to around 65-70 % after being exposed to the busting methods. The lower concentration of oxygen, measured by the Winkler method, could arise from several different factors, one being that it can be difficult to determine the endpoint of the titration. Furthermore, during preparation, the sample is carefully mixed to not introduce additional air into the solution, which may not provide adequate mixing.

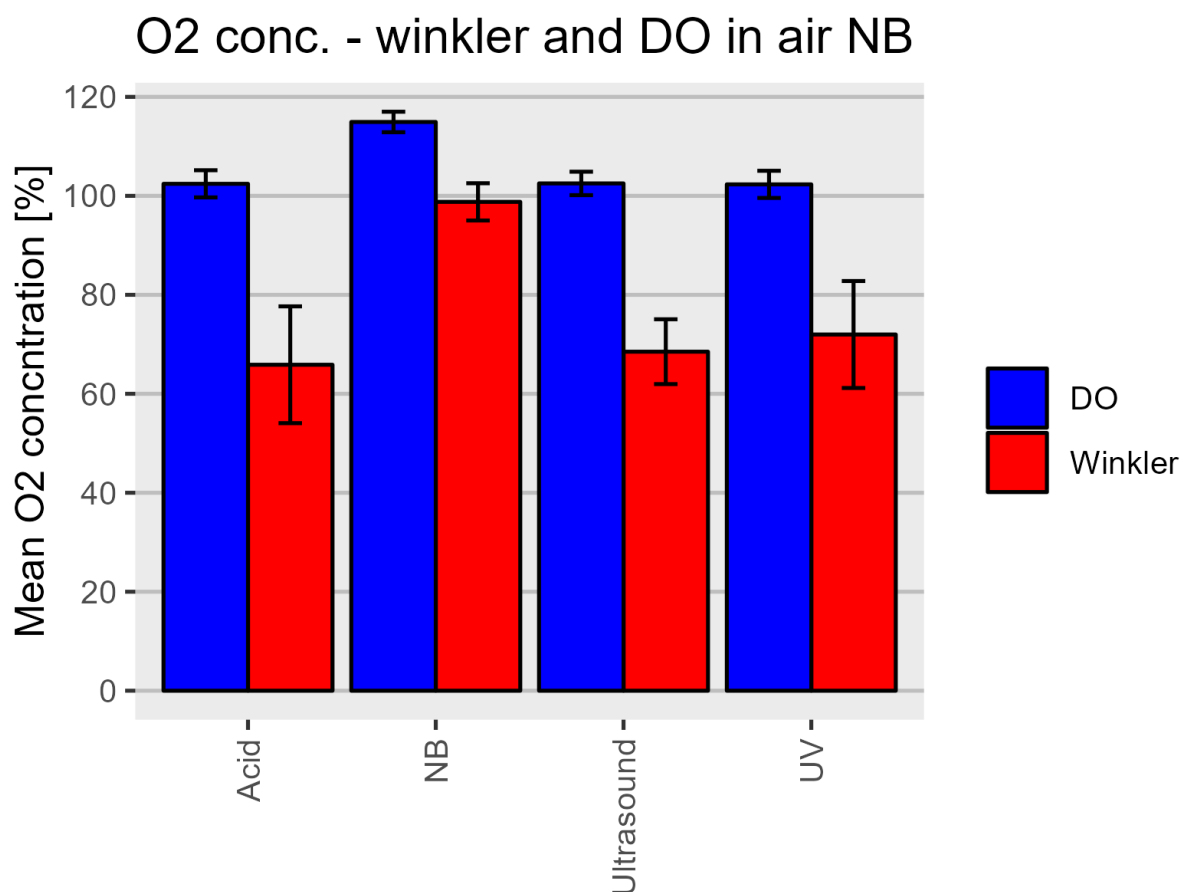


**Figure 6.13:** The mean O<sub>2</sub> concentration with standard deviation per method for air as measured by the Winkler method and DO meter.

**Table 6.4:** The mean O<sub>2</sub> concentration and standard deviation per method for air and O<sub>2</sub> as measured by the Winkler method and DO meter. The concentration of O<sub>2</sub> in the O<sub>2</sub> NB was too high for the DO meter to measure.

		Winkler	DO meter
		mean conc. [%]	mean conc. [%]
Air	NB	98.78 ± 3.76	114.93 ± 2.07
	Acid	65.87 ± 11.80	102.43 ± 2.74
	Ultrasound	68.51 ± 6.55	102.51 ± 2.37
	UV	71.98 ± 10.81	102.32 ± 2.75
O <sub>2</sub>	NB	243.54 ± 25.29	NA
	Acid	140.43 ± 28.00	123.92 ± 21.82
	Ultrasound	110.40 ± 17.59	110.42 ± 21.92
	UV	142.45 ± 30.57	106.65 ± 21.92

### Winkler & DO-meter

From **figure 6.14** it can be seen that the concentration in the O<sub>2</sub> samples for Winkler are significantly higher concentration than the air NB.

From **figure 6.15** it can be seen that the concentration is higher for the O<sub>2</sub> NB samples than the air NB samples.

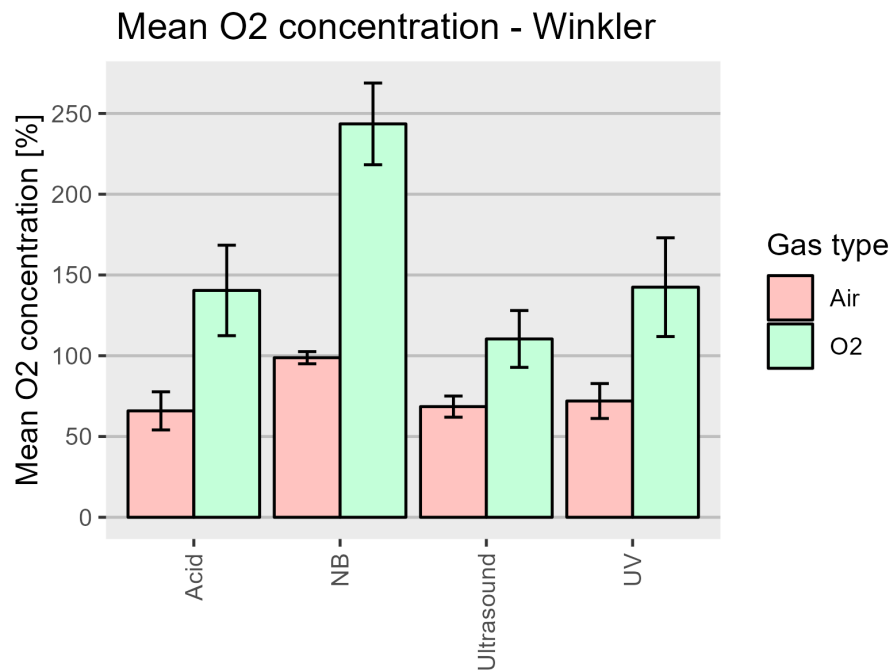


**Figure 6.14:** The mean O<sub>2</sub> concentration with standard deviation per method for air and O<sub>2</sub> as measured by the Winkler method.

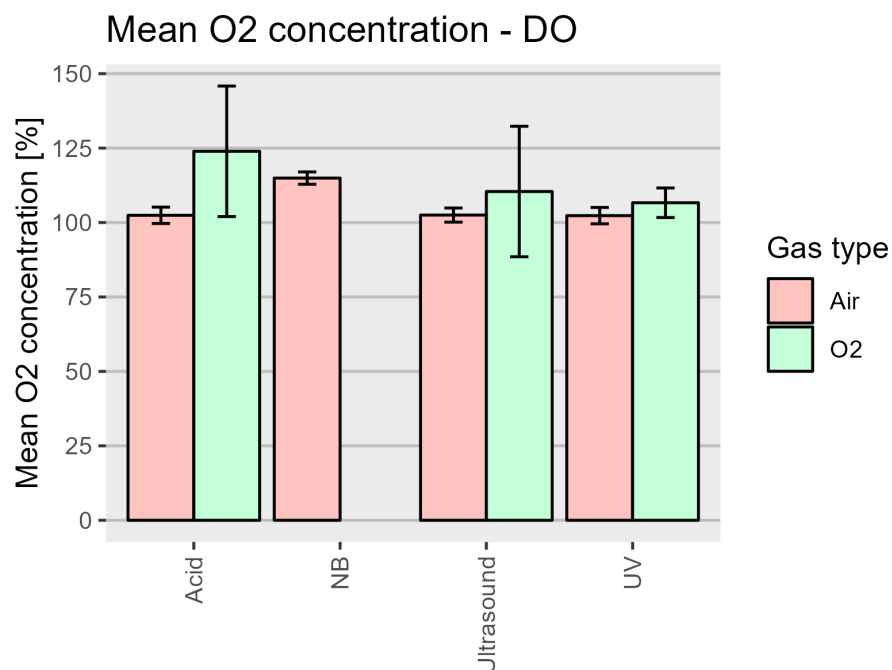


**Figure 6.15:** The mean O<sub>2</sub> concentration with standard deviation per method for air and O<sub>2</sub> as measured by DO meter.

For both the Winkler and DO measurements the standard deviation is larger for O<sub>2</sub> NB than for air. This indicates either a larger difference between the batches in the O<sub>2</sub> experiment or that the methods are more precise at the lower concentration. For the DO meter, it is more likely that the larger variance comes from differences between the batches as the measured concentration is not that much higher in O<sub>2</sub> than in air.



Therefore, the possible source of the increased standard deviation may be due to variance and not the concentration itself. Furthermore, the fact that both Winkler and DO-meter see a larger standard deviation in O<sub>2</sub> than air, indicates that it is caused by variance between the batches.

## 6.2 Radical formation & OMP breakdown

To help determine the effectiveness of the NB-assisted breakdown, benzoic acid was added to different NB solutions and different bursting methods were tested. Hereafter, the benzoic acid concentration was determined by HPLC.

### 6.2.1 HPLC

In order to determine the effect of NB on the breakdown the concentration of benzoic acid is plotted on **figure 6.16**.

Concentration before & after bursting method - breakdown experiment

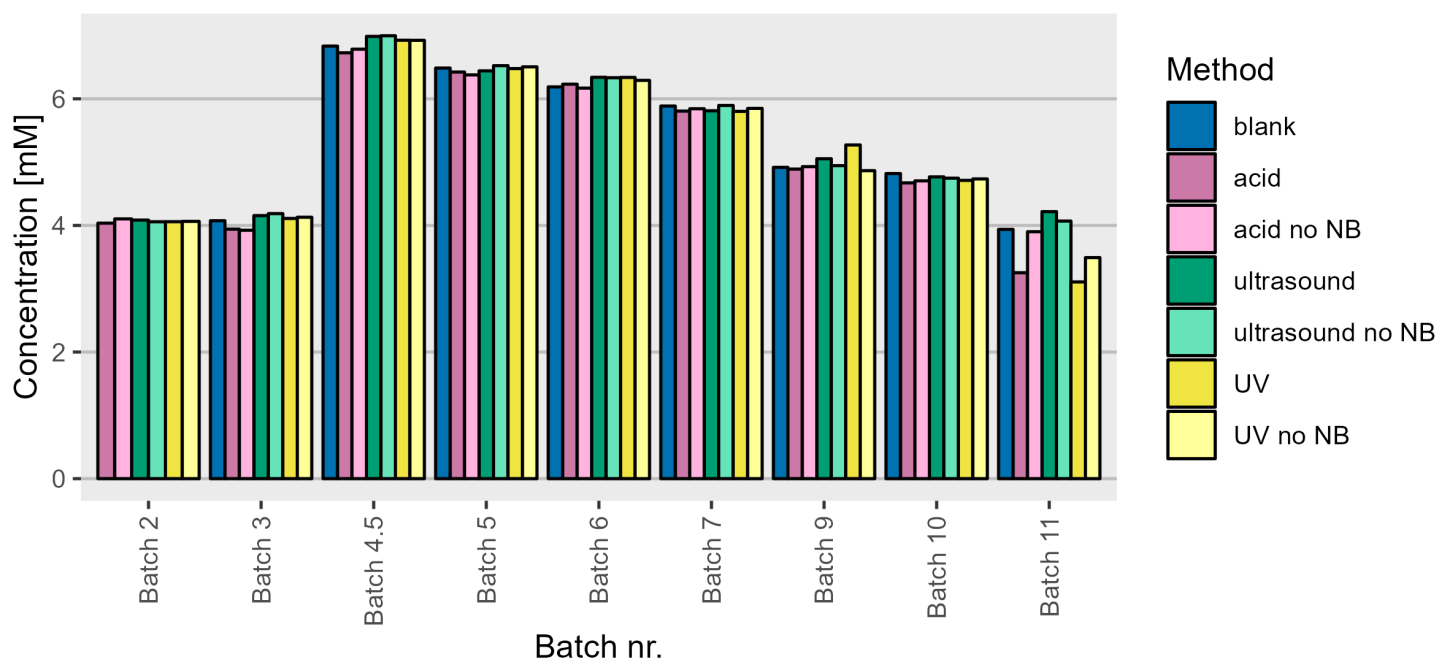


**Figure 6.16:** The concentration of benzoic acid for each batch and each breakdown method. Batch 2-4.5 is O<sub>2</sub> NB, batch 5-7 is air NB and batch 9-11 is CO<sub>2</sub> NB.

It can be seen that the concentration decreased with time as the batches were done over several months, the reason for the increase in batch 4.5 is that a new batch of benzoic acid standard solution was made. For most of the batches, no significant difference can be seen between the no NB and with NB for each method. In batch 9 UV and all the methods in batch 11, a difference is observed. In order to perform statistics and better see the size of the effect, the difference in % ( $\Delta$ breakdown) between with NB ( $c_{NB}$ ) and without NB ( $c_{w.o}$ ) was found with **equation 6.1**.

$$\Delta\text{breakdown} = 100 - \frac{c_{NB}}{c_{w.o}} \cdot 100 \quad (6.1)$$

The mean breakdown % of the benzoic acid can be seen on **figure 6.17**.

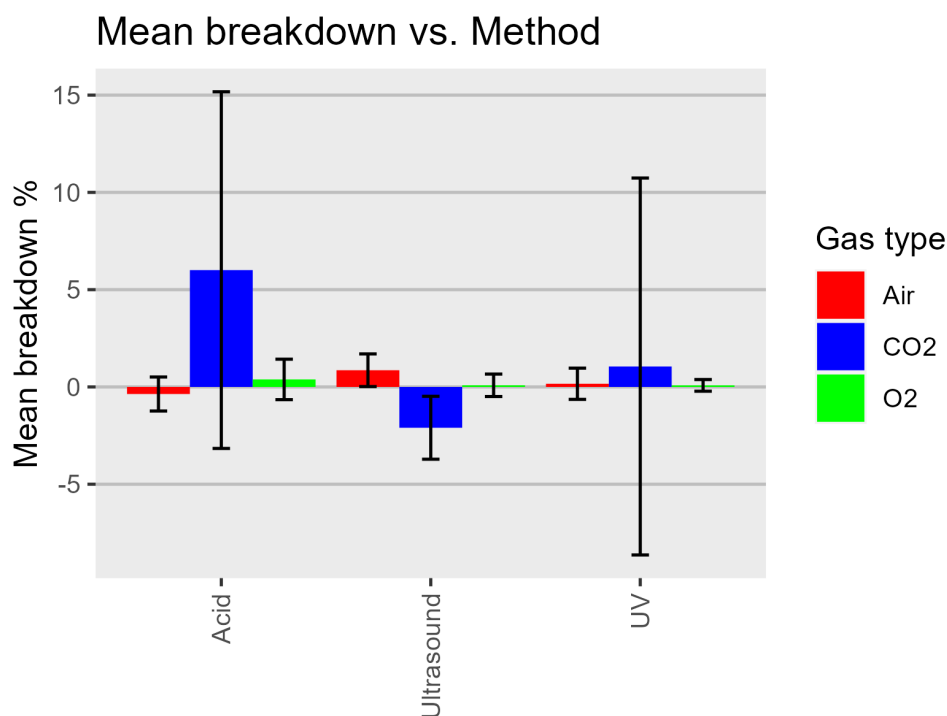


**Figure 6.17:** The mean breakdown (%) of benzoic acid with standard deviation are shown per method for 3 gas types.

For **air** and **O<sub>2</sub>** the breakdown is generally close to zero with the error bars crossing the zero % line, the only exception to this is air NB exposed to ultrasound. The air ultrasound shows a larger degradation than the others in the air series, with the error bars not crossing the zero % line. However, the error bars do touch the line and since they are only one standard deviation, it is not possible to determine whether the NB helps with the degradation. This indicates that air and O<sub>2</sub> NB do not contribute to the degradation of benzoic acid under the investigated parameters.

For **CO<sub>2</sub>** a higher breakdown, compared to the other gasses, is observed for acid, however, the standard deviation is larger than the value. This is due to there being only observed a substantial breakdown in batch 11 whereas for batch 9 and 10 the concentration is around the same for both with and without NB. This indicates that CO<sub>2</sub> NB can break down benzoic acid when combined with acid but since it was only observed for one batch further investigation is needed. CO<sub>2</sub> NB exposed to UV show a small degradation of benzoic acid with a large standard deviation. This arises from an observed breakdown in batch 11 and a prevention of the breakdown in batch 9 where the Nb sample is higher than the no NB sample.

As both a breakdown and prevention of the breakdown are observed it is not possible to determine the effect of CO<sub>2</sub> NB on the breakdown of benzoic acid when combined with UV. The sample exposed to ultrasound shows a negative breakdown indicating that CO<sub>2</sub> NB prevents the breakdown of benzoic acid when exposed to ultrasound which is also found in literature [83]. However, since the standard deviation almost crosses the 0 % line, it is not possible to say with certainty that it inhibits the degradation. But it can be observed that for all the batches that the concentration of benzoic acid in the with NB is larger than the no NB.

The standard deviation for CO<sub>2</sub> is generally quite large both when it is compared to air and O<sub>2</sub>. This mostly arises from the values from batch 11. This indicates that CO<sub>2</sub> or another part

of these samples leads to an instability in the breakdown percentage of benzoic acid. The instability could arise from the influence of carbonic acid  $\text{H}_2\text{CO}_3$  on the equilibrium of benzoic between the acid and base form towards more benzoic acid in the acid form.

As phosphoric acid  $\text{H}_3\text{PO}_4$  was only added to the sample and not the eluent, it was theorised that it might lead to some of the variants that were observed as the water in the eluent might lead to higher pH and therefore could cause the benzoic acid to be in both the acid and base form. It was also possible that  $\text{CO}_2$  could inhibit this change from the acid to the base form, therefore was the retention time and the length of the peak investigated and no significant difference was found between NB and no NB samples from the same bath that had been exposed to the same method. However, there was a significant difference between the batches in both the retention time and the length of the peak which can be found in the supplementary material. So the acid-base effect from  $\text{CO}_2$  does not seem to be the reason for the large variance as the breakdown % is calculated within the same batch from the NB and no NB sample.

## 6.3 Mass transfer experiment

To test the ability of NBs to collect hydrophobic matter on their surface, different solutions with OMP and NB were prepared. The solutions were then tested by way of pH and conductivity. Hereafter the solutions were filtered through a dead-end membrane filtration system, and the retentate and permeate were saved. pH and conductivity were measured, and HPLC was used to determine the concentration of OMP in both retentate and permeate.

### 6.3.1 HPLC

The concentrations in the permeate and the retentate for BPA were calculated from the area under the curve in the HPLC chromatogram and can be seen in **table 6.5**.

**Table 6.5:** Concentration of retentate and permeate for BPA and atrazine in the mass transfer experiment. \* signifying that the sample had no detectable peak. \*\* Atrazine was detected in a sample that did not contain atrazine, likely due to atrazine being retained in the membrane.

	concentration [mg/L]
demi water + BPA retentate	1.1909
demi water + BPA permeate	*
NB + BPA retentate	1.1725
NB + BPA permeate	0.0402
demi water + atrazine retentate	1.6418
demi water + atrazine permeate	0,7464
NB + atrazine retentate	1.6323
NB + atrazine permeate	0.9426
NB permeate atrazine	0.3189**

There were no detectable peaks at the highest points in the standard row for the OMP other than BPA and atrazine, this is possibly due to the low solubility of the tested OMP and the detection limit of the HPLC. These are therefore not included in the HPLC section.

From **table 6.5** it can be seen that the highest concentrations are found in the retentate samples. The permeate of the samples shows a low concentration of BPA with the NB sample showing a small peak and a concentration of 0.0402 mg/L. Demi water + BPA permeate showed no peak that was differentiable from the noise.

These results indicate that the membrane is retaining the BPA as it was not observed in demi water + BPA permeate. The membrane has a molecular weight cutoff at 900 Da and BPA has a molar mass of 228.28 g/mol, therefore it should not hold all the BPA back. The large retention could be caused by several factors one of these being the small volume of permeate.

However, in NB + BPA permeate a small amount of BPA can be seen in the permeate. This could indicate that NB helps facilitate transport across the membrane. This seems unlikely as the BPA is theorized to be on the surface of the NB as the pore size of the membrane is much smaller than the size of the NB thus filtering it out. Therefore, if the NB makes it more favourable for BPA to travel through the membrane it is by another mechanism than adhering to the NB.

The NB might facilitate the transport of BPA across the membrane by collecting the BPA from solution and then adhering to the membrane or collapsing in contact with the membrane, which could lead to a concentration gradient of the BPA near the membrane. However for this to be the driving factor for the increased transport over the membrane, there needs to be a large transport of NB towards the membrane for it to lead to an increased concentration at the membrane surface. This means that the NB carrying the BPA should all gather at the membrane surface for this effect to work, which is counterintuitive as NB doesn't coalesce and spread out into the solution according to Brownian motion. Therefore it is unlikely that the concentration of BPA by NB is the driving factor for the larger concentration of BPA in the permeate for the solution that contains NB than the solution without NB.

From table 6.5 it can be seen that the atrazine concentration is lower in the retentate than in the permeate for the solutions that contain atrazine. For the NB solution without atrazine, a peak was observed in the permeate, this peak is most likely due to atrazine still in the membrane from the demi water + atrazine since no peak was seen in the retentate. The two retentate samples with atrazine have a similar concentration with demi water being slightly higher. For the permeate samples the concentration is highest for the NB sample which further indicates that the NB helps the OMP over the membrane. However, only one experiment per sample was performed further experiments are needed to be certain that it is not run to run variance and it is caused by the NB.

### 6.3.2 pH & conductivity

The results from the pH and conductivity measurements can be seen in **table 6.6** and **figure 6.18 and 6.19**.

The conductivity for the permeate in samples without NB is generally significantly higher than both the feed and the retentate. This could mean that the membrane releases some kind of conductive compound. This compound could be  $\text{Na}_2\text{S}_2\text{O}_5$  which was added to the liquid that the membrane was stored in. The samples with NB generally have a higher conductivity but there is no systematical difference between the retentate and permeate. The conductivity of the retentate for the BPA sample without NB is significantly higher than the others, this is likely due to contamination from the pH probe which had not been properly cleaned after storage. The pH tends to be higher in the feed than in the permeate and retentate. And since none

**Table 6.6:** The conductivity and pH measurements for all OMP for feed, permeate and retentate are recorded in this table.

	Conductivity [ $\mu\text{S}/\text{cm}$ ]			pH		
	feed	permeate	retentate	feed	permeate	retentate
estradiol NB	9.14	9.49	1.458	6	5.388	5.870
	64.8	54.2	50.1	6.431	4.636	5.787
bisphenol-A NB	2.35	20.0	154.8	5.700	5.280	5.342
	62.5	54.2	59.7	6.430	5.854	6.297
atrazine NB	3.28	22.4	1.875	6.210	6.157	5.472
	70.7	49.4	47.4	6.720	6.040	6.196
diclofenac NB	2.52	12.06	1.917	5.643	5.528	5.198
	67.9	48.4	46.2	6.900	5.998	6.188

## Conductivity - mass transfer experiment

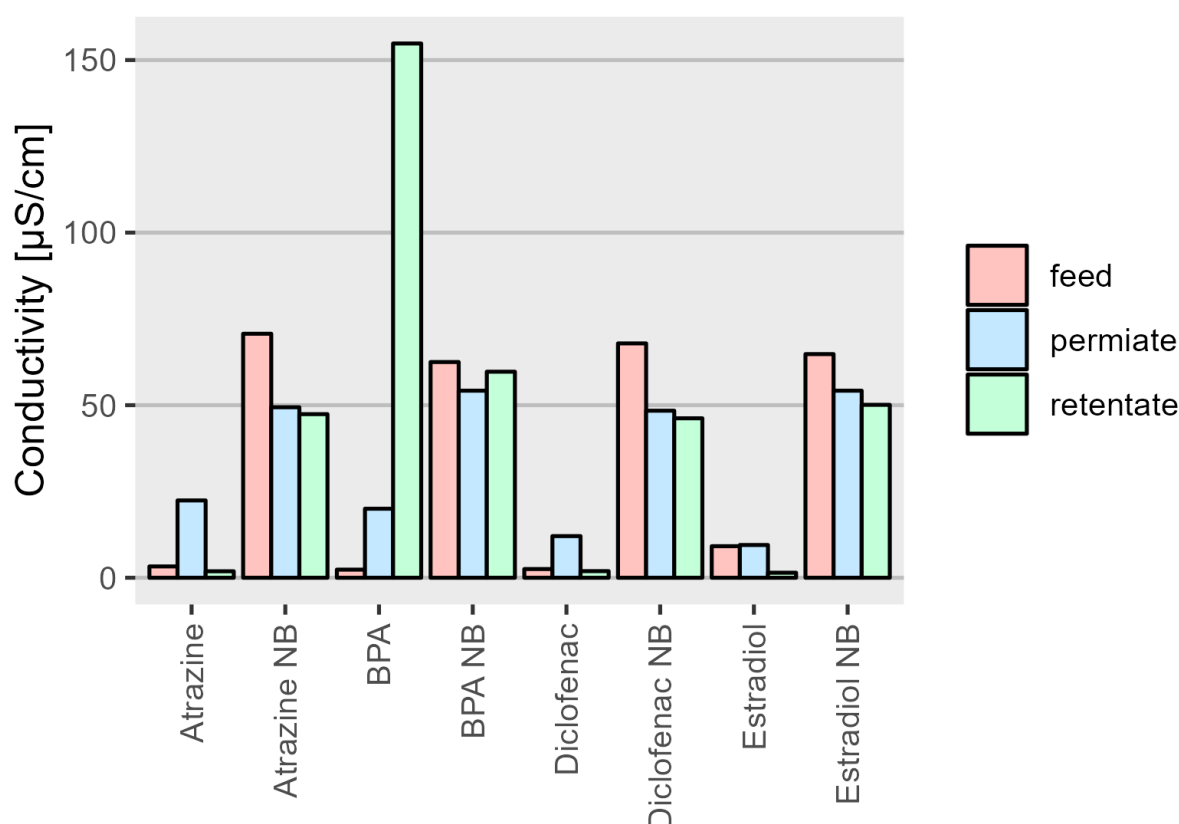


**Figure 6.18:** The conductivity for all OMP for feed, permeate and retentate.

of the chosen OMP are acids or bases, they do not influence the pH value so the change in pH comes from other factors than the OMP and can therefore not be used as an indication for whether or not the OMP have been retained by the membrane. In the NB samples the pH tends to be lower in the permeate than in the retentate this can be explained by the phosphoric acid used as a pH buffer in the BOD water. The membrane is better at retaining divalent ions than monovalent ions and therefore more  $\text{H}_2\text{PO}_4^-$  pass through the membrane than  $\text{H}_1\text{PO}_4^{2-}$  this would lead to a lower pH in the retentate.

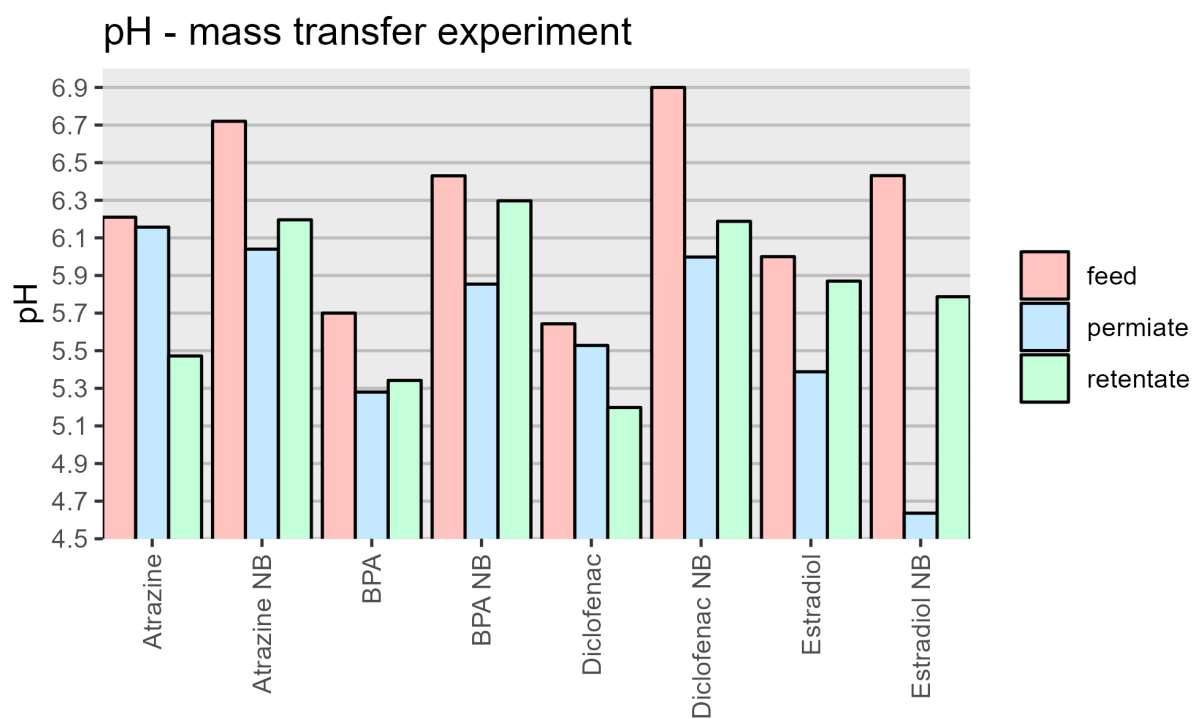


**Figure 6.19:** The pH for all OMP for feed, permeate and retentate.

## Chapter 7

# Conclusion

Nanobubbles with O<sub>2</sub>, CO<sub>2</sub> and air were produced in BOD water in 3 batches of each gas for a total of 9 batches.

The batches were characterized by size, zeta potential and dissolved gas content. Benzoic acid was added to each batch and different bursting methods were attempted.

The size analysis found a general increase in size for both [O<sub>2</sub>] and air on all methods, while CO<sub>2</sub> showed a decrease in ultrasound and a small increase in acid. This decrease is theorized to be caused by the additional acid from the CO<sub>2</sub> equilibrium as the addition of ions affects the size of the double layer [109]. The general sizes of CO<sub>2</sub> NB were also smaller by comparison to the other gasses.

O<sub>2</sub> showed no difference between the methods within the standard deviation which means that the methods didn't impact the size. The zeta potential analysis showed no overall trend, except acid consistently increasing the zeta potential.

No relationship was found between size and zeta potential of NB.

The experiment of the longevity of NB showed that the most stable nanobubbles were air, followed by O<sub>2</sub> and CO<sub>2</sub> being the shortest lived.

The surface saturation of NB showed a slight trend with increasing concentration of SDS. This is however doubtful, as some standard deviations overlap

All the bursting methods showed no credible breakdown of benzoic acid. The CO<sub>2</sub> was found to inhibit the breakdown of benzoic acid when exposed to ultrasound which was also found in literature [83].

The mass transfer of NB was tested by way of conductivity, pH and retention rate over a membrane and determined by HPLC. The conductivity showed no systemic difference, other than NB having a higher conductivity due to the added salts from the BOD solution. The pH showed no change which could be explained.

The HPLC results showed that the membrane retained BPA, and that the sample with NB transported it across the membrane. The proposed mechanism of mass transfer did not explain the results. The experiment should be repeated with a suitable membrane allowing OMP to pass through and not NB.

## Chapter 8

# Further research

In order to better characterise the size and concentration of NB it would be favourable to have a machine capable of nanoparticle tracking analysis (NTA). An NTA works by illuminating the sample with a laser and detecting the scattered light through a camera sensor with a microscope attached. This allows it to detect individual particles and track them over multiple frames from which it is possible to calculate the size of individual particles along with their concentration. This allows it to obtain a more accurate size distribution than DLS as it relies on fluctuations in all the scattered light at once [114].

If the experiments are repeated, extra care must be taken to dilute the sample with solutions of the ion strength so as to not affect the zeta potential and thus size of the nanobubble. Additionally, more care must be taken to keep the samples free from dust and other particles as they can influence both the size and zeta potential measurements.

The age experiments should be repeated again with a consistent interval between sampling. It should also be investigated over a longer time frame than the maximum 58 days.

An NTA would enable the determination of the concentration of NB [114]. This could be used in conjunction with DO measurements to determine the amount of gas in the liquid both dissolved and in the NB. From this the effectiveness of the NB generator in terms of gas in to the system compared to gas in the water.

It is also relevant to further investigate the effects of surfactants on NB further. This could both be through the use of different surfactants from the one investigated in this project and through a more thorough investigation of SDS. It could for example be that a broader range of concentrations of SDS is investigated in order to understand the effect of SDS over a larger range.

The radical formation and breakdown of OMP should be investigated further. This investigation could include the use of electron spin resonance (ESR) that allows for a more direct detection of radicals through a spin trapping reagent [115]. This would allow for more knowledge about the specific form of radicals generated and make for easier detection of radicals.

It could also be relevant to repeat the breakdown and HPLC experiment with benzoic acid where greater care is taken to keep it in either acid or base form. Alternatively, another probe that doesn't require a specific pH could be used and is equally simple to perform HPLC on or another quantitative method.

To better understand the interaction between OMP, NBs and membranes it would be important to repeat the mass transfer experiment with a membrane with a bigger pore size. It would also be relevant to perform the experiment with the chosen OMP with a quantification method that can detect them. Furthermore, it would be interesting to investigate other OMP in order to find out what kind of OMP the NBs are more effective at retaining.



# Bibliography

- (1) Luo, Y.; Guo, W.; Ngo, H. H.; Nghiem, L. D.; Hai, F. I.; Zhang, J.; Liang, S.; Wang, X. C. *The Science of the total environment* **2014**, 473-474, 619–641.
- (2) Yang, Y.; Zhang, X.; Jiang, J.; Han, J.; Li, W.; Li, X.; Leung, K. M. Y.; Snyder, S. A.; Alvarez, P. J. *Environmental Science and Technology* **2022**, 56, 13–29.
- (3) Ijaz, M.; Ahmed, T.; Iftikhar Ahmad, A. In *Hazardous Environmental Micro-pollutants, Health Impacts and Allied Treatment Technologies*; Springer: 2022, pp 205–217.
- (4) Khoo, Y. S.; Goh, P. S.; Lau, W. J.; Ismail, A. F.; Abdullah, M. S.; Ghazali, N. H. M.; Yahaya, N. K. E.; Hashim, N.; Othman, A. R.; Mohammed, A., et al. *Chemosphere* **2022**, 305, 135151.
- (5) Westerhoff, P.; Yoon, Y.; Snyder, S.; Wert, E. *Environmental science & technology* **2005**, 39, 6649–6663.
- (6) Snyder, S. A.; Westerhoff, P.; Yoon, Y.; Sedlak, D. L. *Environmental engineering science* **2003**, 20, 449–469.
- (7) Pruden, A.; Pei, R.; Storteboom, H.; Carlson, K. H. *Environmental Science and Technology* **2006**, 40, 7445–7450.
- (8) Fent, K.; Weston, A. A.; Caminada, D. *Aquatic Toxicology* **2006**, 76, 122–159.
- (9) Sadia, M.; Nollen, I.; Helmus, R.; Laak, T. L. T.; Béen, F.; Praetorius, A.; Wezel, A. P. V. *Environmental Science and Technology* **2023**, 57, 3062–3074.
- (10) R, L.; D, M.; I, S.; D, N.; T, L. **2018**, DOI: 10.2760/614367(online) , 10.2760/701879(print).
- (11) Screening for medicinrester og miljøfremmede stoffer v. Skanderborg Forsyning <https://www.atv-jord-grundvand.dk/wp-content/uploads/2022/06/Moede-89-Carina-Cupit-Bayley-Screening-for-medicinrester.pdf>.
- (12) QToF Discovery Suite - Eurofins Scientific <https://www.eurofins.com.au/environment-testing/company/news/environote-1122-introducing-the-qtof-discovery-suite/>.
- (13) MerEFF-Environmental treatment of wastewater effluents.
- (14) Yao, K.-M.; Habibian, M. T.; O'Melia, C. R. *Environmental science & technology* **1971**, 5, 1105–1112.
- (15) Wang, J.; Chen, H. *Science of the Total Environment* **2020**, 704, 135249.
- (16) 14.7: Wastewater and Sewage Treatment [Accessed 19-01-2024], [https://chem.libretexts.org/Bookshelves/Introductory\\_Chemistry/Chemistry\\_for\\_Changing\\_Times\\_\(Hill\\_and\\_McCreary\)/14%3A\\_Water/14.08%3A\\_Wastewater\\_Treatment](https://chem.libretexts.org/Bookshelves/Introductory_Chemistry/Chemistry_for_Changing_Times_(Hill_and_McCreary)/14%3A_Water/14.08%3A_Wastewater_Treatment).
- (17) Tyagi, V. K.; Khan, A. A.; Kazmi, A. A.; Mehrotra, I.; Chopra, A. *Desalination* **2009**, 249, 571–576.
- (18) Wilson, P. C. *Department of Soil and Water Science. University of Florida* **2010**.
- (19) <https://www.aquasana.com/info/microfiltration-vs-ultrafiltration-vs-nanofiltration-vs-reverse-osmosis-pd.html>.

- (20) <https://www.safewater.org/fact-sheets-1/2017/1/23/ultrafiltrationnanoandro>.
- (21) Cirillo, A. I.; Tomaiuolo, G.; Guido, S. *Micromachines* **2021**, *12*, 820.
- (22) Soriano, Á.; Gorri, D.; Urtiaga, A. *Water research* **2017**, *112*, 147–156.
- (23) Al-Obaidi, M.; Li, J.-P.; Kara-Zaitri, C.; Mujtaba, I. M. *Chemical Engineering Journal* **2017**, *316*, 91–100.
- (24) Lee, S.; Ihara, M.; Yamashita, N.; Tanaka, H. *Water research* **2017**, *114*, 23–30.
- (25) Timmers, P. H.; Siegers, W.; Ferreira, M. L.; Van der Wielen, P. W. *Water Research* **2024**, *249*, 120921.
- (26) Reactivation of granular activated carbon - Carbotecnia — carbotecnia.info [Accessed 19-01-2024], <https://www.carbotecnia.info/learning-center/activated-carbon-theory/activated-carbon-reactivation/?lang=en>.
- (27) Greaves, J. How are coagulants and flocculants used in water and wastewater treatment? <https://www.wcs-group.co.uk/wcs-blog/coagulants-flocculants-wastewater-treatment>.
- (28) Snoeyink, V.; Chen, A. *Science of the Total Environment* **1985**, *47*, 155–167.
- (29) <https://www.mrwa.com/WaterWorksMnl/Chapter%2012%20Coagulation.pdf>.
- (30) Bratby, J., *Coagulation and flocculation in water and wastewater treatment*, Third edition.; IWA Publishing: London, England, 2016 - 2016.
- (31) Sang, D.; Cimetiere, N.; Giraudet, S.; Tan, R.; Wolbert, D.; Le Cloirec, P. *Journal of Water Process Engineering* **2022**, *49*, 103190.
- (32) Takman, M.; Betsholtz, A.; Davidsson, Å.; Cimbritz, M.; Svahn, O.; Karlsson, S.; Østergaard, S. K.; Nielsen, J. L.; Falås, P. *Journal of Hazardous Materials* **2024**, 134449.
- (33) Ozone Water Treatment Disadvantages [Accessed 22-01-2024], <https://atlas-scientific.com/blog/ozone-water-treatment-disadvantages>.
- (34) Jensen, N. W.; Faraji, T.; Ospina, A. G.; Guilloso, R.; Perrin, F. P.; Kristensen, P. K.; Hansen, S. H.; Jørgensen, M. K.; Andersen, M. B. O.; Tranekær, C., et al. **2022**.
- (35) <https://www.freshwatersystems.com/blogs/blog/what-is-ozone-water-treatment-and-how-does-it-work>.
- (36) Michailidi, E. D.; Bomis, G.; Varoutoglou, A.; Kyzas, G. Z.; Mitrikas, G.; Mitropoulos, A. C.; Efthimiadou, E. K.; Favvas, E. P. *Journal of colloid and interface science* **2020**, *564*, 371–380.
- (37) Law, J.; Brar, A. Colloids [https://chem.libretexts.org/Bookshelves/Physical\\_and\\_Theoretical\\_Chemistry\\_Textbook\\_Maps/Supplemental\\_Modules\\_\(Physical\\_and\\_Theoretical\\_Chemistry\)/Physical\\_Properties\\_of\\_Matter/Solutions\\_and\\_Mixtures/Colloid](https://chem.libretexts.org/Bookshelves/Physical_and_Theoretical_Chemistry_Textbook_Maps/Supplemental_Modules_(Physical_and_Theoretical_Chemistry)/Physical_Properties_of_Matter/Solutions_and_Mixtures/Colloid).
- (38) Knüpfer, P.; Ditscherlein, L.; Peuker, U. A. *Colloids and Surfaces A: Physicochemical and Engineering Aspects* **2017**, *530*, 117–123.
- (39) Chaplin, M. <https://water.lsbu.ac.uk/water/nanobubble.html>.
- (40) Yasui, K. In Springer International Publishing AG: 2017; Chapter 3.1 Cavitation Nuclei (Bulk Nanobubbles), pp 99–106.
- (41) YASUI, K. *Japanese Journal of Multiphase Flow* **2016**, *30*, 19–26.

- (42) Mezger, M.; Schöder, S.; Reichert, H.; Schröder, H.; Okasinski, J.; Honkimäki, V.; Ralston, J.; Bilgram, J.; Roth, R.; Dosch, H. *The Journal of chemical physics* **2008**, 128.
- (43) Steitz, R.; Gutberlet, T.; Hauss, T.; Klösgen, B.; Krastev, R.; Schemmel, S.; Simonsen, A. C.; Findenegg, G. H. *Langmuir* **2003**, 19, 2409–2418.
- (44) Peng, H.; Birkett, G. R.; Nguyen, A. V. *Langmuir* **2013**, 29, 15266–15274.
- (45) 2022.
- (46) Gaiduk, A. P.; Pham, T. A.; Govoni, M.; Paesani, F.; Galli, G. *Nature communications* **2018**, 9, 247.
- (47) Lee, J. K.; Samanta, D.; Nam, I.; Nam, H. G.; Zare, R. N. *Biophysical Journal* **2018**, 114, 542a.
- (48) Takahashi, M.; Shirai, Y.; Sugawa, S. *Langmuir* **2021**, 37, 5005–5011.
- (49) Wada, H.; Koido, J.; Miyazawa, S.; Mochizuki, T.; Masuda, K.; Unga, J.; Oda, Y.; Suzuki, R.; Maruyama, K. *Japanese Journal of Applied Physics* **2016**, 55, 07KF06.
- (50) Ruckenstein, E. *Colloids and Surfaces A: Physicochemical and Engineering Aspects* **2013**, 423, 112–114.
- (51) Takahashi, M.; Chiba, K.; Li, P. *The Journal of Physical Chemistry B* **2007**, 111, 1343–1347.
- (52) Khaled Abdella Ahmed, A.; Sun, C.; Hua, L.; Zhang, Z.; Zhang, Y.; Marhaba, T.; Zhang, W. *Environmental Engineering Science* **2018**, 35, 720–727.
- (53) Nirmalkar, N.; Pacek, A.; Barigou, M. *Soft matter* **2018**, 14, 9643–9656.
- (54) Gao, Z.; Wu, W.; Sun, W.; Wang, B. *Langmuir* **2021**, 37, 11281–11291.
- (55) Raja, P. M. V.; Barron, A. R. 2.5: Zeta Potential Analysis [https://chem.libretexts.org/Bookshelves/Analytical\\_Chemistry/Physical\\_Methods\\_in\\_Chemistry\\_and\\_Nano\\_Science\\_\(Barron\)/02%3A\\_Physical\\_and\\_Thermal\\_Analysis/2.05%3A\\_Zeta\\_Potential\\_Analysis](https://chem.libretexts.org/Bookshelves/Analytical_Chemistry/Physical_Methods_in_Chemistry_and_Nano_Science_(Barron)/02%3A_Physical_and_Thermal_Analysis/2.05%3A_Zeta_Potential_Analysis).
- (56) Atkins, P.; Atkins, P. W.; de Paula, J. In Oxford university press: 2014; Chapter 14E.
- (57) Taylor, P *Advances in colloid and interface science* **1998**, 75, 107–163.
- (58) Chaplin, M. Interfacial water and water-gas interfaces, 2007.
- (59) Chaplin, M. Water dissociation and ph, 2007.
- (60) Wang, L.; Ali, J.; Wang, Z.; Oladoja, N.; Cheng, R.; Zhang, C.; Mailhot, G.; Pan, G. *Chemical Engineering Journal* **2020**, 388, 124227.
- (61) Milo, R.; Jorgensen, P.; Springer, M. Average radius of folded protein <https://bionumbers.hms.harvard.edu/bionumber.aspx?&id=100018&ver=16>.
- (62) Kahn, S. Henry's Law [https://chem.libretexts.org/Bookshelves/Physical\\_and\\_Theoretical\\_Chemistry\\_Textbook\\_Maps/Supplemental\\_Modules\\_\(Physical\\_and\\_Theoretical\\_Chemistry\)/Physical\\_Properties\\_of\\_Matter/Solutions\\_and\\_Mixtures/Ideal\\_Solutions/Dissolving\\_Gases\\_In\\_Liquids%2C\\_Henry's\\_Law](https://chem.libretexts.org/Bookshelves/Physical_and_Theoretical_Chemistry_Textbook_Maps/Supplemental_Modules_(Physical_and_Theoretical_Chemistry)/Physical_Properties_of_Matter/Solutions_and_Mixtures/Ideal_Solutions/Dissolving_Gases_In_Liquids%2C_Henry's_Law).
- (63) Alheshibri, M.; Al Baroot, A.; Shui, L.; Zhang, M. *Current Opinion in Colloid & Interface Science* **2021**, 55, 101470.
- (64) Chaplin, M. [https://water.lsbu.ac.uk/water/hydrophobic\\_hydration.html#r506](https://water.lsbu.ac.uk/water/hydrophobic_hydration.html#r506).

- (65) Than, J. Hydrophobic interactions [https://chem.libretexts.org/Bookshelves/Physical\\_and\\_Theoretical\\_Chemistry\\_Textbook\\_Maps/Supplemental\\_Modules\\_\(Physical\\_and\\_Theoretical\\_Chemistry\)/Physical\\_Properties\\_of\\_Matter/Atomic\\_and\\_Molecular\\_Properties/Intermolecular\\_Forces/Hydrophobic\\_Interactions](https://chem.libretexts.org/Bookshelves/Physical_and_Theoretical_Chemistry_Textbook_Maps/Supplemental_Modules_(Physical_and_Theoretical_Chemistry)/Physical_Properties_of_Matter/Atomic_and_Molecular_Properties/Intermolecular_Forces/Hydrophobic_Interactions).
- (66) Krishnan, J. S.; Dwivedi, P.; Moholkar, V. S. *Industrial & engineering chemistry research* **2006**, *45*, 1493–1504.
- (67) Lohse, D. *Nature* **2002**, *418*, 381–383.
- (68) Free Radicals [Accessed 01-02-2024], [https://chem.libretexts.org/Bookshelves/Organic\\_Chemistry/Supplemental\\_Modules\\_\(Organic\\_Chemistry\)/Fundamentals/Reactive\\_Intermediates/Free\\_Radicals](https://chem.libretexts.org/Bookshelves/Organic_Chemistry/Supplemental_Modules_(Organic_Chemistry)/Fundamentals/Reactive_Intermediates/Free_Radicals).
- (69) Illés, E.; Mizrahi, A.; Marks, V.; Meyerstein, D. *Free Radical Biology and Medicine* **2019**, *131*, 1–6.
- (70) Lan, X.; Dai, Y.; Jing, W.; Meng, X.; Liu, F.; Wang, S.; He, A.; Li, N. *Journal of Molecular Graphics and Modelling* **2022**, *114*, 108182.
- (71) Wardman, P. *Journal of Physical and Chemical Reference Data* **1989**, *18*, 1637–1755.
- (72) Deng, Y.; Zhao, R. *Current Pollution Reports* **2015**, *1*, 167–176.
- (73) Feijoo, S.; Yu, X.; Kamali, M.; Appels, L.; Dewil, R. *Reviews in Environmental Science and Bio/Technology* **2023**, *22*, 205–248.
- (74) Zhou, X.; Mopper, K. *Marine chemistry* **1990**, *30*, 71–88.
- (75) He, D.-Q.; Zhang, Y.-J.; Pei, D.-N.; Huang, G.-X.; Liu, C.; Li, J.; Yu, H.-Q. *Journal of Hazardous Materials* **2020**, *382*, 121090.
- (76) Yasui, K.; Tuziuti, T.; Kanematsu, W. *Ultrasonics sonochemistry* **2018**, *48*, 259–266.
- (77) Kanthale, P. M.; Ashokkumar, M.; Grieser, F. *The Journal of Physical Chemistry C* **2007**, *111*, 18461–18463.
- (78) Liu, X.; Zhong, J.; Fang, L.; Wang, L.; Ye, M.; Shao, Y.; Li, J.; Zhang, T. *Chemical Engineering Journal* **2016**, *303*, 56–63.
- (79) Gonzalez, M. G.; Oliveros, E.; Wörner, M.; Braun, A. M. *Journal of Photochemistry and Photobiology C: Photochemistry Reviews* **2004**, *5*, 225–246.
- (80) Moussavi, G.; Mahdavianpour, M. *Chemical Engineering Journal* **2016**, *295*, 57–63.
- (81) Meegoda, J. N.; Hewage, S. A.; Batagoda, J. H. *Environmental Engineering Science* **2018**, *35*, 1216–1227.
- (82) Montazeri, S. M.; Kalogerakis, N.; Kolliopoulos, G. *Scientific Reports* **2023**, *13*.
- (83) han, Z.; Kurikawa, H.; Matsui, H.; He, C.; Wang, K.; Wei, Y.; Dodbiba, G.; Otsuki, A.; Fuhita, T. *Nanomaterials* **2022**, *12*, 237.
- (84) Wardman, P. *Journal of Physical and Chemical Reference Data* **1989**, *18*, 1637–1755.
- (85) Neta, P.; Grodkowski, J. *Journal of physical and chemical reference data* **2005**, *34*, 109–199.
- (86) Nagano, T.; Yamamoto, H.; Hirobe, M. *Journal of the American Chemical Society* **1990**, *112*, 3529–3535.
- (87) Von Sonntag, C.; Schuchmann, H.-P. *Angewandte Chemie International Edition in English* **1991**, *30*, 1229–1253.
- (88) Alfassi, Z.; Marguet, S.; Neta, P. *The Journal of Physical Chemistry* **1994**, *98*, 8019–8023.

- (89) Li, J.; Guo, J.; Dai, H. *Science Advances* **2022**, *8*, eabo0399.
- (90) Lee, J. I.; Huh, H. S.; Park, J. Y.; Han, J.-G.; Kim, J.-M. *Scientific Reports* **2021**, *11*, 19173.
- (91) Falk, M.; Miller, A. G. *Vibrational spectroscopy* **1992**, *4*, 105–108.
- (92) Carbon Dioxide Test, Sigma Aldrich.
- (93) Abril, G; Hesselsøe, M.; Nielsen, A. H. Oxygen measurement by Winkler titration, 2000.
- (94) Galvanic vs Optical Dissolved Oxygen Sensors [Accessed 30-01-2024], <https://www.horiba.com/sgp/water-quality/support/technical-tips/electrodes/galvanic-vs-optical-dissolved-oxygen-sensors/>.
- (95) Optical Dissolved Oxygen Sensors & Principles of Operation [Accessed 30-01-2024], <https://www.hamiltoncompany.com/process-analytics/dissolved-oxygen-knowledge/oxygen-measurement-principles/optical-dissolved-oxygen-sensors-principles-of-operation>.
- (96) The principles of dynamic light scattering <https://wiki.anton-paar.com/en/the-principles-of-dynamic-light-scattering/>.
- (97) Raja, P.; Barron, A. Dynamic Light Scattering [https://chem.libretexts.org/Bookshelves/Analytical\\_Chemistry/Physical\\_Methods\\_in\\_Chemistry\\_and\\_Nano\\_Science\\_\(Barron\)/02%3A\\_Physical\\_and\\_Thermal\\_Analysis/2.04%3A\\_Dynamic\\_Light\\_Scattering](https://chem.libretexts.org/Bookshelves/Analytical_Chemistry/Physical_Methods_in_Chemistry_and_Nano_Science_(Barron)/02%3A_Physical_and_Thermal_Analysis/2.04%3A_Dynamic_Light_Scattering).
- (98) The principles of dynamic light scattering <https://wiki.anton-paar.com/en/zeta-potential/>.
- (99) Raja, P.; Barron, A. Zeta Potential Analysis [https://chem.libretexts.org/Bookshelves/Analytical\\_Chemistry/Physical\\_Methods\\_in\\_Chemistry\\_and\\_Nano\\_Science\\_\(Barron\)/02%3A\\_Physical\\_and\\_Thermal\\_Analysis/2.05%3A\\_Zeta\\_Potential\\_Analysis](https://chem.libretexts.org/Bookshelves/Analytical_Chemistry/Physical_Methods_in_Chemistry_and_Nano_Science_(Barron)/02%3A_Physical_and_Thermal_Analysis/2.05%3A_Zeta_Potential_Analysis).
- (100) Zetasizer Nano User Manual.
- (101) Lohse, D.; Zhang, X. *Rev. Mod. Phys.* **2015**, *87*, 981–1035.
- (102) Hansen, V. K.; Wanstrup, K. Removal of active pharmaceutical ingredients from wastewater by application of nanobubble technology and ultraviolet light, eng, 2023.
- (103) Winkler, L. W. *Berichte der deutschen chemischen Gesellschaft* **1888**, *21*, 2843–2854.
- (104) He, D.-Q.; Zhang, Y.-J.; Pei, D.-N.; Huang, G.-X.; Liu, C.; Li, J.; Yu, H.-Q. *Journal of Hazardous Materials* **2020**, 382.
- (105) Rodriguez, R.; castillo, E.; Sinuco, D. *Journal of Analytical Methods in Chemistry* **2019**, 2019.
- (106) Jacomini, A. E.; Bonato, P. S.; Avelar, W. E. P. *Journal of Liquid Chromatography & Related Technologies* **2003**, *26*, 1885–1894.
- (107) Alquadeib, B. T. *Saudi Pharmaceutical Journal* **2019**, *27*, 66–70.
- (108) Yilmaz, B.; Kadioglu, Y. *Arabian Journal of Chemistry* **2017**, *10*, S1422–S1428.
- (109) Tadros, T. F. In *Handbook of Colloid and Interface Science*, 1st; De Gruyter Reference; De Gruyter: 2018; Chapter 3.
- (110) Nirmalkar, N.; Pacek, A. W.; Barigou, M. *Langmuir* **2018**, *34*, 10964–10973.
- (111) Zhou, Y.; Han, Z.; He, C.; Feng, Q.; Wang, K.; Wang, Y.; Luo, N.; Dodbiba, G.; Wei, Y.; Otsuki, A.; Fujita, T. *Materials* **2021**, *14*, DOI: 10.3390/ma14071808.
- (112) My engineering tools [Accessed 17-05-2024], [https://myengineeringtools.com/Chemical\\_Reactions/Saturation\\_Concentration\\_Oxygen\\_Water\\_Calculation.html](https://myengineeringtools.com/Chemical_Reactions/Saturation_Concentration_Oxygen_Water_Calculation.html).

- (113) witrox-specs <https://loligosystems.com/media/lmvppv0j/witrox-specs.pdf>.
- (114) Eklund, F.; Alheshibri, M.; Swenson, J. *Current Opinion in Colloid & Interface Science* **2021**, 53, 101427.
- (115) Fujita, T.; Kurokawa, H.; Han, Z.; Zhou, Y.; Matsui, H.; Ponou, J.; Dodbiba, G.; He, C.; Wei, Y. *Scientific Reports* **2021**, 11, DOI: <https://doi.org/10.1038/s41598-021-82717-z>.
- (116) Abril, G.; Hesselsøe, M.; Nielsen, A. H. Oxygen measurement by Winkler titration, Modified by M. Hesselsøe in 2001, A.H. Nielsen in 2007, 2000.
- (117) Libretexts Tyndall effect [https://chem.libretexts.org/Bookshelves/Physical\\_and\\_Theoretical\\_Chemistry\\_Textbook\\_Maps/Supplemental\\_Modules\\_\(Physical\\_and\\_Theoretical\\_Chemistry\)/Physical\\_Properties\\_of\\_Matter/Solutions\\_and\\_Mixtures/Colloid/Tyndall\\_Effect](https://chem.libretexts.org/Bookshelves/Physical_and_Theoretical_Chemistry_Textbook_Maps/Supplemental_Modules_(Physical_and_Theoretical_Chemistry)/Physical_Properties_of_Matter/Solutions_and_Mixtures/Colloid/Tyndall_Effect).
- (118) [https://science.nasa.gov/ems/09\\_visiblelight](https://science.nasa.gov/ems/09_visiblelight).
- (119) Seo, H.-B.; Lee, S.-Y. *Colloid and Interface Science Communications* **2023**, 52, 100687.

## Chapter 9

# Appendix - Winkler method

The Winkler method to determine dissolved oxygen content is presented in this appendix [116]. The Winkler method measures the dissolved oxygen content down to  $\pm 0.05 \text{ mg/l}$  whereas membrane electrodes have a precision down to  $0.1 \text{ mg/l}$ .

### Preparation of Winkler method solutions

#### *3 M manganese chloride ( $\text{MnCl}_2$ )*

The solution that was prepared by dissolving 30 g  $\text{MnCl}_2 \cdot 4 \text{H}_2\text{O}$  in 50 mL demineralised water.

#### *3 M sodium iodide ( $\text{NaI}$ ) with 8 M sodium hydroxide ( $\text{NaOH}$ )*

The solution was prepared by dissolving 30 g  $\text{NaI}$  in 50 mL demineralised water and 16 g  $\text{NaOH}$  in 50 mL demineralised water. The two solutions were cooled to room temperature after which they were mixed.

#### *Thiosulfate ( $\text{Na}_2\text{S}_2\text{O}_3$ )*

The solution, for titration, was made by dissolving 1 g  $\text{Na}_2\text{S}_2\text{O}_3 \cdot 5 \text{H}_2\text{O}$  and 0.1 g of  $\text{Na}_2\text{CO}_3$  in 1 L demineralised water.

#### *1.7 mM potassium iodate ( $\text{KIO}_3$ )*

The solution was made by dissolving 0.3567 g  $\text{KIO}_3$  in 1 L demineralised water.

### *Standardization of thiosulphate solution*

As  $\text{Na}_2\text{S}_2\text{O}_3$  is not stable and decomposes over time, the solution was standardised with the use of the  $\text{KIO}_3$  solution. The standardisation was performed by adding approximately 50 mL deionized water to a beaker. 250  $\mu\text{L}$  concentrated sulfuric acid was added followed by 250  $\mu\text{L}$   $\text{MnCl}_2$  solution and 250  $\mu\text{L}$  of the  $\text{NaI}$  and  $\text{NaOH}$  solution. Then 8 mL  $\text{KIO}_3$  solution was added and the mixture was stirred with a magnetic stirrer for approximately 1 min. The solution was then titrated with the  $\text{Na}_2\text{S}_2\text{O}_3$  solution and the concentration of  $\text{Na}_2\text{S}_2\text{O}_3$  was then calculated.

## **Chapter 10**

# **Appendix - HPLC for breakdown experiment**

The area under the peak for the HPLC measurements performed for the breakdown experiment along with the calculated concentration and the % difference are presented in this appendix.



**Table 10.1:** The area of HPLC chromatograms, concentrations of benzoic acid and breakdown in % between NB and no NB. part 1

	method	Area - HPLC	concentration [mM]	diference in % NB/no NB
Batch 2	ultrasound	243,1333	4,08463944	-0,656975223
	ultrasound w.o. NB	241,5464	4,05797952	
	UV	241,5957	4,05880776	0,128066538
	UV w.o. NB	241,9055	4,0640124	
	acid	240,2454	4,03612272	1,637979071
	acid w.o. NB	244,2461	4,10333448	
Batch 3	ultrasound	247,34	4,155312	0,752043824
	ultrasound w.o. NB	249,2142	4,18679856	
	UV	244,6499	4,11011832	0,465592571
	UV w.o. NB	245,7943	4,12934424	
	acid	234,6066	3,94139088	-0,443806996
	acid w.o. NB	233,57	3,923976	
	helt blank	242,5212	4,07435616	
Batch 4.5	ultrasound	415,8432	6,98616576	0,142542638
	ultrasound w.o. NB	416,4368	6,99613824	
	UV	412,2397	6,92562696	-0,021424166
	UV w.o. NB	412,1514	6,92414352	
	acid	400,4111	6,72690648	0,845096302
	acid w.o. NB	403,8238	6,78423984	
	blank	406,7319	6,83309592	
Batch 5	ultrasound	383,4268	6,44157024	1,256356789
	ultrasound w.o. NB	388,3053	6,52352904	
	UV	385,5778	6,47770704	0,41882802
	UV w.o. NB	387,1995	6,5049516	
	acid	382,3343	6,42321624	-0,714473871
	acid w.o. NB	379,622	6,3776496	
	blank sample	386,0864	6,48625152	

**Table 10.2:** The area of HPLC chromatograms, concentrations of benzoic acid and breakdown in % between NB and no NB. part 2

	method	Area - HPLC	concentration [mM]	diference in % NB/W.o.
Batch 6	ultrasound	377,3676	6,33977568	-0,106030248
	ultrasound w.o. NB	376,9679	6,33306072	
	UV	377,2495	6,3377916	-0,736088722
	UV w.o. NB	374,4929	6,29148072	
	acid	370,9103	6,23129304	-1,007486982
	acid w.o. NB	367,2107	6,16913976	
Batch 7	blank	368,3497	6,18827496	
	ultrasound	345,9186	5,81143248	1,423680127
	ultrasound w.o. NB	350,9145	5,8953636	
	UV	345,343	5,8017624	0,807144903
	UV w.o. NB	348,1531	5,84897208	
	acid	345,6181	5,80638408	0,631828868
Batch 9	acid w.o. NB	347,8157	5,84330376	
	blank	350,3689	5,88619752	
	ultrasound	300,7937	5,05333416	-2,206177419
	ultrasound NB	294,3009	4,94425512	
	UV	313,7474	5,27095632	-8,34245547
	UV w.o. NB	289,5886	4,86508848	
Batch 10	acid	291,0831	4,89019608	0,77732915
	acid w.o. NB	293,3635	4,9285068	
	blank	292,7090	4,9175112	
	ultrasound	283,7441	4,76690088	-0,429368813
	ultrasound w.o. NB	282,531	4,7465208	
	UV	280,4584	4,71170112	0,486958842
Batch 11	UV w.o. NB	281,8308	4,73475744	
	acid	278,1049	4,67216232	0,679339917
	acid w.o. NB	280,0071	4,70411928	
	blank	286,8690	4,8193992	
	ultrasound	251,06	4,217808	-3,658690158
	ultrasound w.o. NB	242,1987	4,06893816	
Batch 11	UV	184,9657	3,10742376	11,00696728
	UV w.o. NB	207,8429	3,49176072	
	acid	193,6294	3,25297392	16,60483326
	acid w.o. NB	232,183	3,9006744	
	blank	234,387	3,9377016	

# Chapter 11

## Appendix - Laser test

The presence of NB and the effect of bursting methods were detected by the Tyndall effect.

The Tyndall effect occurs when particles around the same size as the wavelength of the light passing through interfere with its path causing a beam to appear as the light is scattered [117]. As visible light (380-700 nm) lies within the interval of what is defined as colloids, it makes colloids detectable if the Tyndall effect is present [118].

A green laser (532 nm) and a cardboard box with cut holes were used to observe the presence of colloids in suspension. 3 batches (**O<sub>2</sub>, CO<sub>2</sub> and air**) of NB were produced in a standardized salt solution, 4 samples were gathered for each bursting method, 3 with NB and 1 blank, and exposed to the three bursting methods. The results of the laser test can be seen on **figure 11.1, 11.3 & 11.5**.

### 11.1 Air

The blank sample showed the weakest beam for acid and UV. The blank ultrasound showed no discernible difference indicating that colloids (NB) are present. A difference in intensity of the beam between 1-3 for each method is noticeable, which indicates a factor other than the bursting method plays a role.

The ultrasound samples show the least difference which supports that ultrasound may also produce NB, burst them or make them oscillate [110, 119].

The blank ultrasound size measurement shows a different size compared with the NB version, as well as a similar standard deviation as seen on **figure 11.2a**.

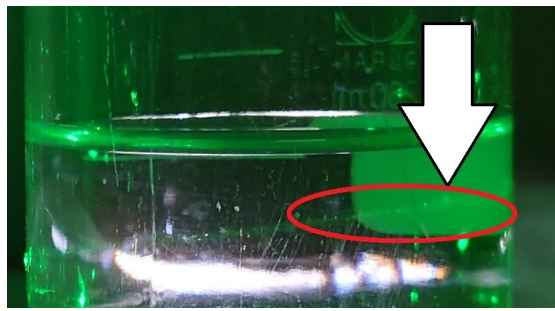
If NB are created, they're more unstable, as the zeta potential is closer to 0 mV as seen on **figure 11.2b**. Every blank sample shows a standard deviation that crosses 0 mV, indicating that if colloids are present, they will aggregate together due to the lack of repulsion from the zeta potential.

Ultrasound on all three batches showed a stronger beam on the blank sample, indicating that NB were created by the method.

The UV sample with NB showed a large standard deviation both for size and zeta potential. The zeta potential shows that impurities are to blame, as a colloidal suspension would have a zeta potential not crossing 0 mV.

### 11.2 CO<sub>2</sub>

The same tendency for the blank sample to be less intense is also observed for CO<sub>2</sub> on **figure 11.3**. Ultrasound also shows a less intense beam, which may be due to the CO<sub>2</sub> not being stable in solution. A difference in intensity is also observed within each method, further reinforcing that factors other than the method affect the Tyndall effect.



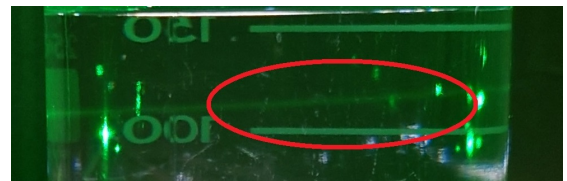
(a) batch 12 acid 1



(b) batch 12 acid 2



(c) batch 12 acid 3



(d) batch 12 acid blank



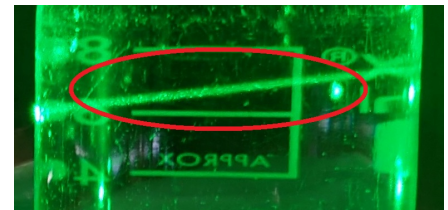
(e) batch 12 Ultrasound 1



(f) batch 12 Ultrasound 2



(g) batch 12 Ultrasound 3



(h) batch 12 Ultrasound blank



(i) batch 12 UV 1



(j) batch 12 UV 2



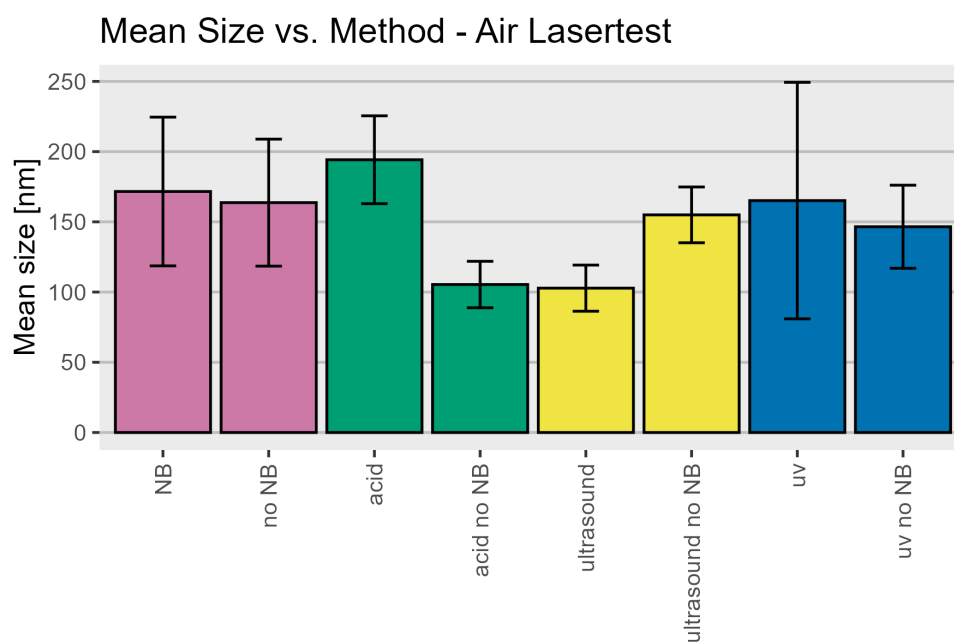
(k) batch 12 UV 3



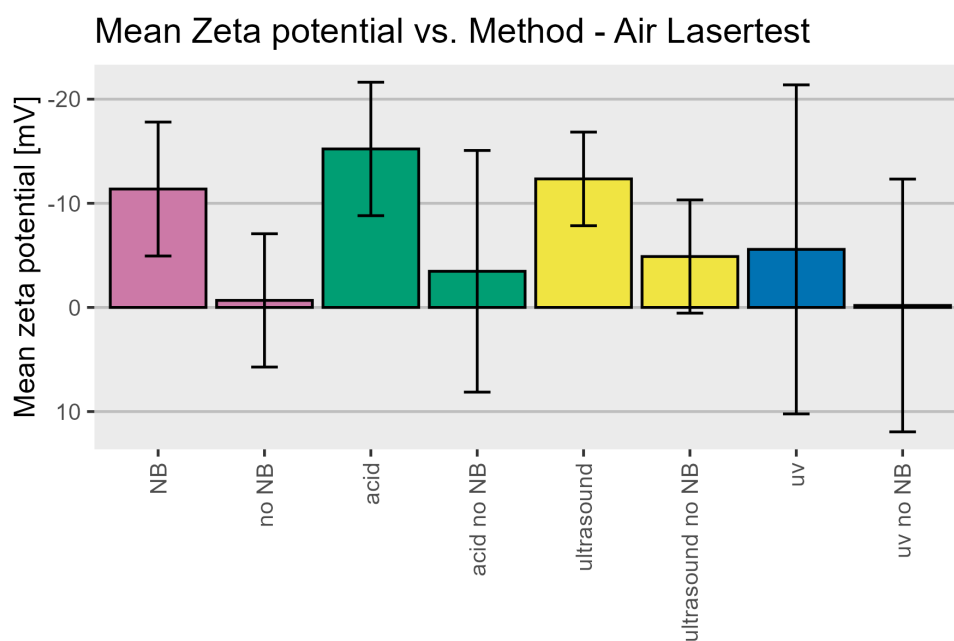
(l) batch 12 UV blank

**Figure 11.1:** Lasertest performed on air NB with 3 different bursting methods.

The size of ultrasound shows a large standard deviation, which indicates that the method both creates and bursts NB as seen on **figure 11.4a**.



(a) Mean size with standard deviation for air lasertest experiment.



(b) Mean zeta potential with standard deviation for air lasertest experiment.

**Figure 11.2:** Size and zeta potential measurement for air. Values are handled the same way as for other size and zeta potential measurements.

The UV also shows a large standard deviation which crosses 0 nm, which may be due to impurities or a low number of colloids/NB.

The acid shows a stable size which may be due to the large zeta potential as seen on **figure 11.4b**.

A positive zeta potential is also observed for UV blank and no NB. Both cases can be attributed to a too low  $k_{cps}$  of 3.3 and 4.5 respectively.

The zeta potential for blank acid and ultrasound shows that if colloids/NB are present, they are not stable.

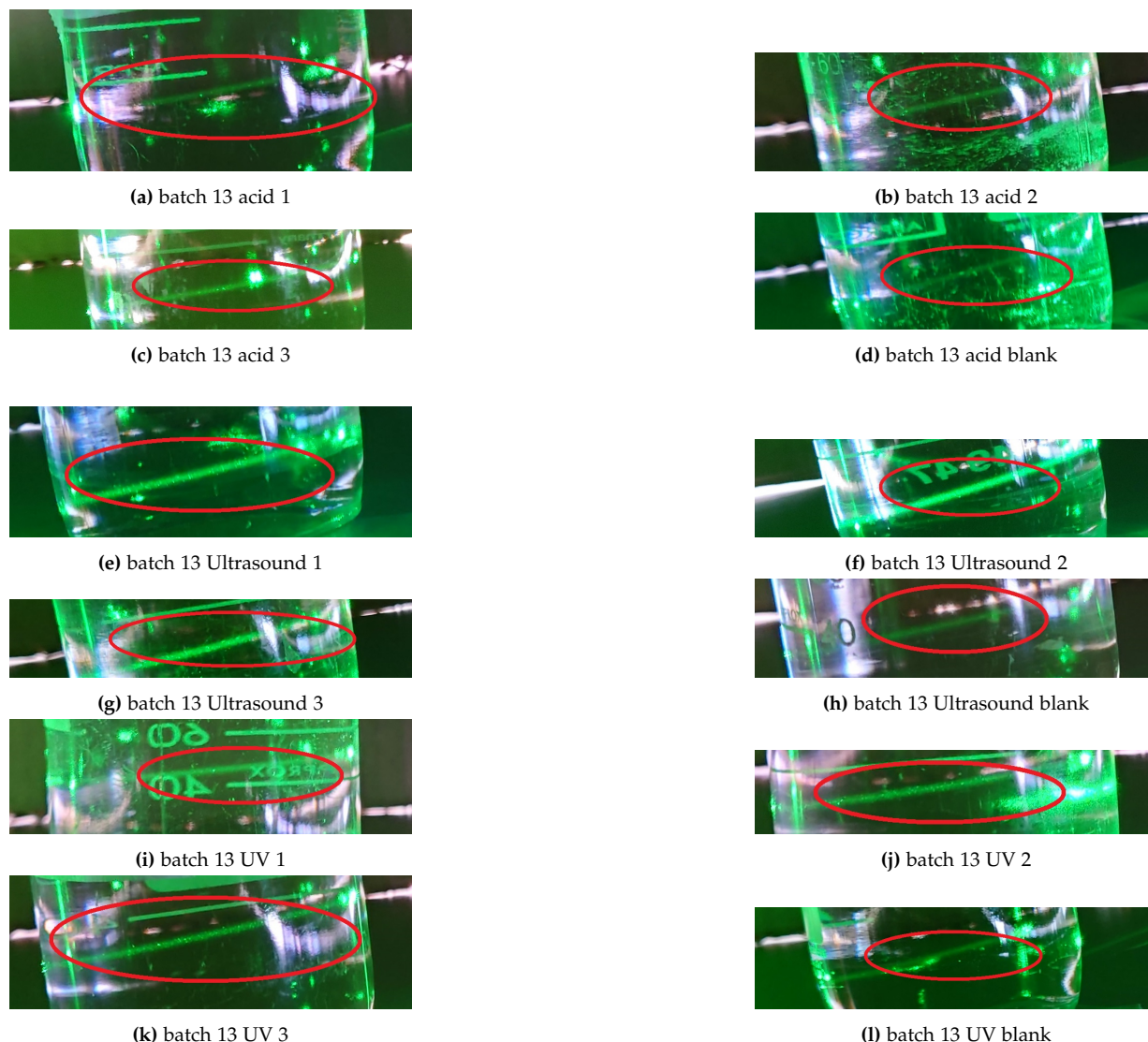
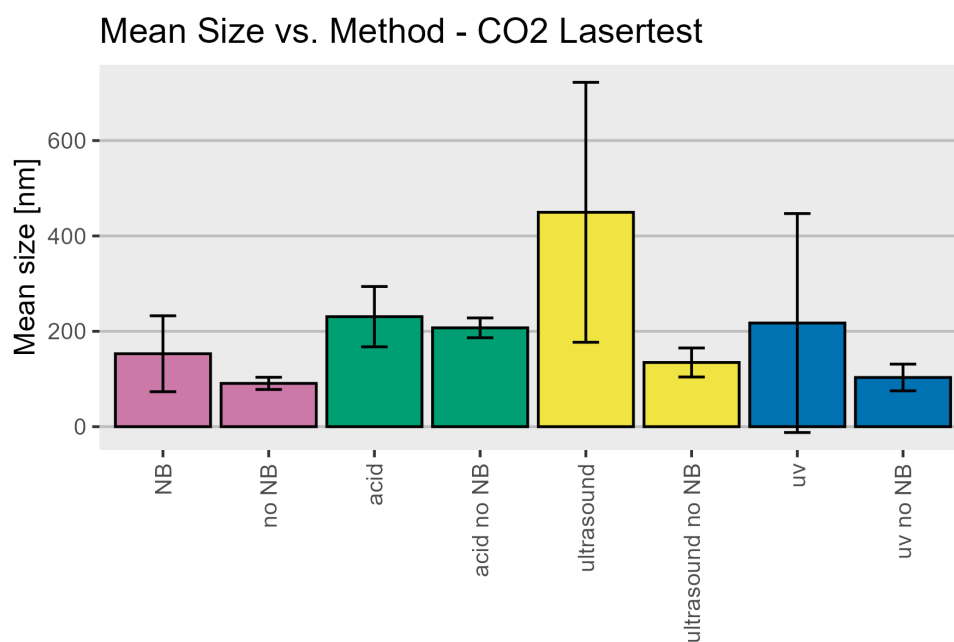


**Figure 11.3:** Lasertest performed on CO<sub>2</sub> NB with 3 different bursting methods

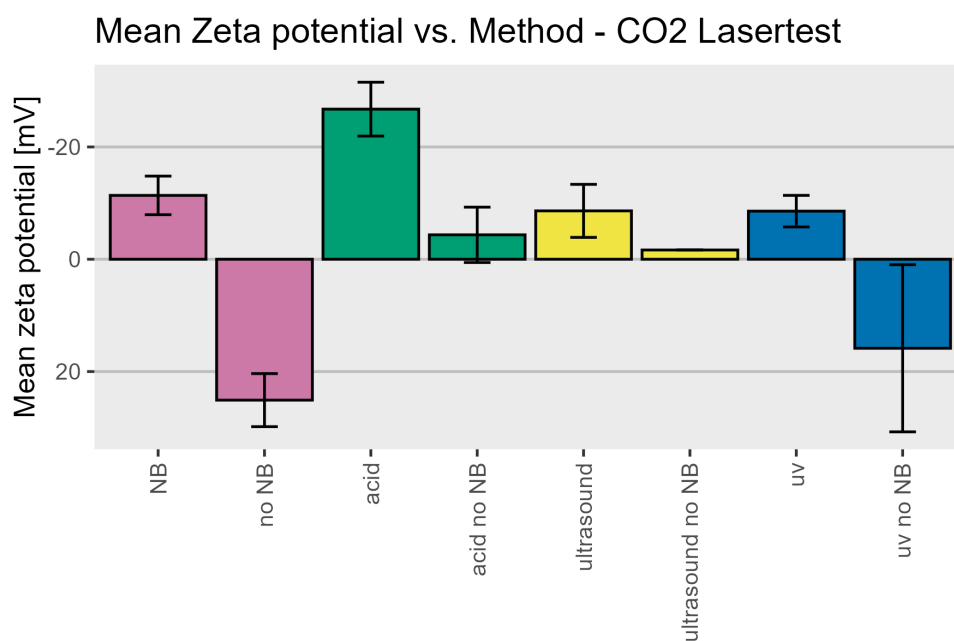
### 11.3 O<sub>2</sub>

The O<sub>2</sub> shows the same tendency as the other of ultrasound being closer in intensity between method and blank as seen on **figure 11.5**. Intensity also differed within each method as with the other gasses.

The blanks for UV and acid also showed a difference between the blank and method, as is



(a) Mean size with standard deviation for CO<sub>2</sub> lasertest experiment.



(b) Mean zeta potential with standard deviation for CO<sub>2</sub> lasertest experiment.

**Figure 11.4:** Size and zeta potential measurement for CO<sub>2</sub>. Values are found the same way as for other size and zeta potentials.



observed for the other gasses.

The size shows a smaller size for acid blank as seen on **figure 11.6a**. The other methods show a larger size for the blank samples. The zeta potential shows a tendency for the blanks to be more negative, stabilizing the colloidal sizes as seen on **figure 11.6b**. Acid and UV with NB shows a large standard deviation compared with their blank samples, indicating a variance within the method.

The ultrasound shows a similar zeta potential which indicate that the repulsion stability of the NB are not compromised.

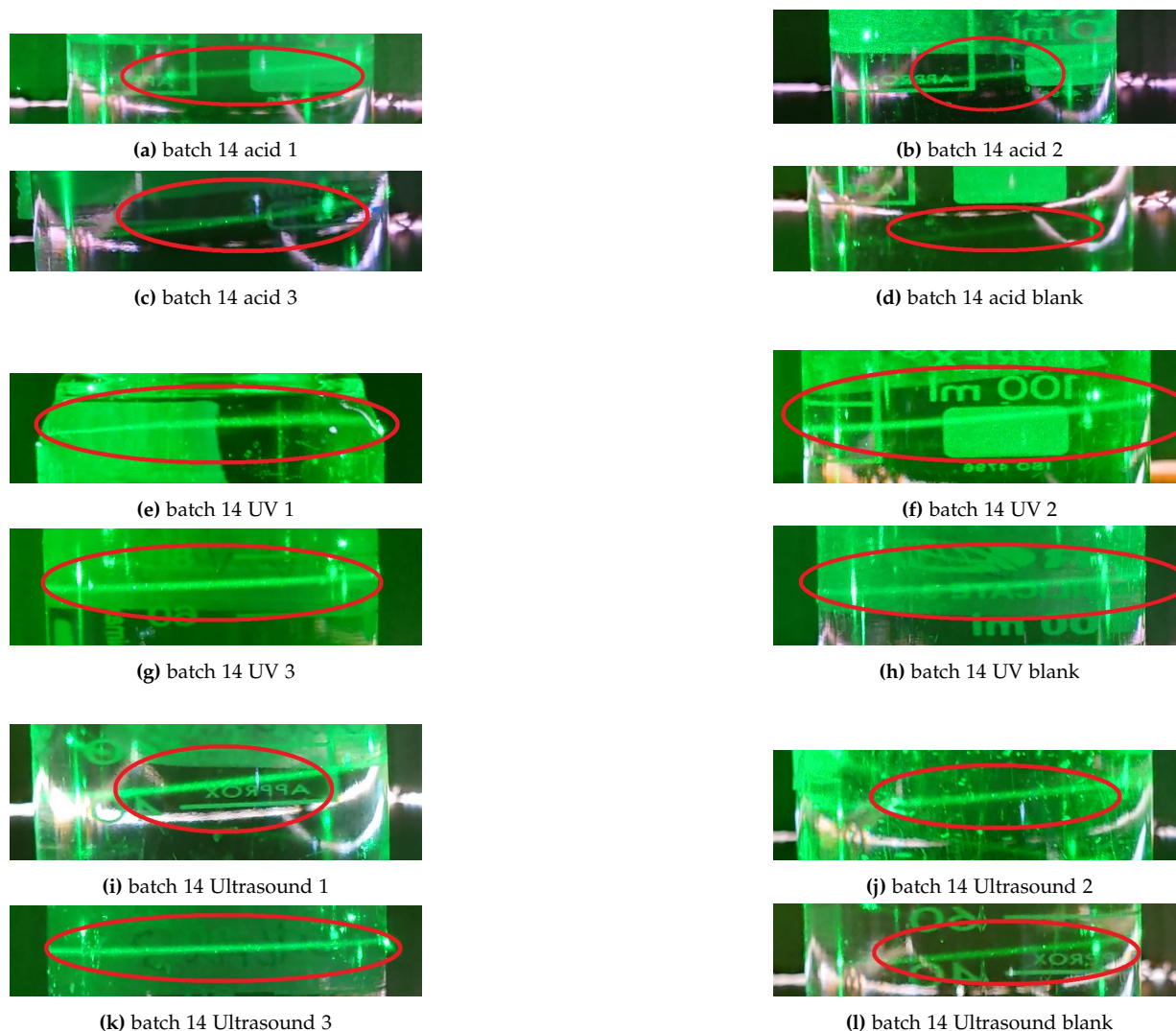
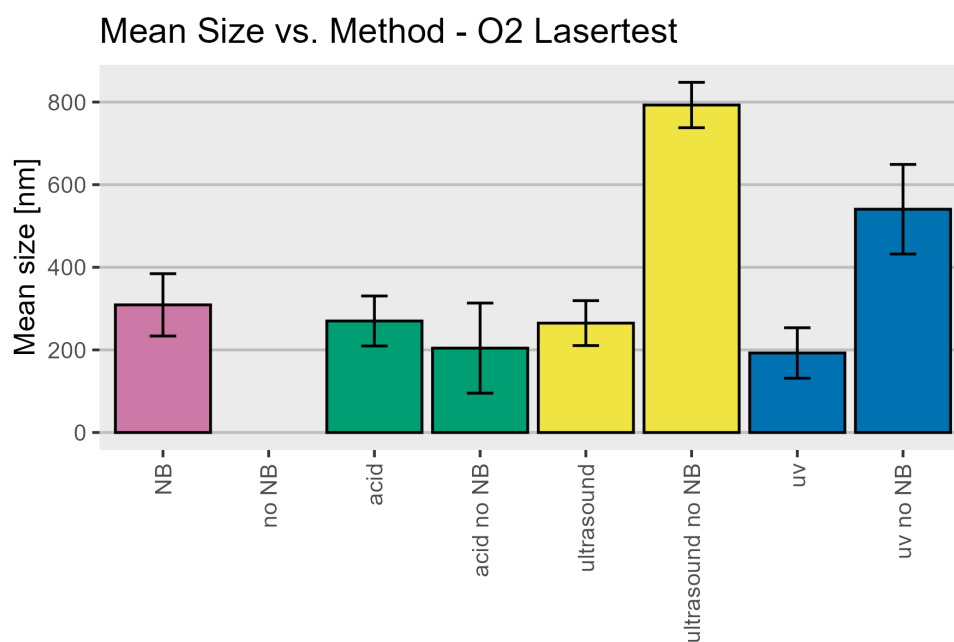


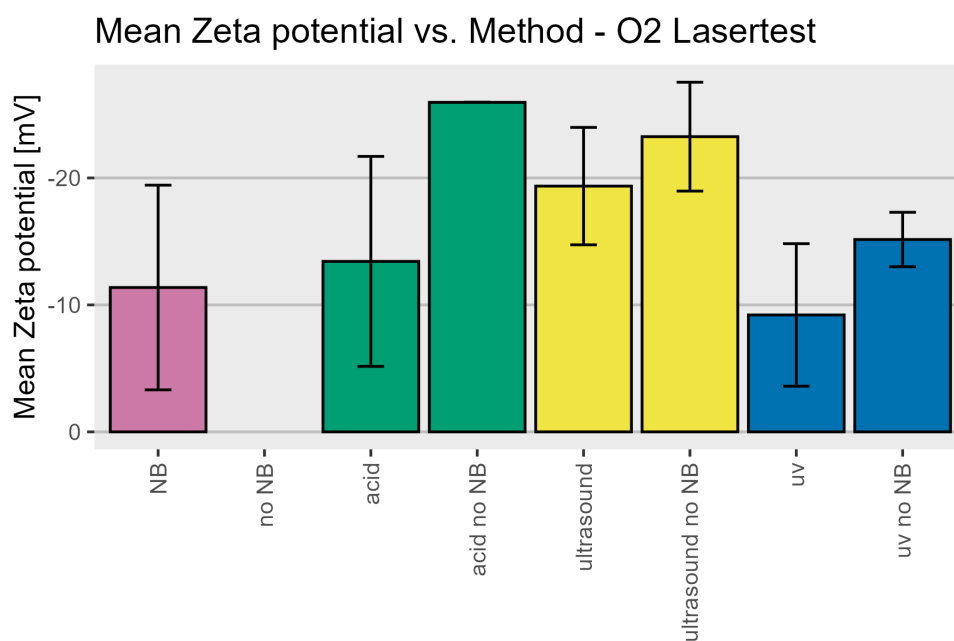
**Figure 11.5:** Lasertest performed on O<sub>2</sub> NB with 3 different bursting methods.

No tendency across the different gasses was observed regarding the Tyndall effect. Although ultrasound showed a difference, this was not consistent across all samples. Furthermore, many samples showed a difference within each method, which may be due to several reasons. Many pieces of glassware used had scratches which may scatter the beam. The cardboard box wasn't cut exact enough only to allow the laser through, which also affected the strength of the beam. The light environment outside the box changed between batches, affecting each batch differently. Furthermore, the laser was handheld and thus prone to slight movement. As the glassware used was cylinder-shaped, the laser could be scattered depending on the incident angle, further complicating the process.





(a) Mean size with standard deviation for O<sub>2</sub> lasertest experiment.



(b) Mean zeta potential with standard deviation for O<sub>2</sub> lasertest experiment.

**Figure 11.6:** Size and zeta potential measurement for O<sub>2</sub>. Values are found the same way as for other size and zeta potentials.

## Chapter 12

# Appendix D - Dissolved CO<sub>2</sub>

The IR spectra for the CO<sub>2</sub> NB were investigated to find the feasibility of using them to determine the CO<sub>2</sub> concentration in the solution. From the IR experiments, the area under the curves have been found and normalized by dividing the area with the area of the NB peak from that batch **table 12.1**. It can be seen that the area from the blank sample is the lowest followed by ultrasound in both batch 10 and 11 the area for acid and UV are close to each other with acid having the highest area however in batch 11 the normalized value is much higher than in batch 10. It was difficult to determine the area under the peak in batch 9 as there was a double peak that interfered in the same region, that double peak could correspond to CO<sub>2</sub> in the gas phase. The double peak can be seen in **figure 12.1**.

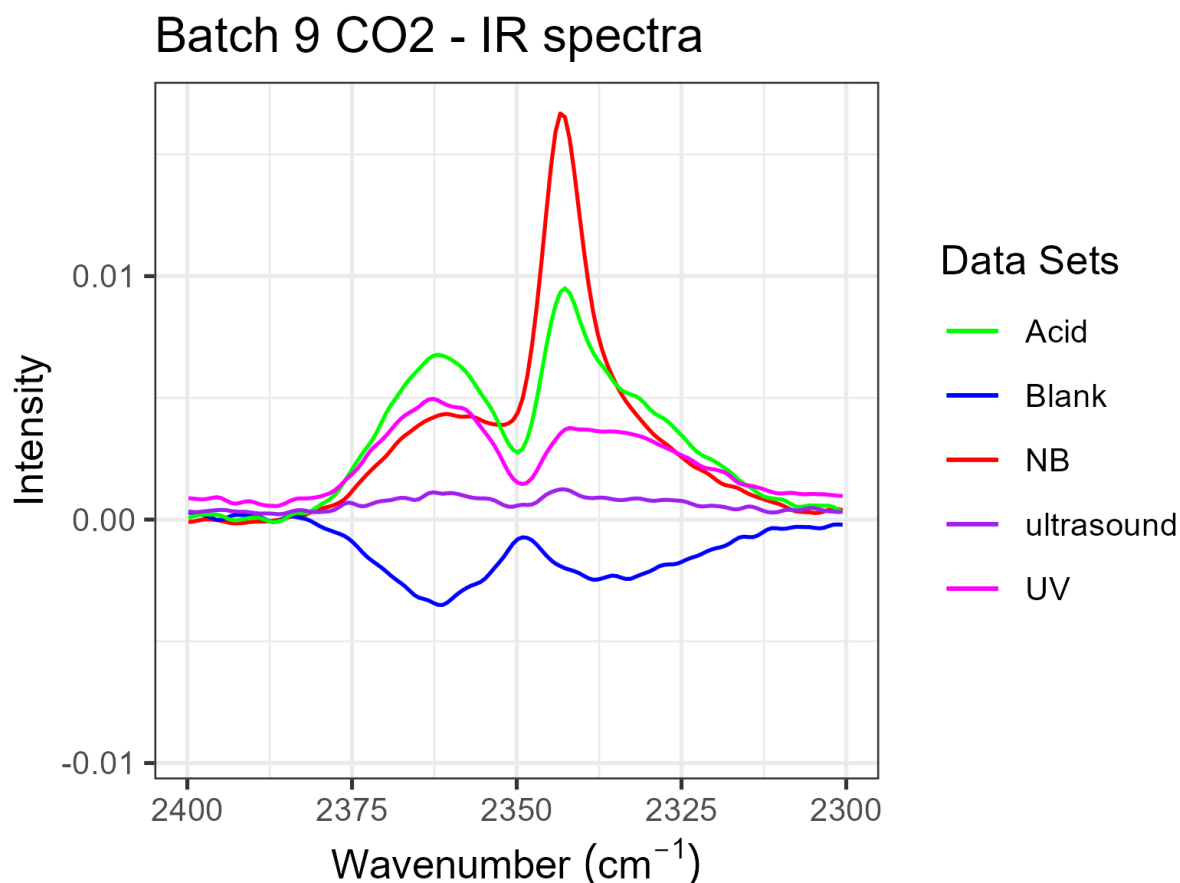


**Figure 12.1:** The IR spectra from batch 9 for each bursting method and a blank without NB.

**Table 12.1:** The normalized area of each peak in the IR spectra for batch 10 and 11.

		normalized area
Batch 10	NB	1
	Blank	0.26
	Acid	0.42
	Ultrasound	0.26
	UV	0.38
batch 11	NB	1
	Blank	0.24
	Acid	0.98
	Ultrasound 1	0.27
	Ultrasound 2	0.28
	UV	0.91

## **Chapter 13**

# **Appendix - kcps values**

The kcps values for all size and zeta measurements are presented in this appendix.

**Table 13.1:** The kpcs values for size and zeta potential measurements for the age experiment.

		DLS	Zeta
O2	age 1	76.9	169.1
	age 2	155.5	67.3
	age 3	132.3	169.3
	age 4	111.1	49.5
	age 5	259.7	97.4
	age 6	114.1	97.4
air	age 1	101.2	82.6
	age 2	215.7	22.8
	age 3	215.1	41.9
	age 4	150.3	58.5
CO2	age 1	225.9	159.1
	age 2	233.2	60.3
	age 3	191.8	797.3
	age 4	158.5	130.5
	age 5	201.6	44

**Table 13.2:** The kpcs values for size and zeta potential measurements for the SDS experiment.

		DLS	Zeta
SDS	no NB	95.2	4.9
	NB	139.6	88.5
	only SDS	83.6	2.3
	SDS 1	170.9	522.8
	SDS 2	142.3	131.8
	SDS 3	158.5	263.3
	SDS 4	19.5	13.9
	SDS 5	178.7	18

**Table 13.3:** The kpcs values for size and zeta potential measurements for the breakdown experiment.

		DLS	Zeta
batch 2	No NB		
	NB	200	39
	Ultrasound	165	10.4
	Acid	86.2	28.3
	UV	156	97.3
batch 3	No NB	178.5	13.3
	NB	132.5	66.8
	Ultrasound	167.6	85
	Acid	179.6	853.8
	UV	662.2	6.7
batch 4.5	No NB	61.3	71.1
	NB	142.3	268.2
	Ultrasound	106	110.8
	Acid	319.3	183.4
	UV	175.3	107.3
batch 5	No NB	95.6	8.8
	NB	360.5	38
	Ultrasound	251.1	76.4
	Acid	143.9	103.3
	UV	146.6	25.4
batch 6	No NB	127.7	8.7
	NB	192.9	47
	Ultrasound	163.6	13.3
	Acid	117.3	3.2
batch 7	No NB	57.5	4.9
	NB	352.1	239.2
	Ultrasound	234.5	48.7
	Acid	103.3	46.4
	UV	48.2	13.9
batch 9	No NB	60	120.9
	NB	231.5	51.2
	Ultrasound	337.2	35.3
	Acid	100.1	6.4
	UV	118.9	12.5
batch 10	No NB	71.9	112.8
	NB	118.5	157.6
	Ultrasound	251.7	18.3
	Acid	180.8	66.1
	UV	163	3.6
batch 11	No NB	122.6	15.9
	NB	360.5	764
	Ultrasound	226.2	971.1
	Acid	98.1	7.8
	UV	171.5	5.3

**Table 13.4:** The kpcs values for size and zeta potential measurements for the laser test.

		DLS	Zeta
air	no NB	70.4	2.8
	NB	173.9	54.7
	ultrasound blank	125.5	2
	ultrasound 1	155.8	19.4
	ultrasound 2	139.5	23.5
	ultrasound 3	138.5	20.9
	Acid blank	54.4	390.4
	Acid 1	132.2	1.2
	Acid 2	101.4	7.2
	Acid 3	64	42
	UV blank	125.5	38.6
	UV 1	145.8	61.2
	UV 2	196.5	97.1
	UV 3	194.3	20.5
O2	uden NB	47.8	4.4
	NB	141.4	33
	ultrasound blank	98.5	966.8
	ultrasound 1	207.9	8.4
	ultrasound 2	314.8	101.7
	ultrasound 3	326.3	47.3
	Acid blank	92.4	37.6
	Acid 1	69.8	19.4
	Acid 2	71.7	3.3
	Acid 3	96.4	1.9
	UV blank	78.1	39.6
	UV 1	195.6	67.6
	UV 2	125.4	639.8
	UV 3	140	49.7
CO2	uden NB	47.8	4.4
	NB	224.3	12.4
	ultrasound blank	73.3	24.5
	ultrasound 1	253.5	185.1
	ultrasound 2	368.5	208.6
	ultrasound 3	101.3	189.1
	Acid blank	80.6	2.9
	Acid 1	106.3	12.7
	Acid 2	279.2	4.8
	Acid 3	118.4	30.9
	UV blank	50.5	3.5
	UV 1	183.2	8.3
	UV 2	251.6	106.4
	UV 3	150	24.5

## **Chapter 14**

# **Appendix - p and F values values**

In this appendix, the F- and P-values for all batches are presented.

**Table 14.1:** One-way ANOVA test performed on size on all batches, producing the F- and P-values in this table part 1.

Batch nr	Method	Size F_Value	Size P_Value
<b>Batch 2</b>	acid	0.2632288	0.6217743
	no NB	4.765913	0.06534126
	Ultrasound	0.4865137	0.5052489
	UV	0.0598581	0.8137373
<b>Batch 3</b>	age 1	0.1429982	0.7245305
	age 2	0.1002285	0.7815448
	age 3	0.01336657	0.9135302
	age 4	0.2332588	0.6543616
	age 5	0.005455403	0.9446673
	age 6	0.8506478	0.4243917
	acid	2.298426	0.2040918
	no NB	0.1139933	0.7526173
	ultrasound	4.517094	0.100734
	UV	0.9515558	0.3845587
<b>Batch 4.5</b>	acid	0.6735433	0.4388696
	no NB	0.8447603	0.3849132
	ultrasound	0.2375462	0.6408762
	UV	0.4678592	0.5159709
<b>Batch 5</b>	age 1	2.049024	0.2022643
	age 2	0.09799594	0.7648438
	age 3	1.664111	0.2665757
	age 4	3.819162	0.0984746
	acid	0.6293092	0.4635736
	no NB	9.203553	0.02895741
	ultrasound	0.2546907	0.631786
	UV	0.5513205	0.4858204
<b>Batch 6</b>	acid	8.13224	0.03575207
	no NB	0.0002304035	0.9883815
<b>Batch 7</b>	acid	0.7830189	0.4055872
	no NB	1.113634	0.3221179
	ultrasound	1.769146	0.2201564
	UV	0.5311496	0.4897829
<b>Batch 9</b>	age 1	0.5578721	0.4794495
	age 2	0.2727013	0.6176386
	age 3	2.117018	0.2054285
	age 4	0.7082886	0.4278244
	age 5	1.829913	0.218202
	acid	0.3267373	0.5883438
	no NB	1.343598	0.2844087
	ultrasound	0.004309037	0.9497944
	UV	0.7770793	0.407284



**Table 14.2:** One-way ANOVA test performed on size on all batches, producing the F- and P-values in this table part 2.

Batch nr	Method	Size F_Value	Size P_Value
<b>Batch 10</b>	acid	5.329356	0.05430349
	no NB	0.06993727	0.8044954
	ultrasound	5.414714	0.05285043
	UV	3.120898	0.1206329
<b>Batch 11</b>	acid	8.760427	0.01815171
	no NB	5.599912	0.04986859
	ultrasound	18.83602	0.002478225
	UV	18.59472	0.002573146
<b>Batch 12</b>	acid	6.971896	0.04595213
	ultrasound	0.1611626	0.7086113
	UV	1.321695	0.3022903
	blank acid	7.723726	0.03203254
	blank ultrasound	0.6504492	0.456583
	blank UV	0.1517135	0.7103528
	no NB	0.4194399	0.5411897
<b>Batch 13</b>	acid	1.634586	0.2418248
	ultrasound	2.93823	0.1248525
	UV	1.677135	0.231427
	blank acid	1.054471	0.3386496
	blank ultrasound	0.5074326	0.5029986
	blank UV	5.793063	0.04271578
	no NB	0.3368008	0.5776581
<b>Batch 14</b>	acid	2.295788	0.1681914
	ultrasound	7.739497	0.02385102
	UV	0.3981603	0.5513047
	blank acid	15.89997	0.01045268
	blank ultrasound	0.06582824	0.8039855
	blank UV	0.7576125	0.4094335
<b>Batch 15</b>	NB SDS 1	0.0005519489	0.9819122
	NB SDS 2	7.163203	0.02808156
	NB SDS 3	0.4144888	0.5377152
	NB SDS 4	0.01362053	0.91037
	NB SDS 5	3.58784	0.09481685
	no NB	3.939634	0.1039316
	SDS	4.827412	0.05925784

**Table 14.3:** Anova test performed on zeta potential on all batches, producing the F- and P-values in this table part 1. Batch 7 has a standard deviation of 0, due to the nature of the data as described in the beginning of **chapter 6**, and thus is not able to be calculated. Batch 5 Ultrasound suffer from the same problem, although is able to be calculated.

Batch nr	Method	Size F_Value	Size P_Value
<b>Batch 2</b>	acid	2.812509	0.1445446
	Ultrasound	0.5071209	0.5082276
	UV	9.599206	0.03628233
<b>Batch 3</b>	age 1	0.5156687	0.49313
	age 2	0.05101343	0.8277621
	age 3	0.02546075	0.8777309
	age 4	0.0218096	0.8867585
	age 5	NaN	NaN
	age 6	2.025366	0.1976952
	acid	0.04742733	0.8348194
	no NB	0.0009825905	0.9758684
	ultrasound	0.06084513	0.8113768
	UV	0.1526832	0.7061839
<b>Batch 4.5</b>	acid	0.6308796	0.4630475
	no NB	0.1875186	0.6801235
	ultrasound	0.308666	0.5958014
	UV	0.07938524	0.7894215
<b>Batch 5</b>	age 1	3	0.1339746
	age 2	0.1363636	0.7246048
	age 3	1.630468	0.2488265
	age 4	4.5	0.07814075
	acid	0.1363636	0.7246048
	no NB	2.142452	0.2031467
	ultrasound	1.01412e+35	5.834077e-64
	UV	0.1363636	0.7246048
<b>Batch 6</b>	acid	1.615449	0.2443325
	no NB	4.203042	0.07951489
<b>Batch 7</b>	acid	NA	NA
	no NB	NA	NA
	ultrasound	NA	NA
	UV	NA	NA
<b>Batch 9</b>	age 1	0.2035473	0.6638511
	age 2	2.640432	0.1553007
	age 3	0.203665	0.663761
	age 4	0.1222654	0.736874
	age 5	3.144122	0.1194822
	acid	1.640893	0.269429
	no NB	2.529258	0.1504167
	ultrasound	00.04346832	0.8400563
	UV	3.545616	0.09646223

**Table 14.4:** Anova test performed on zeta potential on all batches, producing the F- and P-values in this table part 2.

Batch nr	Method	Size F_Value	Size P_Value
<b>Batch 10</b>	acid	2.624756	0.1563358
	no NB	NaN	NaN
	ultrasound	0.3535755	0.5708077
	UV	1.088857	0.3314157
<b>Batch 11</b>	acid	2.499434	0.1579
	no NB	0.3185843	0.5879312
	ultrasound	2.247993	0.1844488
	UV	2.351976	0.1689928
<b>Batch 12</b>	acid	0.6714645	0.4498214
	ultrasound	0.2324429	0.6444278
	UV	0.03514253	0.8574761
	blank acid	0.3713403	0.5688996
	blank ultrasound	0.2053094	0.6663934
	blank UV	0.000000005063395	0.9999452
	no NB	2.032329	0.1970152
<b>Batch 13</b>	acid	0.5715404	0.4782679
	ultrasound	0.0000000009166392	0.9999926
	UV	0.999963	0.350625
	blank acid	2.348086	0.1763236
	blank ultrasound	2.058944	0.2107844
	blank UV	3.758807	0.09370537
	no NB	0.000000001585749	0.9999693
<b>Batch 14</b>	acid	0.1627399	0.6986845
	ultrasound	0.039984	0.8471969
	UV	0.06571376	0.8050535
	blank acid	0.7060584	0.4480475
	blank ultrasound	1.563904	0.2512748
	blank UV	0.210677	0.6601497
<b>Batch 15</b>	NB SDS 1	3.571429	0.1173868
	NB SDS 2	1.085068	0.3377086
	NB SDS 3	0.9528106	0.3738349
	NB SDS 4	0.1040582	0.7579575
	NB SDS 5	1.433386	0.2763635
	no NB	0.5713925	0.4783224
	SDS	0.9687459	0.3630026